ON THE RATE TYPE COMPACTION BEHAVIOUR OF SANDSTONE RESERVOIR ROCK
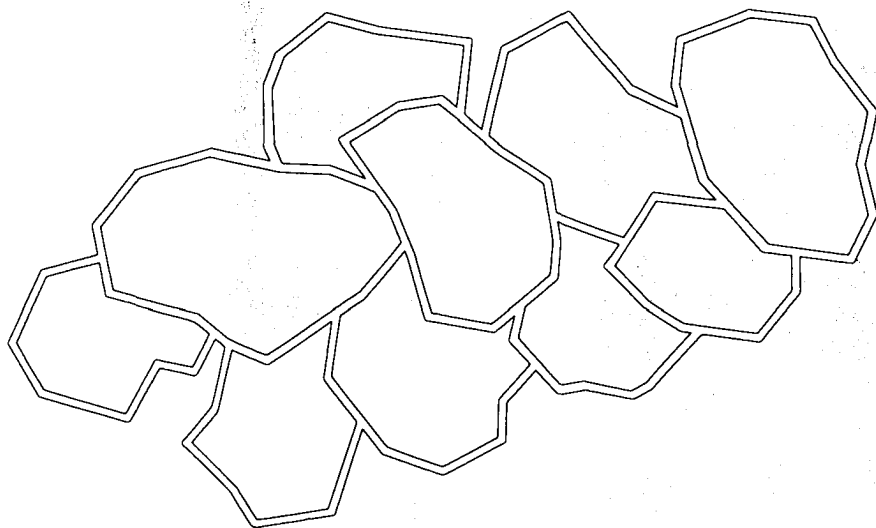
J.A. de Waal

ON THE RATE TYPE
COMPACTION BEHAVIOUR
OF SANDSTONE RESERVOIR
ROCK

33 1' 1 7ᵈ

) 1 7 §2° °

T R diss 14 ᵈ3

ON THE RATE TYPE COMPACTION BEHAVIOUR OF SANDSTONE RESERVOIR ROCK

PROEFSCHRIFT

ter verkrijging van de graad van doctor in de
technische wetenschappen aan de Technische Hogeschool Delft,
op gezag van de Rector Magnificus, prof. dr. J.M. Dirken,
in het openbaar te verdedigen ten overstaan van het College van Dekanen
op dinsdag 6 mei 1986
te 16.00 uur

door

JOHANNES ALOUISIUS DE WAAL

geboren te Amsterdam,
doctorandus in de wiskunde en natuurwetenschappen

Dit proefschrift is goedgekeurd
door de promotor
prof. dr. ir. A. Verruijt

aan Inge
aan mijn ouders

VOORWOORD

Het in dit proefschrift behandelde onderzoek is uitgevoerd op het Koninklijke/Shell Exploratie en Produktie Laboratorium te Rijswijk. Ik wil deze instelling en het management van Shell Research B.V. bedanken voor de grote medewerking die is verleend bij het tot stand komen van dit werk.

CONTENTS

1. INTRODUCTION

The withdrawal of fluids or gases from hydrocarbon or groundwater reservoirs can cause a considerable drop of the reservoir pore pressure. Meanwhile the weight of the layers on top of the reservoir, carried partly by the reservoir rock and partly by the reservoir pore pressure, remains constant. Consequently, when the pore pressure drops, a larger part of this overburden load has to be carried by the rock skeleton. As a result of this increased load, the reservoir rock will be compressed (compacted) until a new equilibrium is reached.

The lateral dimensions of a reservoir are usually large compared to its height. Therefore, considering the prevailing boundary conditions, it can be concluded that upon a drop in pore pressure, the reservoir will mainly deform in the vertical direction. According to Geertsma (1973a) a considerable reduction in reservoir height can be expected when one of the following conditions prevails: 1) a large drop in reservoir pressure, 2) production from a large vertical interval, 3) when the reservoir consists of unconsolidated or weakly consolidated rock or 4) when the reservoir is very shallow. In such cases an accurate prediction of reservoir compaction to be expected during production is essential.

First of all, reservoir compaction can induce considerable amounts of surface subsidence. Subsidence due to the excessive pumping of ground water basins is very common. Some examples are the San Joaquin Valley, California, U.S.A, (9 meter); Tokio, Japan (2.3 meter); Venice, Italy; Galveston, Texas, U.S.A.; Niigata, Japan; Chiba, China; Ravenna, Italy; Tapei, Taiwan; Mexico City, Mexico; Bangkok, Thailand; London, England; Santa Clara Valley, South Central Arizona, USA and Las Vegas, Nevada, U.S.A. (see Corapcioglu, 1984). Many more cases are known however (Bear and Corapcioglu, 1984).

Subsidence due to oil and gas production is considerably less common. Examples are the Goose Creek area near Galveston, Texas (Pratt and Johnson, 1926; Snider, 1927); the Wilmington field, Long Beach, California (approx. 8 meter, Gilluly and Grant, 1949; Mayuga and Allen, 1969; Allen, 1968); Inglewood field, Los Angelos, California (several meters, Yerkes and Castle, 1969); the Nigata gas field, Japan (several meters, Okumara, 1969; Hirono, 1969); the Po river delta gas producing area, Italy (Ciabatti, 1963); the oil fields along the Bolivar Coast of Lake Maracaibo, Venezuela (6-7 meter, van der Knaap and van der Vlis, 1967; Merle et al, 1975; Schenk and Puig, 1983) and the Groningen gas field, the Netherlands (Schoonbeek, 1976), where the subsidence presently amounts to some 15 cm.

In extreme cases, the surface subsidence can have considerable

environmental, technical and financial consequences. It can result in flooding of coastal areas that are near sea level (van der Knaap and van der Vlis, 1967), influence the flow of water, change the artesian head and result in thawing of permafrost layers (Mitchell and Goodman, 1978). In addition it can have a considerable influence on the design criteria of production facilities, e.g. on platform design in the case of offshore fields (van Ditzhuizen and de Waal, 1984). The associated surface stress field can become tensile in certain area's which in extreme cases above shallow fields can result in the occurrence of surface fractures, while the associated differential horizontal movements can result in damage to surface structures (Pratt and Johnson, 1926; Lofgren, 1974; Holzer and Papeyen, 1981; Holzer 1984). Even compaction induced activation of existing fault planes resulting in mini-earthquakes and considerable damage to production facilities has been reported (Richter, 1958; Lee, 1978; Kosloff et al., 1980a).

At the reservoir level, the compaction can result in damage to casing, tubing and liners (Kennedy, 1961; Patillo and Smith, 1982; Wooley, 1984). In addition the porosity reduction of the reservoir rock usually results in a lower permeability (Fatt and Davies, 1952; McLatchie et al, 1958; Brighenti, 1967; Jones, 1975). On the other hand, the reservoir compaction can act as a very effective production mechanism, especially in heavy oil fields and its contribution must be taken into account in material balance equations (see e.g. Finol, 1975). In fact for the heavy oil fields near Lake Maracaibo, reservoir compaction forms a major production mechanism (van der Knaap and van der Vlis, 1967; Merle et al, 1975, Schenk and Puig, 1983).

Because of the vital importance of early recognition and accurate prediction of reservoir compaction and associated surface subsidence, a considerable amount of scientific effort has been spent on the subject over the last sixty years. For sandstone reservoirs this effort has resulted in a framework of theoretical and laboratory procedures which are commonly accepted and which are summarised in section 2. Over the last decade it has become apparent however that application of these procedures to a number of well documented (sandstone reservoir) field cases results in strong discrepancies between the predicted and the observed field behaviour as will be discussed in section 3.

Given the vital importance of being able to properly predict reservoir compaction and the associated surface subsidence, a research program has been carried out in an attempt to resolve these discrepancies. The results of this investigation are presented in detail in the remaining sections of this thesis.

The compaction behaviour of carbonates, which can differ considerably from that of sandstones because of the phenomenon of pore collapse, has been the subject of a number of separate studies, the results of which have been reported elsewhere (van Ditzhuijzen and de Waal, 1984; Smits and de Waal).

2. HISTORICAL BACKGROUND

2.1 Compaction model development

2.1.1 Early work

Compaction model development started with the classical work of Terzaghi (1923, 1943), which because of its success in describing the one-dimensional compaction behaviour of a wide variety of porous media, contributed strongly to the development of the science of soil mechanics. Terzaghi considered the deformation of a laterally confined porous column on top of which a constant load is suddenly applied. He assumed the column to behave like an elastic rubber sponge saturated with liquid, in which the rate of compaction is governed by the rate at which fluid can be expelled from the column. Subsequently Terzaghi arrived at a differential equation describing the resulting deformation process, by coupling the Darcy flow equation (Darcy, 1856) to a linear elastic stress-strain relation via the continuity equation.

The theory was later extended to include permeability and compressibility variations along the porous column (see e.g. Taylor and Merchant, 1940; Verruijt, 1969, 1984) and the effects of the motion of the solid matrix, which was neglected in the original analysis (Philip, 1968), but it remains restricted to one-dimensional problems. The next major step forwards was therefore made by Biot, who extended the theory to three-dimensional systems. In a number of publications Biot showed that under the assumptions of isotropy and a reversible elastic stress-strain relation, the deformation of a porous medium can be described theoretically as an extension of the theory of elasticity (Biot, 1935, 1941, 1955, 1956 and 1957). In his theory however Biot introduced a set of deformation constants which are rather impractical from an experimental point of view. Therefore Gassmann (1951) and Geertsma (1957a, 1966, 1973a,b) reformulated the theory in terms of deformation constants more suitable for practical experimental determination. In Geertsma's formulation (Geertsma 1973b) the resulting stress-strain relation, for which he introduced the term poroelasticity, reads:

$$\sigma_{ij} = 2G \left[\epsilon_{ij} + \frac{\upsilon}{(1 - 2\upsilon)} e \, \delta_{ij} \right] + (1 - \beta)p\delta_{ij} \qquad (2.1)$$

where

σ_{ij} = stress component related to the bulk stress system (compressive stress taken positive, contrary to Geertsma's convention)

ϵ_{ij} = strain component

e = $Tr(\epsilon_{ij})$ = dilation or relative volume change of the bulk material

G = bulk shear or rigidity modulus

υ = Poisson's bulk ratio

p = pore fluid pressure

β = c_r / c_b = ratio between rock matrix and rock bulk compressibility

δ_{ij} = Kronecker delta

Bulk compressibility c_b, Poisson's ratio υ and shear modulus G are interrelated by the equation:

$$c_b = \frac{3(1 - 2\upsilon)}{2G(1 + \upsilon)} \qquad (2.2)$$

Lubinski (1954) and Geertsma (1957b) pointed out that this stress-strain relation is very similar to that used in the much older theory of thermoelasticity:

$$\sigma_{ij} = 2G \left[\epsilon_{ij} + \frac{\upsilon}{1 - 2\upsilon} e \delta_{ij} \right] - 2G \frac{1 + \upsilon}{1 - 2\upsilon} a T \delta_{ij} \qquad (2.3)$$

where

T   temperature variation with respect to the reference state of stress and strain

a   coefficient of linear thermal expansion

The transformation between the two stress-strain relationships is given by:

$$3aT \rightarrow - c_b (1-\beta)p \qquad (2.4)$$

Therefore, for many poroelastic problems an analogous but already solved thermoelastic problem exists. Care has to be taken in using these solutions as the analogy between poroelasticity and thermoelasticity is not complete (identical in all respects) merely because the stress-strain relationships are similar. Major differences can be caused by the body forces that are generated when fluid flow occurs in a porous medium. In addition the boundary conditions can be different.

Attempts to solve the coupled problem of fluid flow and rock deformation have been made by several authors (e.g. Finol, 1975; Verruijt, 1979; Sandhu, 1982; Abou Sayed, 1982). The problem is greatly simplified however when the pore pressure field is known and can be used as input (see Geertsma 1966).

2.1.2 The nucleus approach

An example of particular interest is the use of the so-called nucleus of strain concept to solve the poroelastic problem of the displacement field associated with the compaction of a buried porous sediment. For the case of a hydrocarbon reservoir compacting as a result of depletion, the nucleus approach was introduced by McCann and Wilts (1951), in their (unsuccessful) attempt to arrive at a better understanding of the subsidence behaviour above the Wilmington field. The concept was originally developed in the theory of thermoelasticity and is discussed in detail by Goodier (1937) and Nowacki (1962). The displacement field around such a nucleus of strain in an homogeneous elastic half space with a traction free surface was solved independently by Mindlin and Cheng (1950) and by Sen (1950). For the poroelastic case this solution describes the displacement field resulting from a pore pressure drop in a single point below the surface. Outside a nucleus at a depth of burial $z = c$ (for the geometry of the problem see Fig. 1), the displacement per unit volume and unit pressure change at a radial distance R_1 from the nucleus amounts to (Geertsma 1973b):

$$\vec{u}_e^\star = -\frac{c_m}{4\pi} \left[\frac{\vec{R}_1}{R_1^3} + \frac{(3 - 4\upsilon)\vec{R}_2}{R_2^3} - \frac{6z(z + c)\vec{R}_2}{R_2^5} + \right.$$

$$\left. - \frac{2\vec{k}}{R_2^3} \left[(3 - 4\upsilon)(z + c) - z \right] \right] \tag{2.5}$$

where

$$c_m = \frac{(1 - \beta)(1 - 2v)}{2G(1 - v)} \text{ , the uniaxial compressibility} \qquad (2.6)$$

$$R_1^2 = r^2 + (z - c)^2$$
$$R_2^2 = r^2 + (z + c)^2$$
$$\vec{k} = \text{unit vector in z-direction}$$
$$v = \text{Poisson's ratio}$$

Hence for the subsidence at the free surface above the nucleus:

$$u_z^*(r,0) = - \frac{c_m (1 - v)}{\pi} \frac{c}{(r^2 + c^2)^{3/2}} \qquad (2.7)$$

which shows that the surface subsidence is inversely proportional to $R^3 = (r^2 + c^2)^{3/2}$ the cube of the distance from the nucleus.

The displacement field associated with a compacting porous reservoir of finite dimensions is obtained by integrating the nucleus solution over the total reservoir volume. An approach also well known in thermoelasticity (see e.g. Nowacki 1962). Evangelisti and Poggi (1970) obtained a numerical solution for the integration over an idealised disc shaped reservoir. while Geertsma (1973b) derived an exact analytical solution for this problem. For reservoirs of more complicated shape the integration can only be carried out numerically (see e.g. Geertsma and van Opstal 1973).

For a more extensive discussion on the use of the nucleus of strain concept to model reservoir compaction and surface subsidence see (Geertsma, 1973b; Geertsma and van Opstal, 1973 and Gambolati, 1972). Major conclusions for the homogenous case are:

1. The volume of the surface subsidence bowl equals $2(1-v)$ times the reduction in reservoir volume and this ratio is independent of reservoir geometry.

2. The ratio between maximum subsidence (in the center of the bowl) and the reservoir height reduction is essentially determined by the ratio between the depth of burial and the lateral extent of the reservoir. Compaction of small deeply buried reservoirs results in uplift of the

in reservoir volume however.

Williamson (1974) further extended the work to multi-layered reservoirs, while Gambolati (1972) investigated the influence of the ratio of reservoir rock stiffness over surrounding rock stiffness on the nucleus solution.

2.1.3 The finite element approach

An alternative procedure to calculate the displacement field associated with a compacting reservoir is provided by the Finite Element Analysis (FEA) technique. Like many boundary problems in mathematical physics the FEA technique can be characterised by a variational principle. It can be shown from elasticity theory, that for the correct stress and strain distribution the resulting potential energy is at a minimum (Fung 1965). In the FEA method this' least energy principle is applied through structural idealisation. A sufficient number of points is selected in the body and along its boundaries. The spacing is in principle random. But it is advantageous to use a systematic spatial distribution which can be computer generated, and to apply the densest spacing where the displacement gradients are expected to be largest. Connecting the points to their neighbours by straight lines subdivides the body into the elements that give the method its name.

By means of the relations between displacements and strains and the stress-strain equation, the potential energy P of the body can be expressed as a function of all nodal displacements and the solution of the problem is obtained by minimising P. As each node only affects the displacements in adjacent elements a number of short linear equations results equal to the number of nodal points. If properly arranged, the coefficient matrix of this set of equations forms a large narrow band symmetric and diagonally predominant matrix, which can be solved numerically e.g. by using the Gauss/Seidel iterative method. The introduction of boundary conditions is straightforward by substitution of the given displacement and load vectors in the appropriate nodal points. For a detailed discussion of the finite element method see (Zienkiewicz, 1971) and (Zienkiewicz and Naylor, 1973).

The FEA method was first applied to Biot's equations by Sandhu (1968) and has since then been used by various other investigators as summarised in (Sandhu, 1982). Along a similar approach Geertsma and van Opstal (1973) calculated the radially symmetric displacement field associated with a compacting disc shaped reservoir. An excellent agreement with the known analytical solution for the homogeneous case (based on the nucleus of strain

concept) was obtained.

The FEA method has the advantage that it allows complex geometries, arbitrary boundary conditions, heterogeneity, anisotropy as well as non-linearity to be included in the calculations. The disadvantage of the method is that, especially for three-dimensional analysis, it is more complex, labour intensive and computer intensive. Consequently it is more expensive and more error prone than the nucleus approach. In addition the required detailed input information is usually not available.

For the case of a linear elastic multi-layered half space with different elastic constants for each layer, a hybrid procedure can be followed, provided the reservoir is located within one layer. In this procedure the reservoir is subdivided into rectangular grid blocks and the FEA method is applied to calculate the displacement field resulting from a unit pressure drop in a single grid block. Under the assumption of linear elasticity, the total displacement field is then obtained by a summation procedure over all reservoir blocks.

2.2 Laboratory measurements

As shown by Biot (1935) and by Geertsma (1957a), the deformation properties of a homogeneous isotropic linear elastic porous medium can be characterised by its porosity and three independent elastic constants. From an experimental point of view, a practical choice of elastic constants consists of:

1. The bulk compressibility c_b or the uniaxial compressibility c_m which are interrelated by the equation:

$$c_m = \frac{1}{3} (1 - \beta) \left(\frac{1 + \upsilon}{1 - \upsilon} \right) c_b \qquad (2.9)$$

    Equation (2.9) can be derived from equations (2.1), (2.2) and (2.6) and was confirmed experimentally by Teeuw (1971). For some recent work on this relationship see Lachange and Andersen, (1983).

2. Poisson's ratio υ.

3. The rock matrix compressibility c_r (also called the grain

compressibility), or alternatively its ratio to the bulk
compressibility β $(= c_r/c_b)$.

The bulk compressibility c_b is usually determined by measuring the
volumetric change of a cylindrical sample under the influence of an
increasing external hydrostatic pressure, applied via an impermeable sleeve
surrounding the sample, while keeping the pore pressure constant. Under such
conditions, as can be shown from equations (2.1) and (2.2):

$$c_b = -\frac{1}{V_b} \left(\frac{dV_b}{d\sigma}\right)_p \tag{2.10}$$

where

$$V_b \quad = \quad \text{the bulk volume of the sample}$$
$$\sigma \quad = \quad \text{the externally applied hydrostatic stress}$$

The uniaxial compressibility c_m and Poisson's ratio v are usually
determined in a triaxial cell on a cylindrical sample by increasing the
axial stress, while adjusting the lateral stress to keep the lateral strain
zero. Often the pore pressure is kept atmospheric. Such experiments are
called uniaxial compaction experiments in this thesis. Under such conditions
as can be shown from equations (2.1) and (2.6):

$$c_m \quad = (1 - \beta) \frac{1}{h} \left(\frac{dh}{d\sigma_z}\right)_{\epsilon_r = 0} \tag{2.11}$$

while

$$v \quad = \quad \left(\frac{\sigma_r}{\sigma_z + \sigma_r}\right)_{\epsilon_r = 0} \tag{2.12}$$

where

$$h \quad = \quad \text{sample length}$$
$$\sigma_z \quad = \quad \text{externally applied axial stress}$$

σ_r =   externally applied radial stress

ϵ_r =_ radial strain

Poisson's ratio can theoretically vary between -1 and 0.5. In practice it varies between 0 and 0.5. A value of 0.25 is often assumed.

The matrix or grain compressibility c_r can in principle be determined from the volume change resulting from simultaneously increasing the external hydrostatic pressure and the pore pressure as under such conditions:

$$c_r = \frac{1}{V_b}\left(\frac{dV_b}{d\sigma}\right)_{\sigma=p} \qquad (2.13)$$

Usually however, the literature values for the bulk compressibility of solid quartz (0.26×10^{-5} bar^{-1}) or solid calcite (0.08×10^{-5} bar^{-1}) are assumed (Adams and Williamson, 1923). More detailed descriptions of typical experimental procedures and equipment can be found in (Geertsma, 1957a) and in (Teeuw, 1971, 1973).

The mechanical properties of reservoir rock have in fact been measured by many authors (see e.g. Fatt, 1952, 1953, 1958; Hall, 1953; Geertsma, 1957a, 1973a; Roberts and de Souza, 1958; van der Knaap and van der Vlis, 1967; Teeuw, 1973; Newman 1973; Martin and Serdengecti, 1984). From this large data set the following general observations can be made for sandstones over the pressure range of interest during reservoir depletion:

1. Laboratory measured compressibilities of sandstone reservoir rocks range over several orders of magnitude, depending on rock type, degree of cementation, porosity, stress range, loading cycle etc. Typical ranges are shown in Fig. 2.
2. As the degree of cementation decreases, the compressibility generally increases, while the deformation behaviour changes from almost elastic and reversible for tight (low porosity) rock, to cataclastic and largely irreversible for unconsolidated sands. Typical examples are shown in Figs. 3 and 4.
3. The compressibility is in general found to be stress dependent as also illustrated by Figs. 3 and 4.
4. Poisson's ratio decreases with decreasing compressibility, from a typical value of 0.35 for unconsolidated sands to values well below 0.2

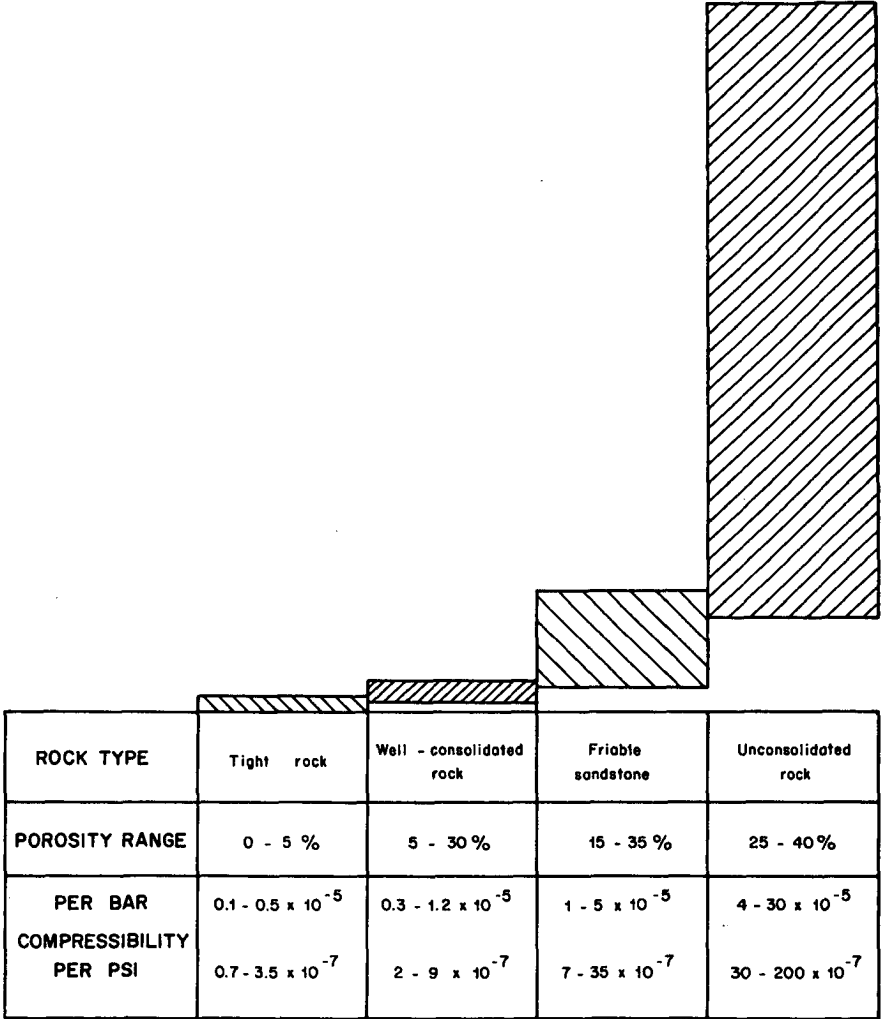| ROCK TYPE	Tight rock	Well – consolidated rock	Friable sandstone	Unconsolidated rock
POROSITY RANGE	0 - 5 %	5 - 30 %	15 - 35 %	25 - 40 %
PER BAR COMPRESSIBILITY PER PSI	$0.1 - 0.5 \times 10^{-5}$ $0.7 - 3.5 \times 10^{-7}$	$0.3 - 1.2 \times 10^{-5}$ $2 - 9 \times 10^{-7}$	$1 - 5 \times 10^{-5}$ $7 - 35 \times 10^{-7}$	$4 - 30 \times 10^{-5}$ $30 - 200 \times 10^{-7}$

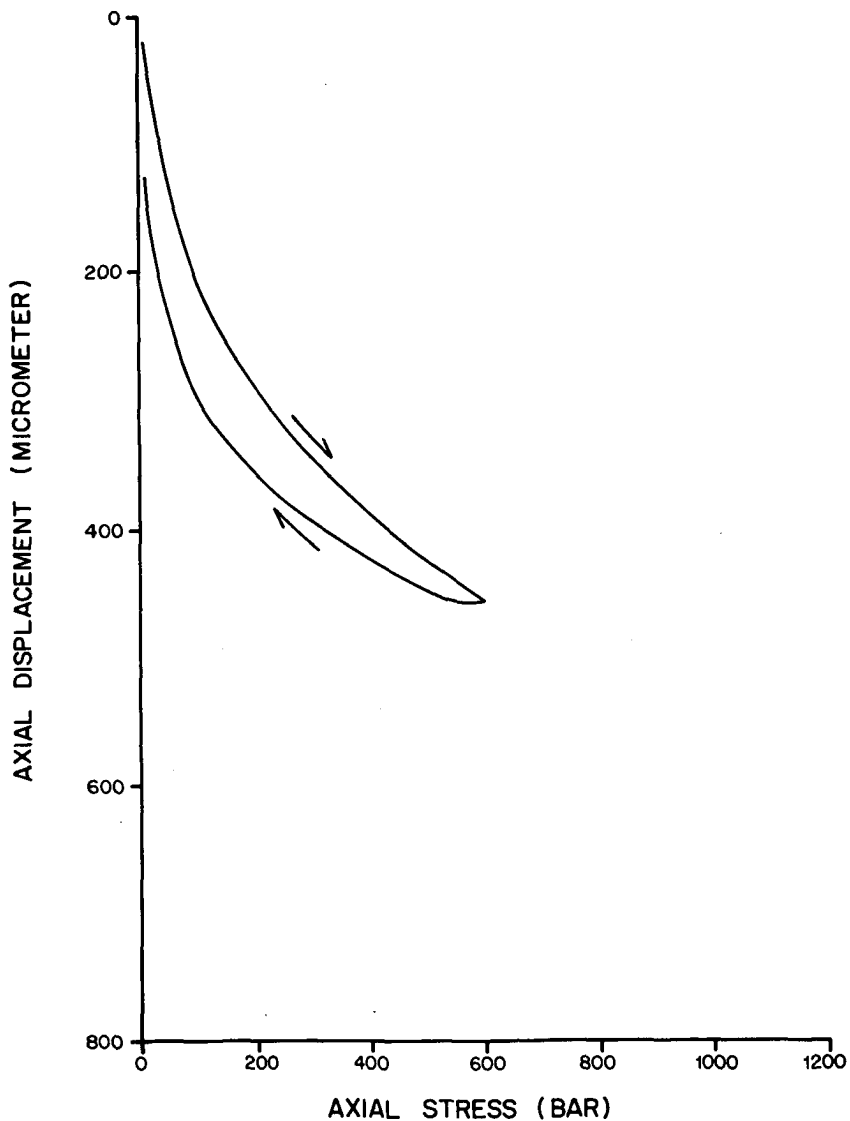# FIG.2 RANGE IN COMPRESSIBILITY OF VARIOUS ROCK TYPES (AFTER GEERTSMA, 1973a)

22

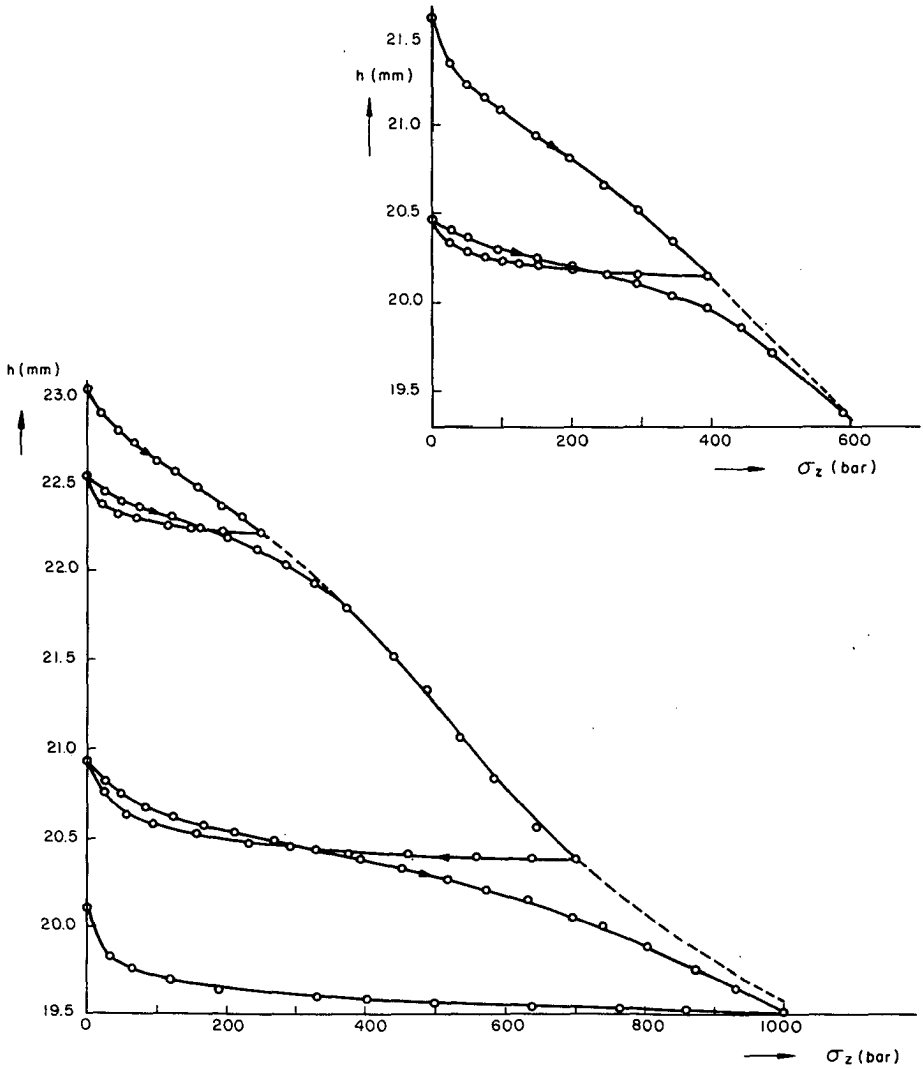FIG.3 TRIAXIAL COMPACTION OF LOW
POROSITY SANDSTONE

FIG.4 COMPACTION BEHAVIOUR OF A DRY, ARTIFICIALLY PACKED 450 μ SAND, WITH RELOADING CYCLES FROM ZERO LOAD

for tight rocks.

5.   Static elastic constants are in general quite different from those
      determined dynamically (e.g. using acoustic measurements).

2.3 Application to field cases

Based on the framework described in the previous paragraphs, the
following   approach has become commonly accepted in the recognition,
prediction and monitoring of reservoir compaction and surface subsidence:
For every compaction prone reservoir (large vertical interval, large
pressure drop, high compressibility rock or shallow depth of burial), a
rough calculation is made, to estimate the maximum possible compaction and
subsidence using the equation:

$$\Delta h \simeq c_m \, h_o \, \Delta p \qquad\qquad\qquad (2.14)$$

where

  Δh =   approximate maximum subsidence/compaction
  c_m =   rough guess of applicable uniaxial compressibility
  h_o =   approximate thickness of depletion interval
  Δp =   estimated maximum pressure drop

The calculation can be somewhat refined by taking the ratio between
reservoir compaction and surface subsidence into account. To this end the
reservoir is approximated by a disc (or a number of discs) of constant
thickness, for which Geertsma's analytical solutions (e.g. equation (2.8))
can be applied (Geertsma, 1973b). If the outcome of this calculation
indicates maximum reservoir compaction and surface subsidence less than say
10 cm, no further action is usually taken. If larger numbers are predicted,
a more detailed study is normally carried out consisting of:

1.   A series of hydrostatic or preferably uniaxial compaction experiments
      covering the pressure range of interest, on a minimum of 20 – 30
      representative core samples taken from various parts of the field if
      possible.
2.   An attempt to correlate the obtained compressibilities with some log
      derivable parameter, such as porosity.

3. Subdivision of the reservoir in grid blocks and assignment of depth, thickness, pore pressure drop and uniaxial compressibility to each block.

4. Calculation of the deformation field and possibly the stress field resulting from depletion profiles as predicted by reservoir simulations, using either the nucleus of strain or the FEA approach.

If as a result of such a detailed study considerable amounts of compaction and subsidence are still expected, further refinements are included based on increasing geological, reservoir engineering and rock mechanical information as soon as such data become available.

In addition, provisions are usually made for monitoring the surface subsidence and the reservoir compaction. Onshore this is done by setting up a leveling network to monitor the subsidence (Boot, 1973). Offshore, platform airgap data can be used in combination with pipeline and/or seabottom surveys. A recent technique is based on accurate platform position determinations using satellites. Expected accuracy of this latter technique is in the mm range. The reservoir compaction is sometimes monitored in dedicated observation wells by measuring the distance between radioactive bullets, shot in the formation or by accurately measuring the distance between casing joints, provided the casing is properly cemented to the formation (Allen, 1969; Loos, 1973). Natural compaction in the near surface layers is sometimes measured independently to account for its contribution to the total surface subsidence (Loos, 1973).

Unfortunately, for many historical field cases the influence of reservoir compaction was only realised after the observation of considerable surface subsidence. As a result, for most field cases only limited data is available over the early production period. An exception is formed by the Groningen gas field, where the potential importance of reservoir compaction was realised well before the start of production (Schoonbeek 1976).

2.4 Literature

Many review articles on reservoir compaction and surface subsidence have been written, e.g. (Geertsma, 1966, 1973a; Poland and Davies, 1969, 1981; Verhandelingen, 1973; Chilingarian 1975/76; Rieke et al, 1978; Saxena, 1981; Chilingar et al, 1983). In addition numerous articles can be found in the proceedings of a number of conferences especially dedicated to the problem of reservoir compaction and surface subsidence: (Proceedings, 1969, 1977, 1978, 1982, 1984).

3. DISCREPANCIES BETWEEN PREDICTED AND OBSERVED FIELD BEHAVIOUR

Over the last decade it has become apparent that application of the procedures as described in section 2, to a number of well documented field cases (all sandstone reservoirs), results in strong discrepancies between predicted and observed field behaviour. Some examples are:

1. In the case of the <u>Wilmington field</u> the original predictions, based on the extrapolation of the initial field behaviour, resulted in a gross underestimate of the ultimate subsidence, indicating a strongly non-linear compaction behaviour (Christian and Hirschfield, 1974; Kosloff and Scott, 1980a, 1980b; Helm, 1984). The non-linear behaviour is illustrated by the subsidence of a typical benchmark as a function of the average reservoir pressure drop as shown in Fig. 5 (derived from Lee, 1978). In addition, attempts to match the surface contour lines of the observed subsidence bowl with those calculated using an FEA approach were unsuccessful. Matching the depth of the subsidence bowl by tuning the estimated reservoir compressibility, resulted in a subsidence bowl of much larger radial extent than actually observed (Kosloff and Scott, 1980a). The field behaviour could only be simulated by assuming a "cap type" material behaviour of the reservoir rock (Kosloff and Scott, 1980b). This results in a very low compressibility up to a certain drop in pore pressure followed by a much higher compressibility during the subsequent pressure drop. The principle is illustrated in Fig. 6. Such material behaviour is in fact typical for certain clay types described by the "Cam Clay" model (Roscoe and Poorooshasb, 1963; Wroth, 1977) and for certain carbonate rocks (Blanton, 1981; van Ditzhuizen and de Waal, 1984). The compaction in Wilmington is mainly caused by unconsolidated sandstones however (Allen and Mayuga, 1970) and no detailed explanation for the postulated material behaviour was given (although erosion, ground vibration and viscous effects were suggested as possible causes).

2. In <u>Bachaquero</u>, a careful analysis of available field data, led to the conclusion that there appeared to exist so-called "threshold pressures" (Kennedy, 1961; Merle et al., 1975). Pore pressure drops up to the threshold pressure did not result in very significant surface subsidence. Upon approaching and surpassing the threshold pore pressure drop, surface subsidence increases rapidly however. Based on the
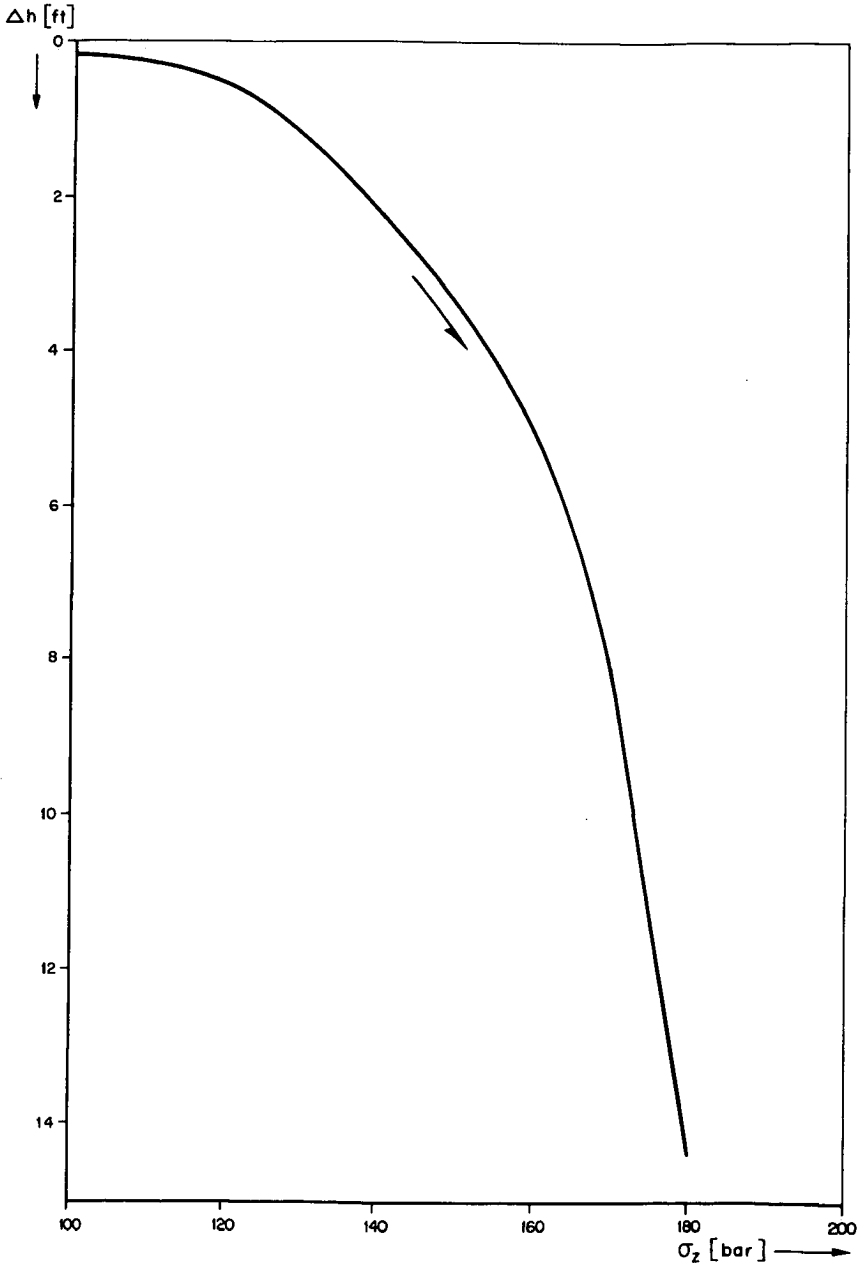
FIG.5 WILMINGTON: SUBSIDENCE OF
TYPICAL BENCHMARK AS A FUNCTION
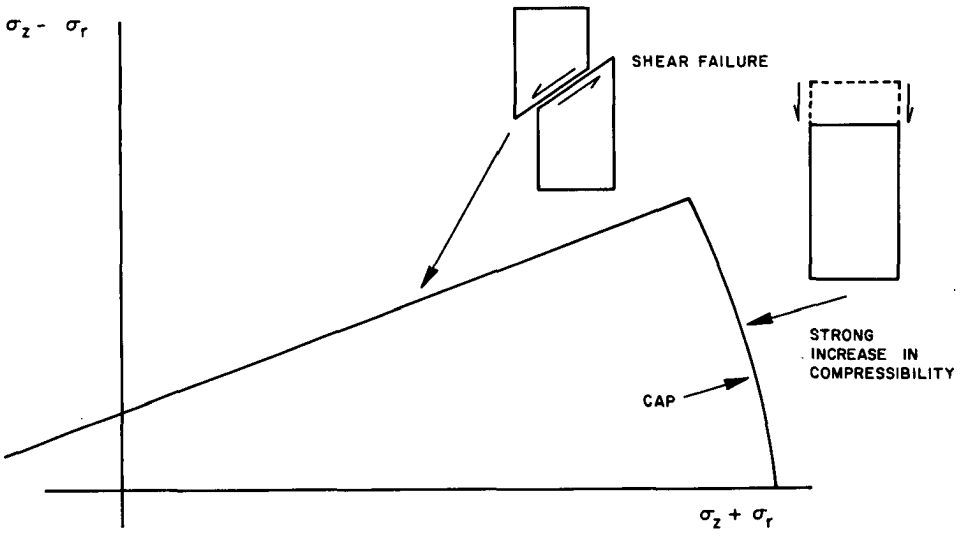OF VERTICAL EFFECTIVE STRESS.
(DERIVED FROM LEE, 1978)

FIG.6 ILLUSTRATION OF CAP-TYPE MATERIAL BEHAVIOUR

available surface subsidence and reservoir pressure data, Merle et al (1975), using an inversion algorithm, were able to back calculate the reservoir compaction for the various blocks in the field. Some results are shown in Fig. 7. From their work it became clear that the threshold pressure increases with increasing reservoir block depth. The work was considerably refined at a later stage. From this latter work an additional anomaly became apparent. For the more shallow reservoir blocks, average compressibilities during the production period (ignoring the non-linearities) seemed to be comparable to those predicted on the basis of laboratory core measurements. But for the deeper blocks the in-situ compressibilities appeared to be up to an order of magnitude lower as shown in Fig. 8. Meanwhile, from a geological point of view there was no explanation for such a different behaviour. Recently a cap-type material behaviour similar to that introduced for Wilmington, has been proposed to explain the observed field behaviour (Perez and Toscaz, 1984).

3. Threshold pressures have also been observed for the other Lake Maracaibo reservoirs such as <u>Tia Juana</u> (Schenk and Puig, 1982), in the <u>San Joaquin Valley</u> (California), were the subsidence is mainly related to ground water extraction (Propkovitch, 1982), and in a number of other field cases (Holzer, 1981, 1984; Martin and Serdengecti, 1984).

4. In the case of the <u>Groningen</u> gas field, the possibility that significant surface subsidence could occur as a result of reservoir depletion was recognised before the start of production. As a result, an extensive monitoring network was set up consisting of:

   a. A surface leveling network
   b. Shallow observation wells to measure the contribution of natural near surface layer compaction to the total surface subsidence
   c. In-situ compaction monitoring wells, using radioactive bullets shot into the reservoir formation

In addition a study was started at the "Koninklijke/Shell Exploratie en Produktie Laboratorium" (KSEPL) to predict the amount of reservoir compaction to be expected. As a result of this study an almost linear relation was predicted between the reservoir pressure drop and surface subsidence culminating in the late sixties in a predicted maximum subsidence of approximately 100 cm at the end of the production period. The work was reported by Geertsma and van Opstal in 1973.

By 1974 it became clear that the actual subsidence as measured in the field by surface levelings was considerably less than predicted. The discrepancy was attributed to possible sample disturbance, resulting in
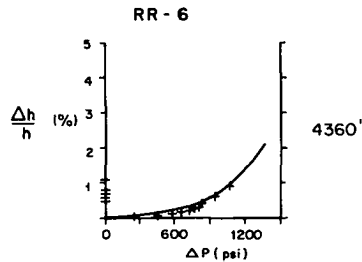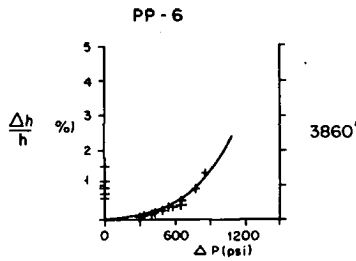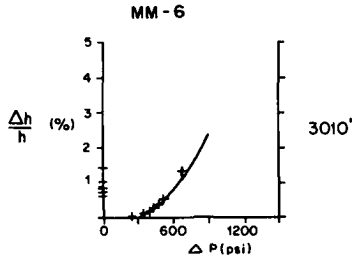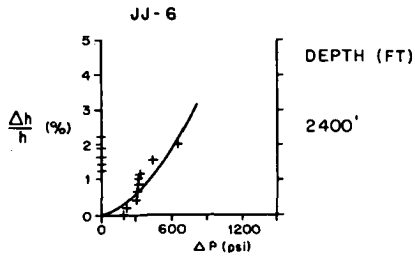
(△h = COMPACTION ; h = INITIAL GROSS THICKNESS)
(AFTER MERLE ET AL, 1975)

FIG.7 BACHAQUERO, FIELD DATA: COMPACTION BEHAVIOUR AT DIFFERENT DEPTHS.
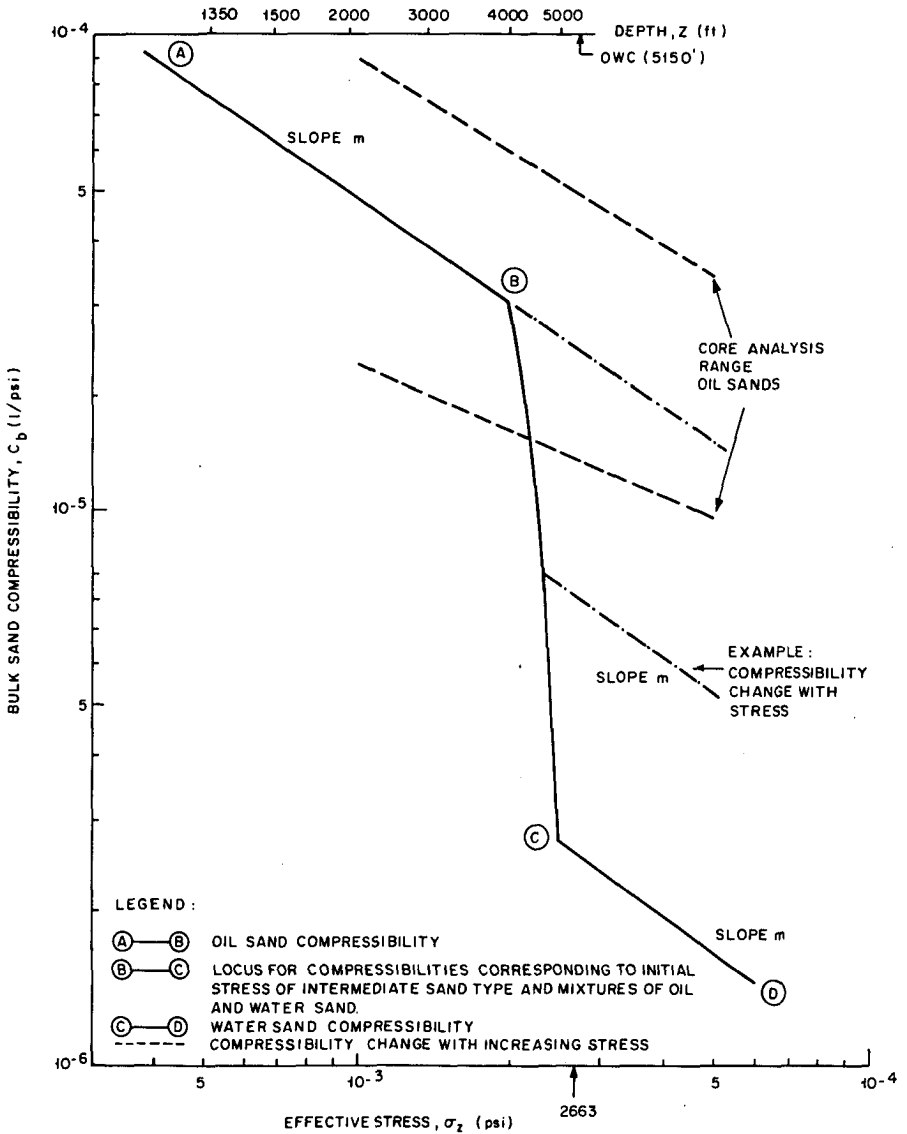
FIG.8 INITIAL ROCK COMPRESSIBILITY, BACHAQUERO FIELD

laboratory compressiblities which are not representative for the in-situ reservoir rock. Hence, the value of the in situ compressibility used in the calculations was adjusted to obtain a good fit between calculated and observed surface subsidence. Based on the adjusted value of the in-situ compressibility, a maximum subsidence of 30 cm was predicted at the end of the production period (Schoonbeek, 1976).

The new predictions were in good agreement with the actual field behaviour until 1981. After that date, the actual subsidence started to deviate more and more from the predicted linear behaviour, resulting in 1984 in an actual subsidence some 15 % larger than predicted.

4. POSSIBLE EXPLANATIONS

Given the vital importance of being able to accurately predict reservoir compaction and surface subsidence, the existing discrepancies between predicted and observed (sandstone reservoir) field behaviour were considered unacceptable. Therefore it was decided to start an investigation into the cause of these discrepancies. Basically two types of anomalies were recognised:

1. Differences between laboratory measured and field derived reservoir rock compressibilities. Examples are the Groningen gas field and the deeper Bachaquero reservoir blocks.

2. Apparent non-linear field behaviour as observed e.g. in Wilmington and the Bolivar coast.

Based on a careful analysis the following factors were recognised as possible causes for these discrepancies:

1. Incorrectness of the theory relating reservoir compaction and surface subsidence

2. Invalidity of the effective stress concept

3. Core disturbance

4. Previous deeper burial of reservoirs during their geological history

5. Temperature effects

6. Deviations from the assumed in-situ stress state

7. Loading rate effects

8. Pressure lag effects

Each of these hypotheses is discussed in more detail in the following paragraphs, in some cases together with the experimental procedures that have been carried out to test them.

4.1 Relation between reservoir compaction and surface subsidence

It was considered very unlikely that the observed discrepancies could be explained by assuming that the Geertsma/van Opstal theory, which relates reservoir compaction and surface subsidence, is incorrect. This is based on the following arguments:

1. In Bachaquero, the observed subsidence bowl volume equals that of the produced volume of hydrocarbons (at reservoir conditions) (Merle et al,1975). As over the production period considered, compaction was essentially the only drive mechanism, and as a stiff basement is present in Bachaquero, this is in exact agreement with the Geertsma/van Opstal theory.

2. In Bachaquero, San Joaquin and Wilmington, comparison of the surface subsidence of individual benchmarks with reservoir compaction measurements based on casing collar and radioactive bullet surveys in nearby wells, confirmed the one to one relation between subsidence and compaction as predicted by the Geertsma/van Opstal theory (Nunez and Escojido, 1977; Lofgren, 1961; Allen, 1969).

3. In Groningen, the agreement between predicted and initially observed subsidence profiles along cross-sections through the field was very good after scaling down all predicted subsidence contour lines by a factor of three (Schoonbeek, 1976). Moreover in-situ reservoir compaction measurements, based on distance measurements between radioactive bullets shot in the formation, suggested that reservoir compaction was also considerably smaller than predicted on the basis of the conventional laboratory core measurements (Mess, 1978).

Given the above arguments, it was concluded that the relation between reservoir compaction and surface subsidence is described correctly by the Geertsma/van Opstal theory. In addition it was concluded that the observed discrepancies therefore had to be due to differences between the laboratory and the in-situ compaction behaviour of the reservoir rock.

4.2 Invalidity of the effective stress concept

Rewriting equation (2.1) in the form:

$$\sigma_{ij} - (1 - \beta)\, p\, \delta_{ij} = 2G\, [\, \epsilon_{ij} + \frac{\upsilon}{(1 - 2\upsilon)}\, e\, \delta_{ij}] \qquad (4.1)$$

and taking the trace on both sides results in:

$$\sigma_{ii}/3 - (1 - \beta)p = c_b^{-1} e \qquad (4.2)$$

hence the bulk volume compaction e is only a function of $\sigma_{ii} - (1-\beta)p$ or for most samples only a function of the effective stress $\sigma_{ij} - p$ (as for most reservoir rocks $\beta \ll 1$). This "effective stress" principle is used in many laboratory compaction experiments, in which the reservoir compaction due to a drop in p is simulated by increasing σ_{ij} (keeping the pore pressure at atmospheric level). Thus a simple experiment replaces the more complex in-situ loading conditions. The invalidity of the effective stress concept was considered very unlikely as it has been experimentally confirmed by several investigators (Fatt, 1958; van der Knaap, 1958; Newman and Martin, 1977; Morita and Gray, 1984).

4.3 Core disturbance

It was considered very well possible that the coring action, the related stress relief and temperature change and the subsequent core handling procedures (transportation, sawing, drilling of samples etc.), results in core material which is not fully representative any more for the in-situ reservoir rock (Verhandelingen, 1973; Schoonbeek, 1976). The problem of the possible influence of such core disturbances was considered by several authors (Mattax et al, 1975; Mess, 1978; Dasseault 1980; Dasseault and van Domselaar, 1982). For a very weakly consolidated or unconsolidated sandstone the uniaxial compressibility measured during the first and the second laboratory loading cycle can differ by a factor of five (Mess, 1978). Upon surpassing the maximum stress level reached in the first cycle, the compressibility in the second cycle rises again, reaching first cycle values (Fig. 4).

The first laboratory loading of a core plug usually is a reloading up to the effective stress level sustained in the field. Therefore, during such first cycle laboratory loading, a similar increase of the compressibility can be expected around this stress level in the ideal case of an undisturbed core sample (Mess 1978). In fact in soil mechanics such a behaviour is often observed in tests on clay samples (Casagrande, 1936). For clay samples originating from Bolivar Coast reservoirs, van der Knaap and van der Vlis (1967) reported sharp increases in the compressibilities near the in-situ stress level. In general this behaviour is not observed on sandstone samples, indicating considerable disturbance to be the rule rather than the exception.

It was decided to continue the study of core disturbance along the lines of Mess and to extend the work to consolidated sandstones. First, a
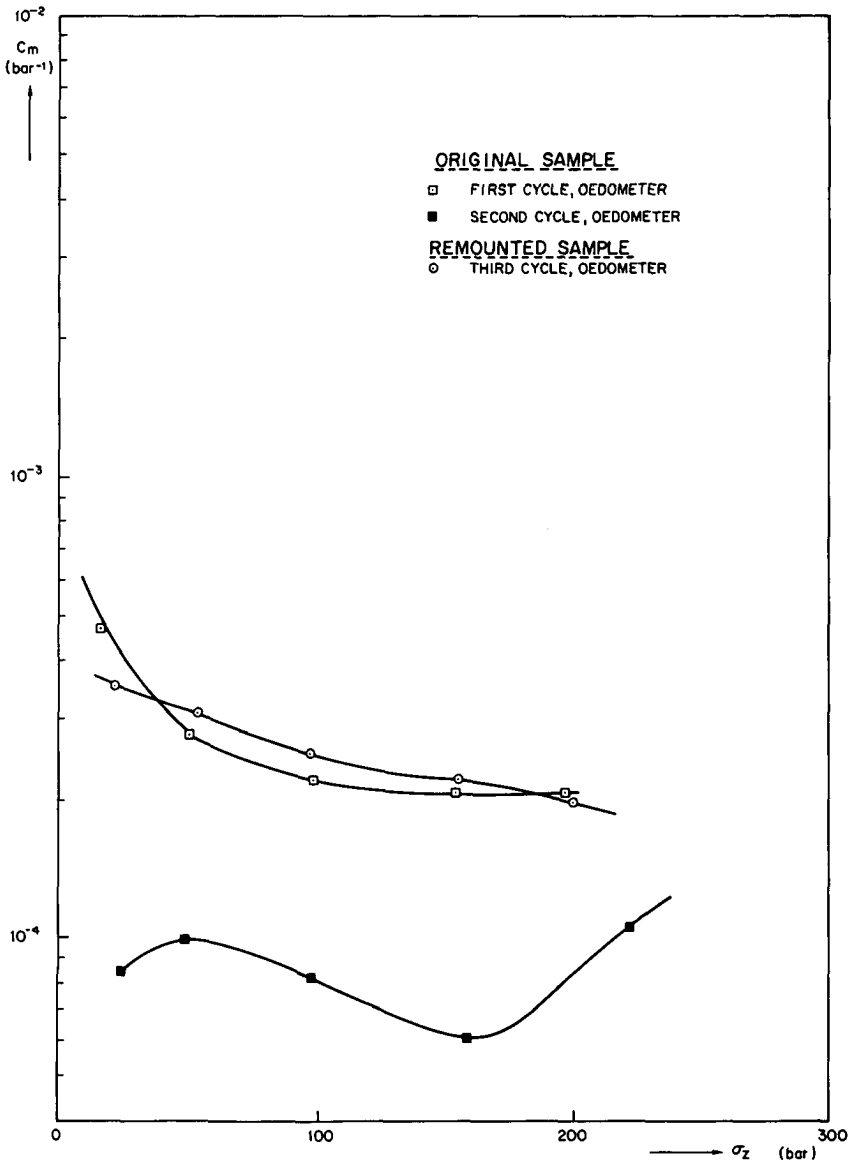
FIG.9 INFLUENCE OF SAMPLE HANDLING ON COMPACTION BEHAVIOUR OF UNCONSOLIDATED SAND
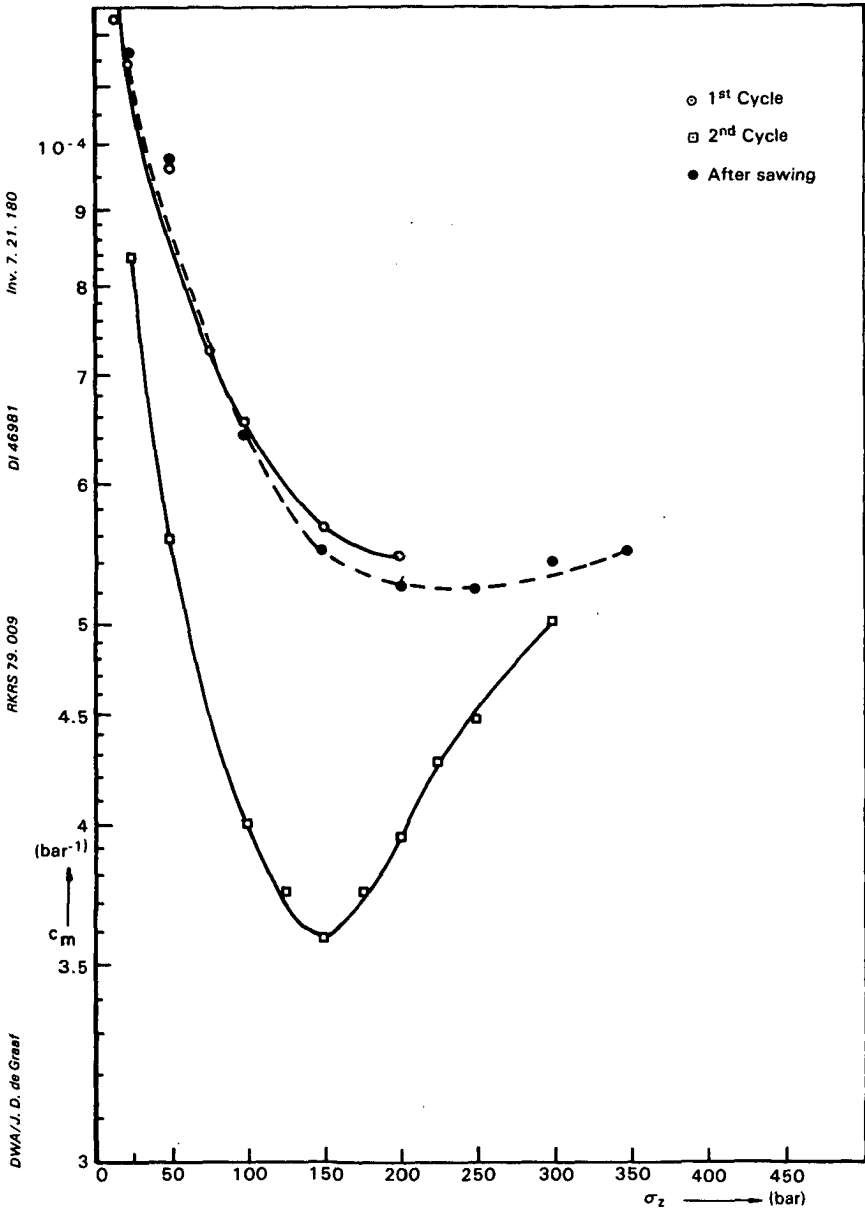
FIG.10 COMPACTION BEHAVIOUR OF CONSOLIDATED SANDSTONE AFTER SAWING

number of compaction experiments were carried out on very fresh core material (within a few hours from coring), but also these experiments showed no indications of the in-situ loading of the rock.

Next, the influence of removing and subsequently remounting samples after one or two laboratory loading cycles was studied. For the friable sandstones loaded in the triaxial compaction cell, no loss of "memory" was found during the subsequent loading cycle. For unconsolidated sands, removal and remounting resulted in return to first cycle behaviour however (Fig. 9).

Subsequently the influence of sawing on the compaction behaviour of friable and consolidated sandstone cores was studied by removing a thin slice from a number of samples after the first or second loading cycle, using a circular saw. In all cases the samples showed first cycle compressibilities upon reloading, indicating complete loss of memory (see Fig. 10). Similar results were obtained on 1 inch diameter samples drilled from a 2 inch diameter plug that had been subjected to a first loading cycle. Recently though some indications of in-situ loading have been found in the laboratory compaction behaviour of core samples from a very compressible but slightly consolidated reservoir rock.

It thus appears that sawing and drilling or even careful core manipulation (in case of unconsolidated sands), which inevitably occur during the preparation of samples for compaction experiments, completely remove the influence of the previous (in-situ) loading history for most sandstones. It also appears that the resulting first loading cycle compressibility is more or less reproducible. This suggests that the first cycle laboratory compressibility as measured on relatively undisturbed core samples should be used to predict field behaviour. It also suggests that core disturbance does not explain the discrepancies discussed in section 3. The subject will be further discussed in section 9.3.2.

4.4 Previous deeper burial

Laboratory measurements on unconsolidated sand samples (Mess, 1978) showed that reloading of a reservoir core sample after partial unloading, results in compressibilities that are initially much lower than those measured during the first loading cycle (Fig. 11). A similar partial unloading occurs in-situ when a reservoir is uplifted or geo-pressurised during its geological history. Therefore, upon the depletion of such a reservoir one would expect an initially low reservoir compressibility, which, upon surpassing the previously attained maximum stress level, will

gradually increase to values characteristic for a first loading cycle.

The resulting transition zone qualitatively resembles the field behaviour as observed in the San Joaquin Valley, in Wilmington and in Bachaquero and could also explain the initial low reservoir compressibility observed in Groningen. Previous deeper burial or geopressure of these reservoirs has indeed been proposed or considered as a possible explanation of the observed field behaviour (Merle et al, 1975; Schoonbeek, 1976; Propkovitch, 1982). To explain the increase in threshold pressure with increasing depth, as observed in Bachaquero, it has to be assumed that the reservoir has rotated as well during its geological history. Meanwhile in Bachaquero and Groningen, there are no geological indications for a previous deeper burial.

A further study on the influence of stress history on subsequent compaction behaviour of consolidated and unconsolidated sandstones was considered useful however. The related measurements consisted of: 1) interruption of loading (at various stress levels) during a uniaxial compaction experiment (resulting in a constant load on the sample); 2) uniaxial compaction after such an interruption; 3) uniaxial compaction after complete unloading and 4) uniaxial compaction after various amounts of partial unloading at various stress levels. The results of these experiments will be summarised in section 6, details are given in section 9.2 and in Appendix A.

4.5 Temperature effects

Laboratory experiments are usually carried out at room temperature. Actual reservoir temperatures are normally higher, ranging from slightly above room temperature for shallow reservoirs, to around 100 degrees C for deeper reservoirs such as the Groningen gas field. Given the deformation mechanisms considered to be important in sandstone reservoir rock (to be discussed in detail in section 8.1), very little influence of such temperature differences was expected, as confirmed experimentally by others (see e.g. Morita and Gray, 1984). A scouting experiment, further confirming these expectations was carried out at elevated temperature. More detail will be given in sections 6 and 7.3.2.

Cm (bar⁻¹) — vertical axis label: $C_m \ (bar^{-1})$

Legend:
- ○ $\sigma_z : 0-400-100$
- □ $100-700-400 \ (\text{previous } \sigma_{z_1 max} = 400)$
- △ $400-1000-0 \ (\text{previous } \sigma_{z_1 max} = 700)$
- ▨ Reloading from $0-700 \ (\text{prev.} \sigma_{z_1 max} = 400)$
- ▲ Reloading from $0-1000 \ (\text{prev.} \sigma_{z_1 max} = 700)$
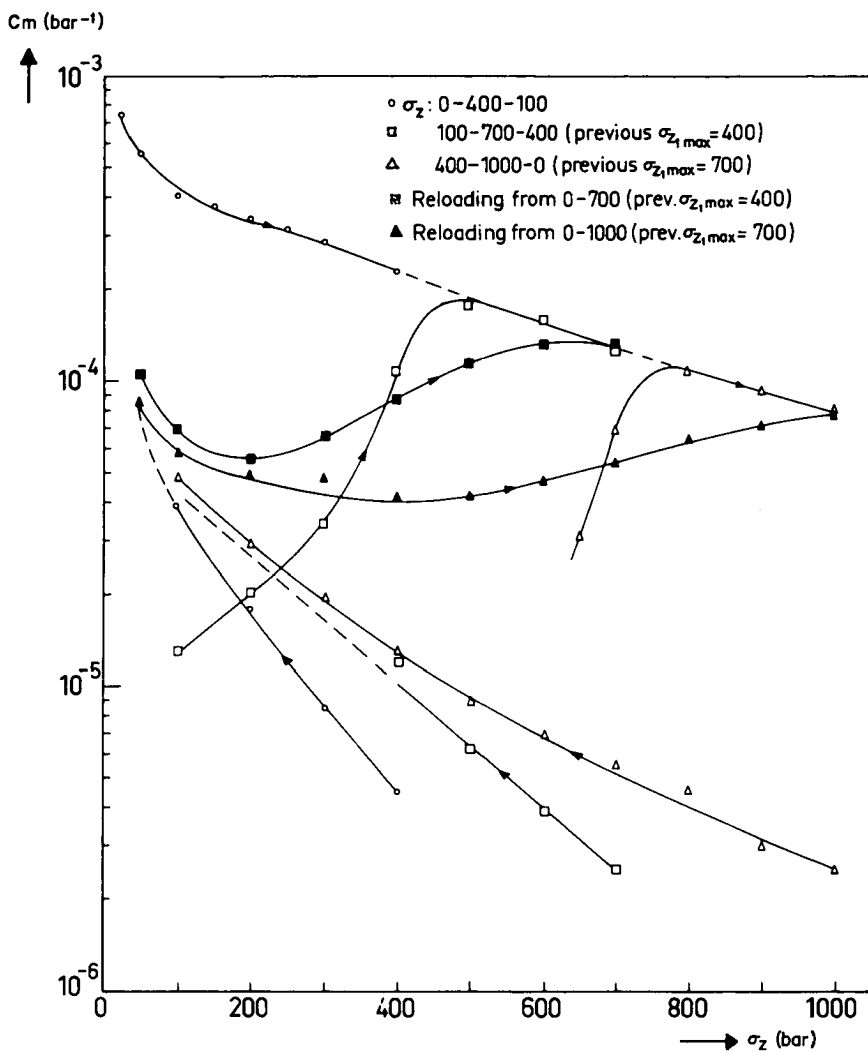
Horizontal axis: $\sigma_z \ (bar)$

FIG.11 UNIAXIAL COMPRESSIBILITY OF WATER-SATURATED, RESEDIMENTED POST-EOCENE BOLIVAR COAST SAND FOR VARIOUS LOADING HISTORIES (AFTER MESS,1978)

41

4.6 Effects of the in-situ stress state

In general uniaxial compressibility measurements are carried out by increasing the axial load on a cylindrical sample, while adjusting the lateral stress to keep the lateral strain zero during the complete loading cycle. In the reservoir, lateral strains will also be small due to the prevailing boundary conditions, but only during the (geologically very short) depletion period. Hence the in-situ lateral stress at the start of the production depletion can in principle be quite different from that measured in the laboratory at the corresponding vertical stress (e.g. as a result of tectonic movements over geological time or as a result of thermal stresses caused by temperature changes during the burial process).

Under the assumption of linear elasticity however, this should not influence the compressibility during subsequent uniaxial compaction as a result of production. In addition, in-situ horizontal stress levels in most reservoirs have been found to be quite comparable to those derived from uniaxial compaction experiments (Breckels and van Eekelen, 1981). Investigation of the possible effects of the in-situ stress state was therefore not considered to be very important and measurements were not continued after some scouting work.

4.7 Loading rate effects

The loading rate in the field is quite different from that applied in the laboratory. In the field, the reservoir rock is loaded very slowly during geological times (geological loading rate). This is followed by a much faster further loading during the production period (depletional loading rate). In the laboratory, a constant loading rate is usually applied (laboratory loading rate), which from a practical point of view has to be even considerably higher than the depletional loading rate.

Teeuw (1973) showed that the applied laboratory loading rate had some influence on the measured uniaxial compressibility of artificially sedimented sand packs. As can be seen in Fig. 12, the effect is rather small. Based on these results it had therefore been concluded that the difference between the average laboratory and the average depletion loading rate could result in an underestimate of at most 10 percent of the uniaxial compressibility. This effect was considered not very significant at the time.

The fact that the loading rate in the field is suddenly increased

Compaction, % of height at 260 bar

Vertical pressure, bar

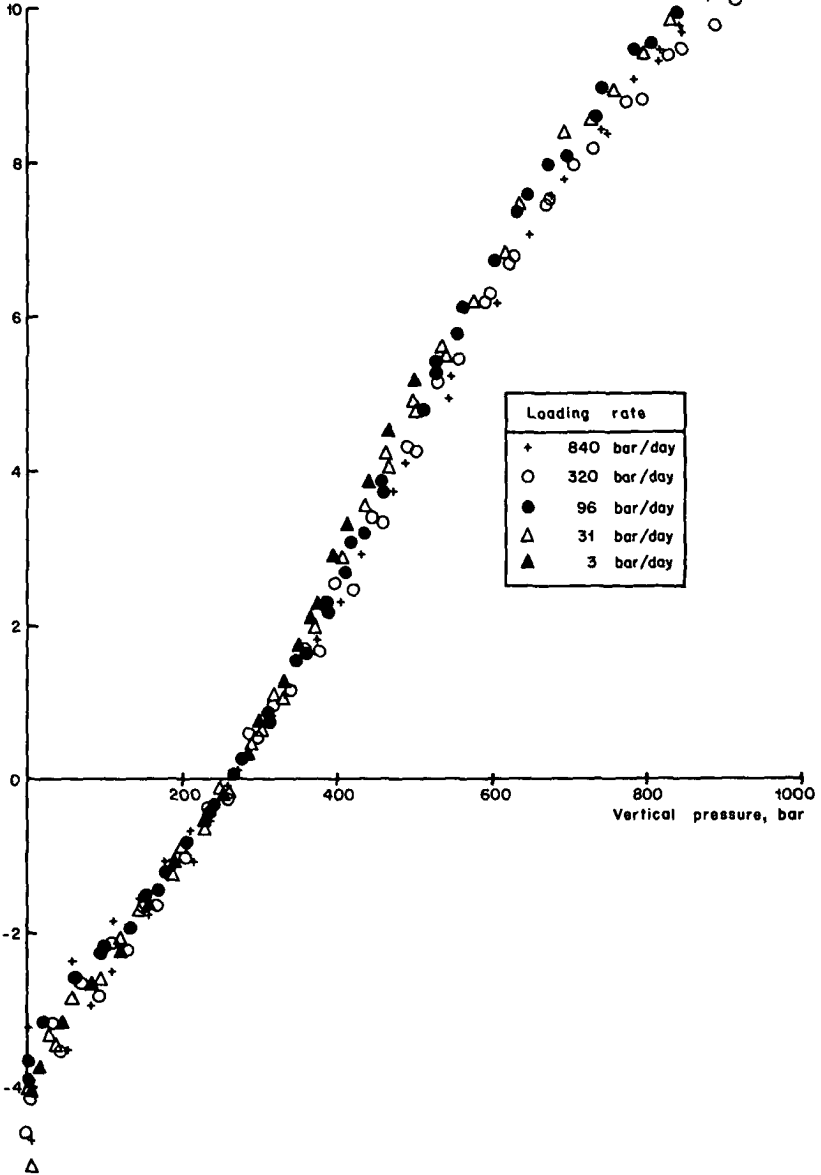| Loading	rate
+	840 bar/day
O	320 bar/day
●	96 bar/day
△	31 bar/day
▲	3 bar/day

FIG.12 RELATIVE COMPACTION OF
ARTIFICIAL SAND PACKINGS
MEASURED AT DIFFERENT LOADING
RATES
(AFTER TEEUW,1973)

tremendously upon the start of production (by up to six to seven orders of magnitude) was apparently not realised before (except very recently by Martin and Serdengecti, 1984) and hence its effect was never studied in depth. It was decided to investigate its possible influence in detail by uniaxial compaction experiments in which the loading rate is suddenly changed within a loading cycle (and at various stress levels). The detailed results of these experiments, are given in Appendix A and are extensively discussed in sections 6 - 10. On the basis of these results it is now understood that the observed discrepancies between predicted and observed field behaviour are due to rate effects.

4.8 Influence of pressure lags

Initially, it was considered possible that the field observed transition zones could be due to pressure lag effects between high and low permeability layers and/or parts in the reservoir as proposed by several authors (Domenico and Mifflin, 1965; Gambolati and Freeze, 1973; Helm, 1975, 1976, 1984; Schenk and Puig, 1983). Pressure measurements would essentially "see" the pressure in the most permeable layers, while compressibility later apparently increases when the pore pressure also starts to drop in the low permeability layers.

A separate study has been carried out to investigate the importance of such pressure lag effects. Resulting model calculations showed that the maximum non-linearities than can be caused by pressure lags are to weak to explain the observed non-linear field behaviour (Smits and de Waal).

5. EXPERIMENTAL PROGRAMME, EQUIPMENT AND PROCEDURES

5.1 TYPES OF EXPERIMENTS

The following types of uniaxial compaction experiments have been carried out:

1. Compaction at constant stress (creep).
2. Compaction during loading after an interruption period at constant stress, i.e. compaction upon reassumption of loading after creep.
3. Compaction during reloading after partial or complete unloading.
4. Compaction during experiments in which the loading rate was suddenly changed.
5. Compaction during reloading after sample manipulation (sawing, drilling, cutting and remounting).
6. One uniaxial compaction experiment at elevated temperature.

5.2 Sample selection

The above types of experiments were carried out on the following unconsolidated and consolidated materials:

1. Artificially sedimented sand packs of 170 μm and 450 μm quartz grains.
2. Core samples from a reservoir to be denoted here as reservoir A (mainly unconsolidated silty sands, North American continent, depth around 1000 m). The core material was drilled with a plastic sleeve inner barrel, frozen at the well site, and kept frozen until the start of the laboratory experiments.
3. Core samples from a reservoir to be denoted here as reservoir B (unconsolidated sands and silts, Far East, depth around 600 m). The core was drilled with the rubber sleeve coring technique.
4. Remoulded core samples. These were obtained by re-sedimenting the grains of some of the above core samples after completion of the initial loading program to study the influence of extreme sample disturbance.
5. Artificially sedimented packs of 170 μm steel beads.
6. Artificially sedimented packs of fine-grained aluminium oxide powder.

7. Towards the end of the experimental programme, when improved laboratory equipment became available, a series of measurements was carried out on core samples from various Rotliegendes reservoirs (friable to well consolidated sandstones, Northern Europe, depths around 3000 m). Most of these samples originated from the Groningen gas field in the Netherlands.

5.3 Sample preparation

Reservoir samples were obtained by sawing discs of reservoir material from the core. Subsequently vertical cylindrical plugs were drilled from these discs. In the case of unconsolidated material this procedure was applied to frozen core material. The drill bit was then cooled with liquid nitrogen. An alternative procedure consisted of cutting the unconsolidated samples with a cylindrical knife, after the outer part of the disc had thawed. The plugs, with a diameter of 50.8 mm (2") and a height of approximately 25 mm, were then mounted in the (oedometer or triaxial) measuring cell after which the measuring programme was applied (allowing sufficient time for thawing in the case of unconsolidated samples). Reservoir samples were not cleaned, but compacted in "native state".

To obtain artificially sedimented packings of 170 μm and 450 μm sand and steel grains, use was made of a particle distributor (Wygall, 1963). Remoulded samples were sedimented with a funnel, as the grain size distribution of such samples is in general too large to successfully apply a particle distributor. Before testing, all artificially sedimented packings were partially saturated with tap water.

5.4 Experimental procedures

5.4.1 The oedometer compaction cell

Initially, the experimental programme was limited to unconsolidated materials: reservoir samples, remoulded reservoir samples and artificially sedimented sand packs. The advantage of these materials is that the experimental equipment required is rather simple, while the deformations to be studied are rather large. The majority of these experiments were carried out in an oedometer cell (Fig. 13). In this type of cell, the sample is compacted by increasing the vertical load by means of a piston. Lateral expansion of the sample is prevented by the rigid steel cylinder of the

LOAD

DIAL GAUGE

STEEL BALL

PISTON

O-RING

SAMPLE

PERMEABLE DISC

CYLINDER
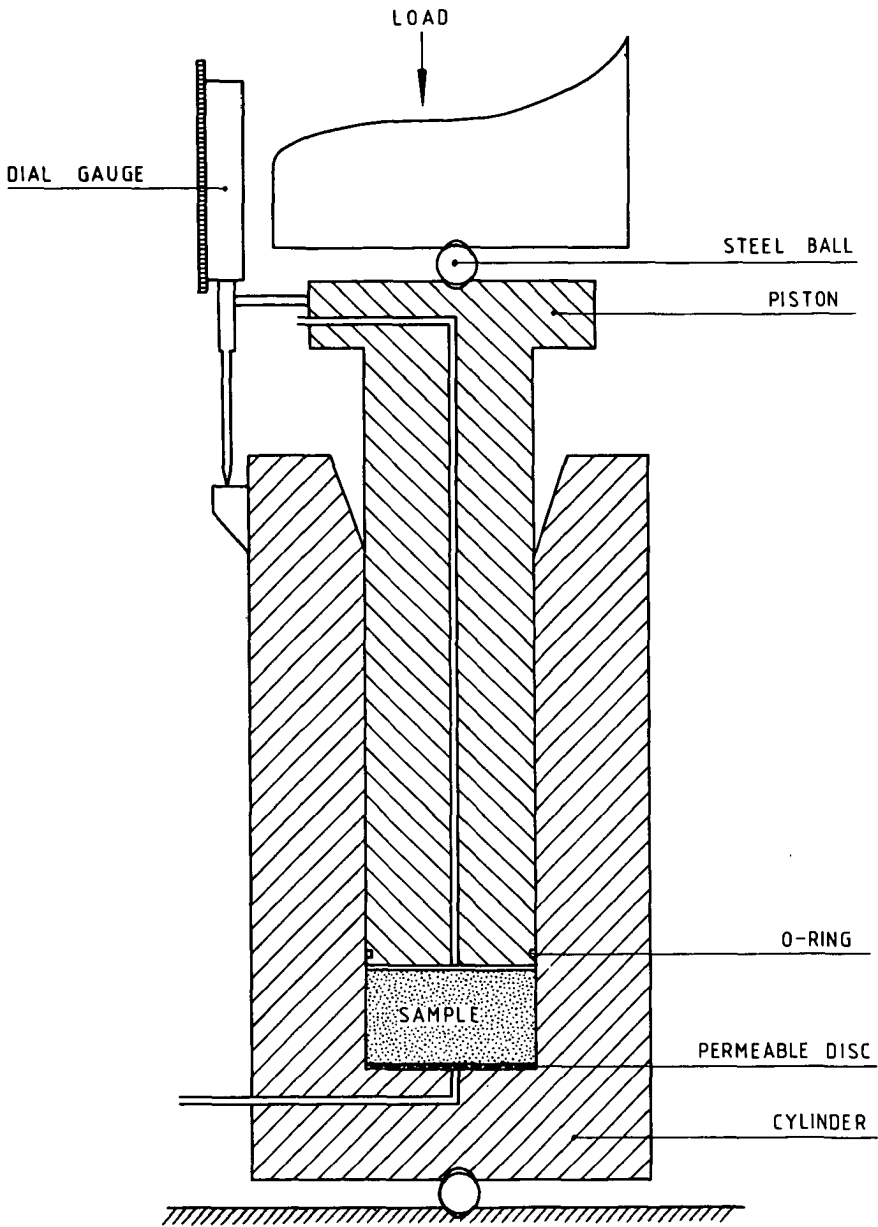
FIG.13 UNIAXIAL COMPACTION CELL
(OEDOMETER)

oedometer. Wall friction effects are kept within acceptable limits by using relatively thin samples. For two inch diameter plugs a maximum height of 25 mm can be used (Mess, 1978).

During the oedometer experiments, the axial deformation (measured with an electrical displacement transducer or LVDT) was recorded as a function of axial pressure (measured with an electrical pressure gauge) on an x-y recorder. Initially, stepwise loading was applied by means of an automated pressure build-up system. By changing the interval between subsequent steps a variety of loading rates could be applied, also allowing changes in loading rate within a loading cycle. During all these experiments the pore pressure was kept at an atmospheric level.

5.4.2 The triaxial compaction cell

At a later stage, more sophisticated equipment was developed consisting of new pressure build-up systems, and a computerised data acquisition and data reduction system, while the experimental programme was extended to friable and even well consolidated sandstones, for which improved triaxial compaction cells were constructed. The major improvement with respect to the old triaxial compaction cells (Teeuw, 1973) consists of the use of a radial displacement transducer as described below.

In the triaxial cell (Fig. 14), the sample is placed between two pistons which are used to apply the axial load (to a maximum of 1000 bar) which is supplied by an external load frame. Radial pressure (to a maximum of 350 bar) is applied via an impermeable viton sleeve surrounding the sample. The axial displacement is measured with two external LVDT's of which one is shown in Fig. 14. As a result a correction has to be applied for the piston deformation (Fig. 15). It was found that the piston deformation is different during a first and a second loading cycle. After a few days at zero pressure the piston shows first cycle behaviour again.

The radial displacement is measured with a radial displacement transducer (RDT). This transducer consists of an elastic metal strip, which is clamped on two buttons which are in direct contact with the sample (Fig. 16). By means of strain gauges on the metal strip, the radial displacement of the sample between the buttons can be measured (Fig. 17). The resolution of the radial displacement transducer is better than 1 μm. Calibration runs showed the influence of the radial pressure, which is felt by the transducer, to be small (Fig. 18). Electrical feedthroughs in the triaxial cell allow the RDT to be connected to the related electronic measuring equipment. Flow channels in the axial pistons allow the measurement of axial

AXIAL LOAD

AXIAL
DISPLACEMENT
TRANSDUCER

PORE-PRESSURE
INLET

RADIAL-PRESSURE
INLET

ACOUSTIC TRANSMITTER

SLEEVE
CORE SAMPLE

RADIAL
DISPLACEMENT
TRANSDUCER

PERMEABLE DISC

ACOUSTIC RECEIVER

ELECTRICAL
FEEDTHROUGH
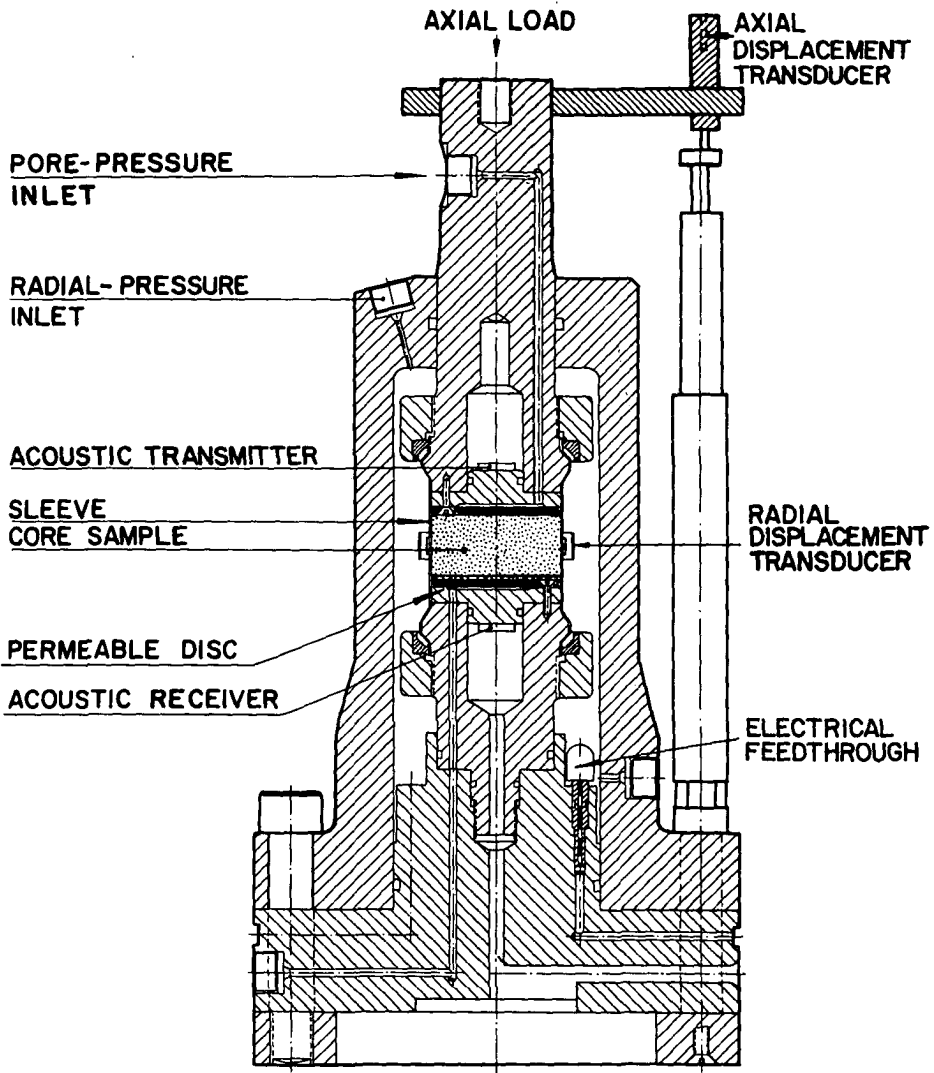
FIG.14 2'' TRIAXIAL COMPACTION CELL
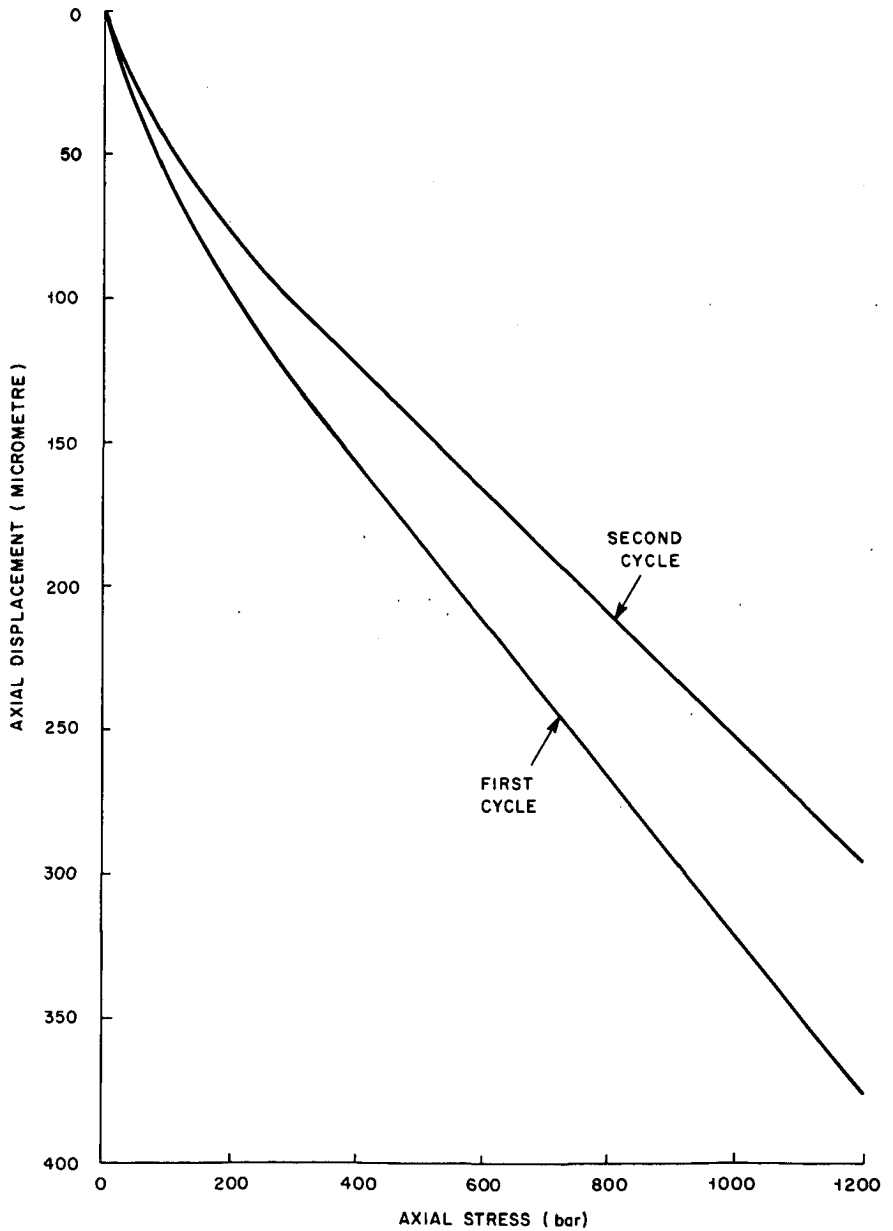
FIG.15 AXIAL CALIBRATION: APPARENT
AXIAL DISPLACEMENT DUE TO
DEFORMATION OF THE STEEL
PISTONS OF THE TRIAXIAL CELL
VERSUS AXIAL STRESS.

STRAIN GAUGES

ELASTOMER SLEEVE

SAMPLE

COPPER RING

PRESS-BUTTON
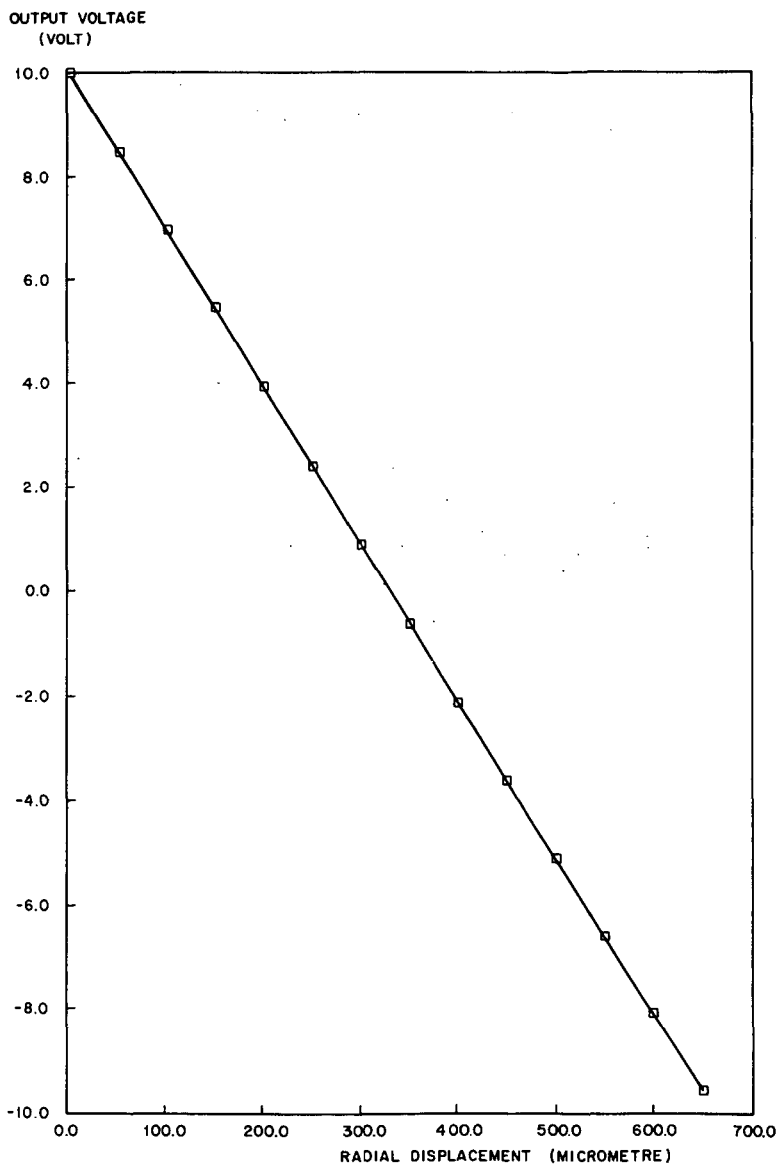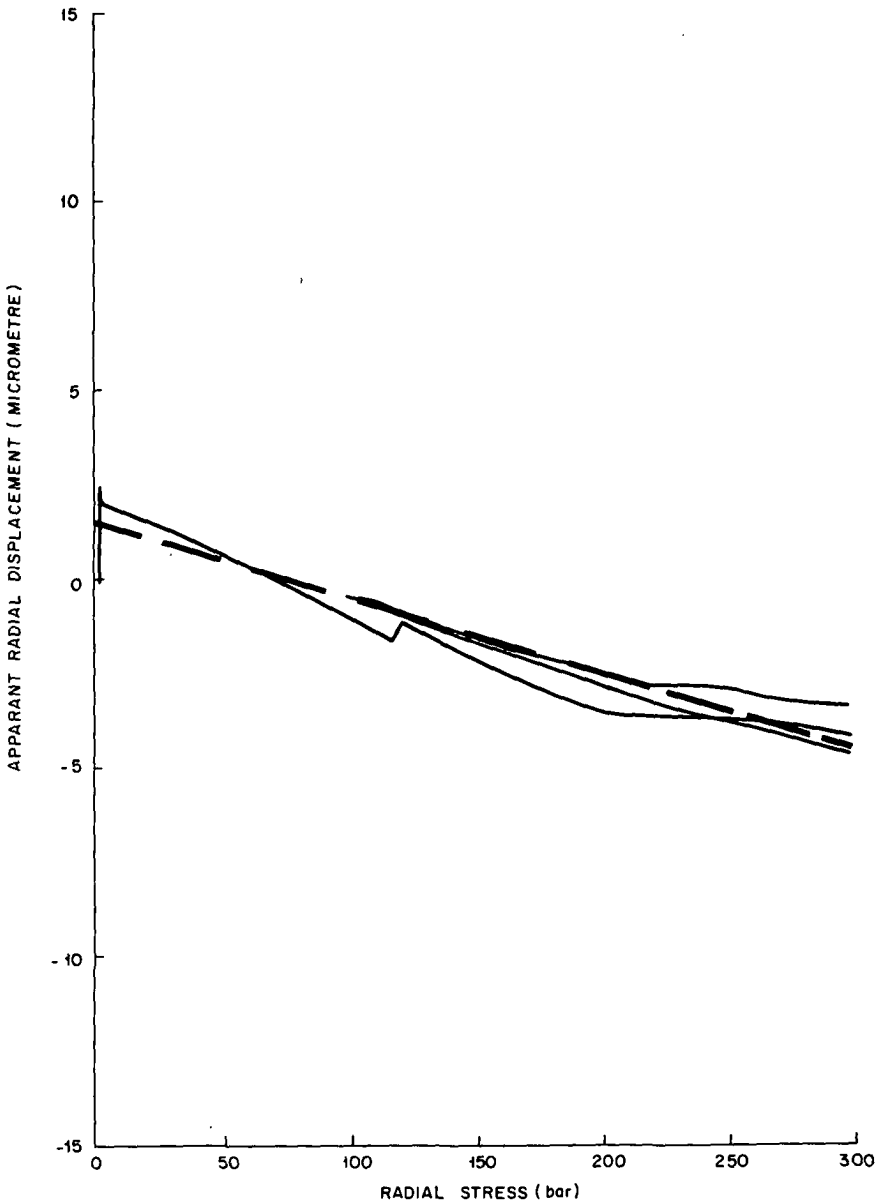
COUNTERWEIGHT
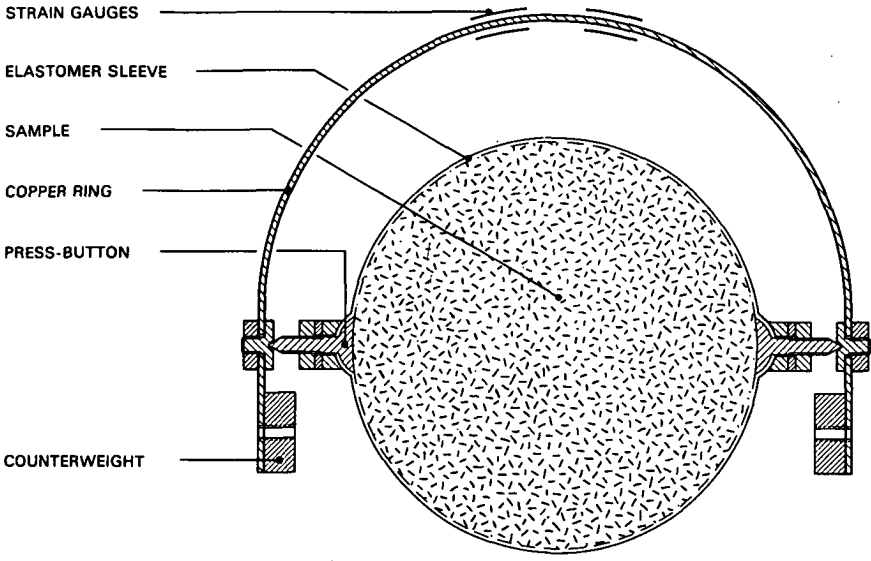
FIG.16 RADIAL DISPLACEMENT TRANSDUCER

FIG.17 CALIBRATION OF RADIAL
DISPLACEMENT TRANSDUCER

FIG.18 RADIAL CALIBRATION:
SENSITIVITY OF THE RADIAL
DISPLACEMENT TRANSDUCER TO THE
PRESSURE OF THE SURROUNDING OIL.

permeability during a compaction experiment, while acoustic transducers in the pistons allow the measurement of compressional and shear wave velocities.

5.4.3 Pressure build-up system

A schematic overview of the total pressure build-up system is shown in Fig. 19. The essential part of the pressure build-up system consists of stepping motor driven, high precision pressure regulators. These regulators were modified to obtain a very good linear relationship between outlet pressure and regulator knob rotation. The use of stepping motors allows a very large range of pressure build-up rates. The maximum pressure build-up rate is approximately 8000 bar/h. From a practical point of view, the lower limit is in the order of 1 bar/h. Therefore variations in loading rate can be applied over almost four orders of magnitude.

The axial load is measured with a load cell placed between the axial piston of the triaxial cell and the ram of the external load frame. Measurements showed the difference between the measured load and that actually applied on the sample during pressure build-up to be constant (independent of stress level and loading rate) and less than a few bar. Hysteresis is less than 6 bar. Radial pressure is measured with a commercial high precision electric pressure gauge, calibrated against a dead-weight pressure gauge.

5.4.4 Data acquisition system

The following parameters are measured:
1. axial load
2. axial pressure
3. radial pressure
4. pore pressure
5. axial pressure build-up rate
6. radial pressure build-up rate
7. pore pressure build-up rate
8. axial deformation
9. radial deformation.

Using signal conditioners, all the electrical signals from the transducers corresponding to these parameters are brought in a 0-10V range, after which they are fed into A/D converters. These in their turn are connected to a HP9825 desktop controller. A schematic diagram of the data

FIG.19 PRESSURE BUILD-UP SYSTEM

AXIAL STRESS
RADIAL STRESS

10V

VCO

MOTOR CONTROL

M

400 bar

VCO

MOTOR CONTROL

M

400 bar

8V

± 2V

BRIDGE AMPLIFIER

RDT IN

10V
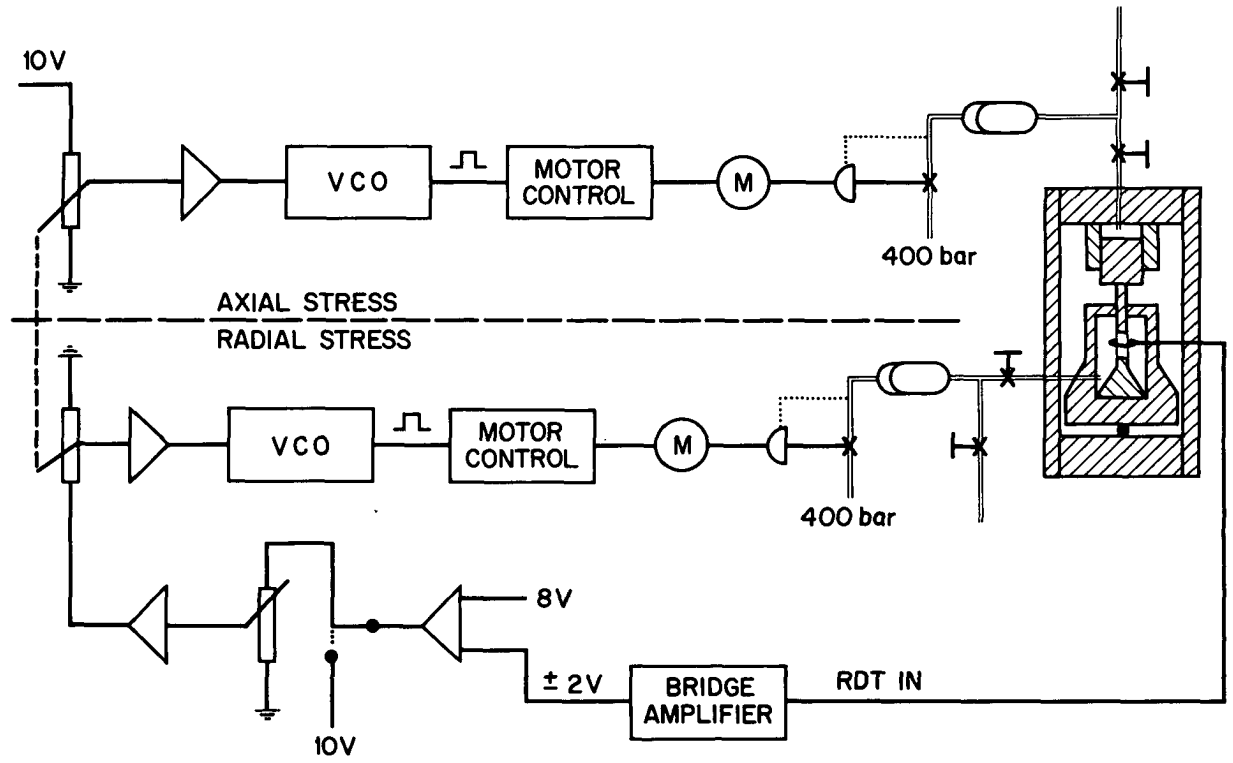
acquisition system is shown in Fig. 20. A data acquisition programme was written for the HP9825 controller allowing:

1. Calibration and definition of the various signals.

2. Measurement of a selected set of up to 28 transducers as a function of time at a given scan rate.

3. Measurement of the selected set of transducers at given increments of the variable measured by one of these transducers (e.g. the axial load).

4. Input of up to 10 manually measured parameters (e.g. permeability and acoustic travel time) and comments.

5. Printing of (a subset of) the measured data during the experiment.

6. Storage of the acquired data on tape.

7. Generation of alarm signals when one of the signals of a pre-selected set of transducers reaches a value outside pre-defined upper or lower boundaries.

8. Changing the set of scanned transducers, scan rate, alarm boundaries etc. during the experiment.

9. Transfer of the acquired data to a mainframe computer after finalising an experiment.

10. Automatic adjustment of the radial pressure build-up rate to keep the radial displacement zero.

For the mainframe computer, software was developed to generate tabulations and plots of the experimental data (including corrections, smoothing, derivatives etc.).

FIG.20 DATA ACQUISITION SYSTEM

UNIVAC / VAX

PDP 11/70

2400 BAUD

HP 98035 CLOCK

HP 9825 CENTRAL PROCESSOR

HP 9878 I/O EXPANDER

MAX.28 TRANSDUCERS

PCS A/D CONVERTERS

VALIDYNE SIGNAL CONDITIONERS

TI SILENT 700 PRINTER

KEYBOARD

CASSETTE TAPE

DISPLAY

STRIP PRINTER

DEVICES INTERNAL TO HP 9825
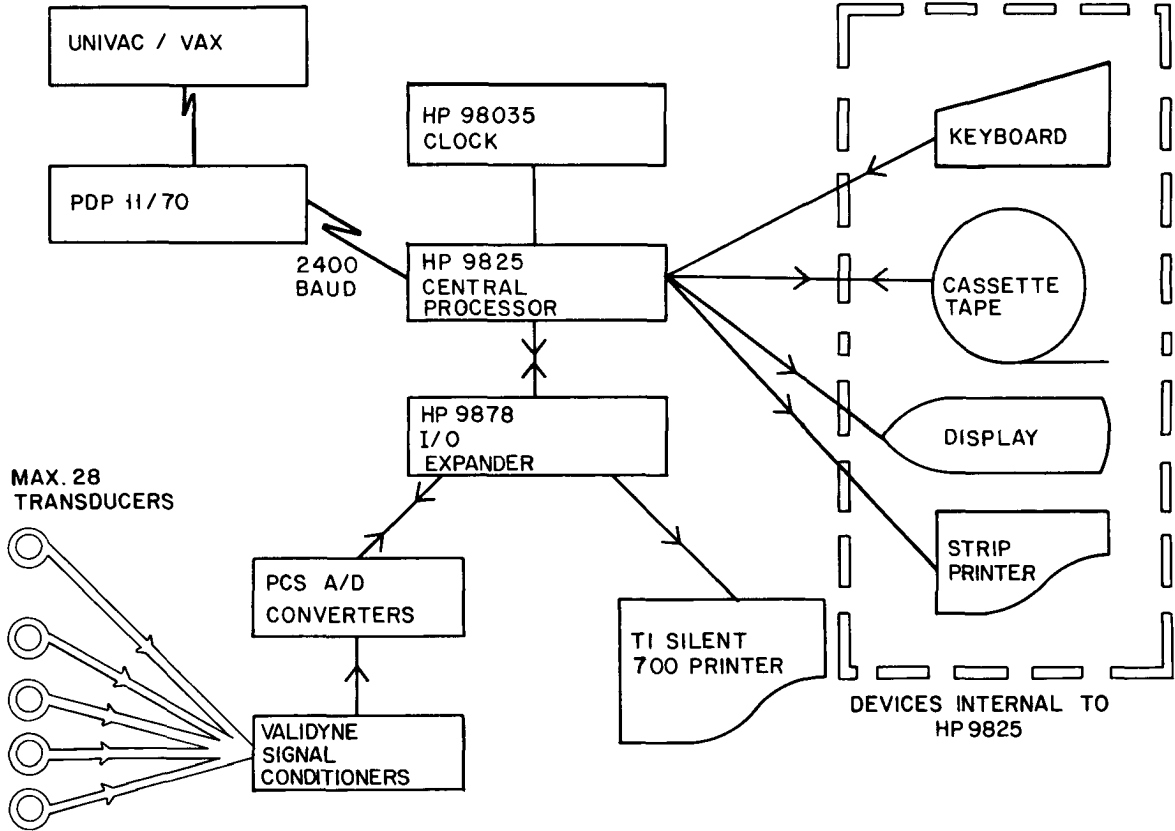
6. EXPERIMENTAL RESULTS

The results obtained during the experiments on unconsolidated sands are given in detail in Table A1 and Figs. A1-A14 of Appendix A. The rate type compaction model, discussed in section 7, was originally developed on the basis of these data. At a later stage the experimental programme was extended to consolidated sandstones, confirming the applicability of the model for friable and consolidated sandstones and resulting in refinement of the model. As an example of such data, results obtained on wells EKL-12 and ZDP-12 of the Groningen gas field are given in Tables A2-A4. It has been found that the compaction behaviour of all samples (both consolidated and unconsolidated) in the various experiments is qualitatively very similar giving the following results:

1. Compaction curves at different but constant loading rates appear to form a fan of lines (dashed curves in Fig. 21, further referred to as "virgin" compaction curves). The lower the loading rate, the more the sample will be compacted at a given stress level. The compressibility along the virgin compaction curves (i.e. the slope of the compactin curves) will from here on be denoted by $c_{m,o}$.

2. The shifts $\Delta\sigma_z$ between compaction curves for different constant loading rates $\dot{\sigma}_z$ are quite systematic and related to stress level, and can be described with good accuracy by the empirical equation (see also Fig. 22):

$$\Delta\sigma_z = \sigma_{z,1}[(\dot{\sigma}_{z,2}/\dot{\sigma}_{z,1})^b - 1] \tag{6.1}$$

    where b is a material constant which depends on rock type (see Table 6.1).

3. Every time the loading rate is suddenly increased within a loading cycle, a compaction curve like A'-B' or B-C in Fig. 21 will result. A sudden decrease in loading rate will result in a compaction curve like A-B (also see Figs. A1-A7, A9-A11, A13-A15). In both cases the resulting compaction curve will finally reach the virgin compaction curve corresponding to continuous loading at the new loading rate. The width of the transition zone can be considerable. During the experimental program, transition zones of up to 80 bar have been measured (see Fig. A5).

4. Interruption of loading ($\dot{\sigma}_z = 0$, resulting in constant load) is

A   DECREASE IN LOADING RATE $\dot{\sigma}z = \dot{\sigma}z,3$
B   INCREASE IN LOADING RATE $\dot{\sigma}z = \dot{\sigma}z,4$
C   INTERRUPTION OF LOADING $\dot{\sigma}z = 0$
D   RE-START OF LOADING $\dot{\sigma}z = \dot{\sigma}z,3$

Δh

A'
B'
A
C'
B
E'
C
D'
F'
D

$\dot{\sigma}_z = \dot{\sigma}_{z,4}$

$\dot{\sigma}_z = \dot{\sigma}_{z,1}$

A'   INCREASE IN LOADING RATE $\dot{\sigma}z = \dot{\sigma}z,2$
B'   INTERRUPTION OF LOADING $\dot{\sigma}z = 0$
C'   RE-START OF LOADING $\dot{\sigma}z = \dot{\sigma}z,2$
D'   PARTIAL UNLOADING
E'   RELOADING $\dot{\sigma}z = \dot{\sigma}z,2$

E

$\dot{\sigma}_z = \dot{\sigma}_{z,3}$

$\dot{\sigma}_{z,4} > \dot{\sigma}_{z,3} > \dot{\sigma}_{z,2} > \dot{\sigma}_{z,1}$

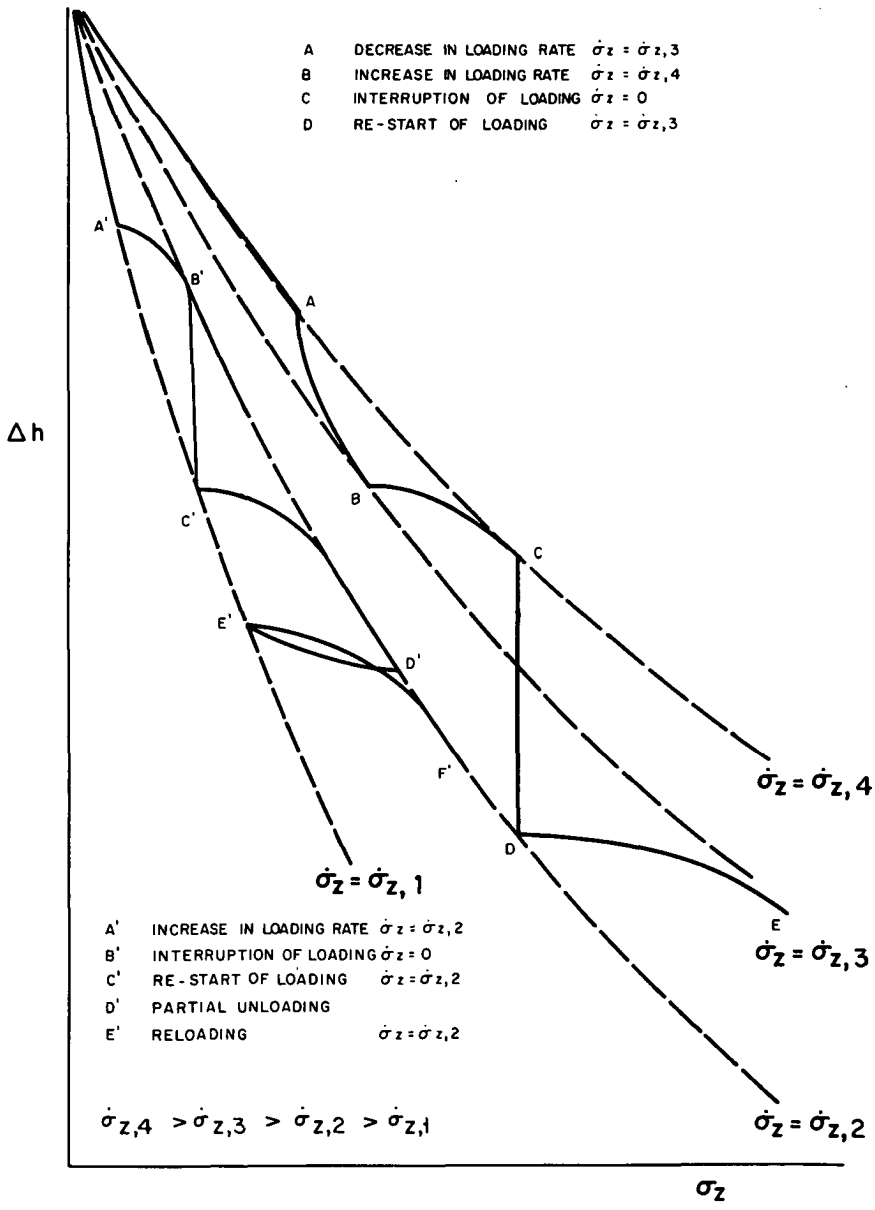$\dot{\sigma}_z = \dot{\sigma}_{z,2}$

σ_z

FIG.21 CONDENSED PICTURE OF
COMPACTION BEHAVIOUR

followed by creep (C-D and B'-C' in Fig. 21, see also Figs. A7, A9 and A10). When loading is re-assumed (which corresponds to an increase in loading rate), the sample shows a compaction behaviour similar to that after an increase in loading rate (D-E and C'-D' in Fig. 21. If the loading rates applied before and after the interruption are equal, the virgin compaction curve followed before the interruption is again reached (B'-D' in Fig. 21). If these loading rates are different, the virgin compaction curve corresponding to the new loading rate is reached after the transition zone (e.g. from A-C to B-E in Fig. 21).

5. The compaction behaviour during reloading after partial unloading (previously studied by Mess (1978)), strongly resembles that observed after constant loading (creep) or after an increase in loading rate (E'-F' in Fig. 21, see also Figs. A4, A5, A7-A10, A12 and A14). For larger amounts of unloading, a different compaction behaviour results which will be discussed in some more detail in section 9.2, but which is not important within the scope of this thesis.

6. The behaviour described above has a large influence on the uniaxial compressibility c_m, which is directly related to the slope of the curve of Δh versus σ_z according to:

$$c_m = (1 - \beta) \frac{1}{h(\sigma_z)} \left(-\frac{dh(\sigma_z)}{d\sigma_z} \right)_{\epsilon_r = 0, \ \Delta p = 0} \qquad (6.2)$$

where

$h(\sigma_z)$	=	sample height at axial stress σ_z
ϵ_r	=	radial strain (compression positive)
ϵ_z	=	axial strain (compression positive)
p	=	pore pressure
β	=	$c_r / c_{b,o}$

E.g. when the loading rate is increased, the uniaxial compressibility initially becomes much lower but later it increases again. Conversely when the loading rate is decreased, the uniaxial compressibility initially becomes much higher.

7. No differences with respect to the above findings were found between the compaction behaviour of artificially sedimented sand packs, and that of consolidated and unconsolidated (original and remoulded) reservoir samples.

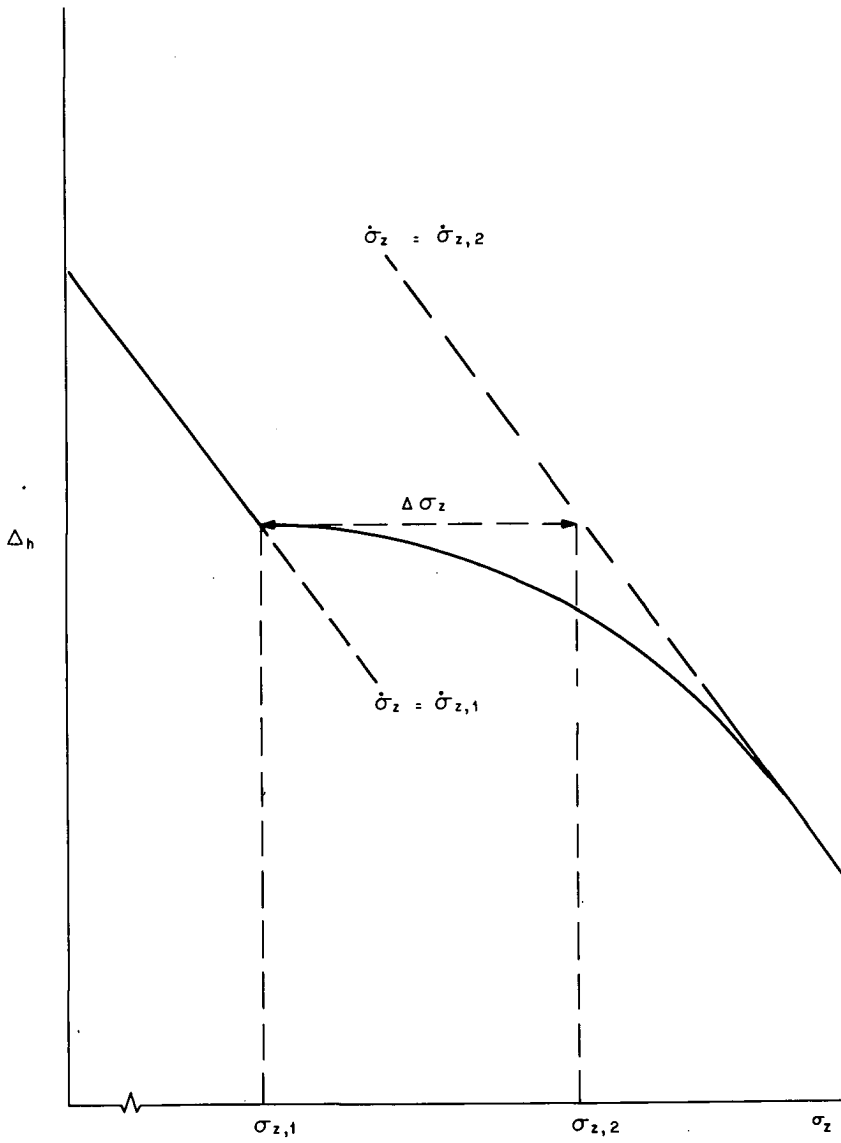8. The compaction behaviour after an arbitrary loading history is restored

FIG.22 DEFINITION OF $\Delta \sigma_z$, $\sigma_{z,1}$ AND $\sigma_{z,2}$

to first cycle behaviour by not too large a mechanical disturbance e.g. as encountered during the coring process and sample preparation procedures (see section 4.3).

9.   No major differences were found between the compaction behaviour at 20 degrees C and that in an experiment at 90 degrees C (see section 7.3.2).

Table 6.1   Laboratory measured b-values

Rock type	$c_{m,o}(10^{-5}$ bar$^{-1})$	b
Well consolidated sandstones	< 1	< 0.010
Consolidated sandstones	1 - 5	010 - 0.018
Unconsolidated sandstones	10 - 40	018 - 0.022
Steel beads	1	0.005
Aluminium powder	5	0.005

---

7. THE RATE TYPE COMPACTION MODEL

7.1 The general compaction curve

The transition curves resulting upon reassumption of loading after creep, upon an increase in loading rate and upon reloading after partial unloading have a similar shape and position relative to the constant loading rate compaction curve that is finally reached. This even holds for experiments carried out at different stress levels and on different samples. This suggests that all transition curves can perhaps be described by one general compaction curve after application of an appropriate normalisation procedure, using the compaction curve finally reached as a reference.

Such a normalisation procedure has indeed been found. The axial stress σ_z is divided by a normalising stress $\sigma_{z,o}$, which is related to the stress level. It is determined by the intersection point of the transition curve and a line defined by $\sigma_z'(\epsilon_z) = 0.9\,\sigma_z(\epsilon_z)$ (see Fig. 23). In the case of the virgin line being curved, the auxiliary line is constructed relative to a straight line approximation of the virgin line finally reached. This particular definition has been chosen for reasons of convenience, but could in principle be replaced by any other, yielding a point with a fixed orientation relative to the virgin compaction curve that is finally reached.

The axial displacement ϵ_z' (arbitrarily taken zero at $\sigma_{z,o}$) is divided by $\sigma_{z,o}$ and by the uniaxial compressibility $c_{m,o}$ of the virgin compaction curve finally reached. As a result of this normalising procedure, a dimensionless plot of $\epsilon_z'/(c_{m,o}\sigma_{z,o})$ versus $\sigma_z/\sigma_{z,o}$ is obtained in which the virgin compaction curve finally reached is represented by a straight line with slope unity (by definition).

In Figs. 24-31, the normalised transition curves resulting from loading (at constant rate) after creep, after increases in loading rate and after partial unloading at various stress levels and for various sandstones are compared. All the curves have been normalised according to the above procedure. The resulting normalised compaction curves combine into one general compaction curve (solid line in Figs. 24-31).
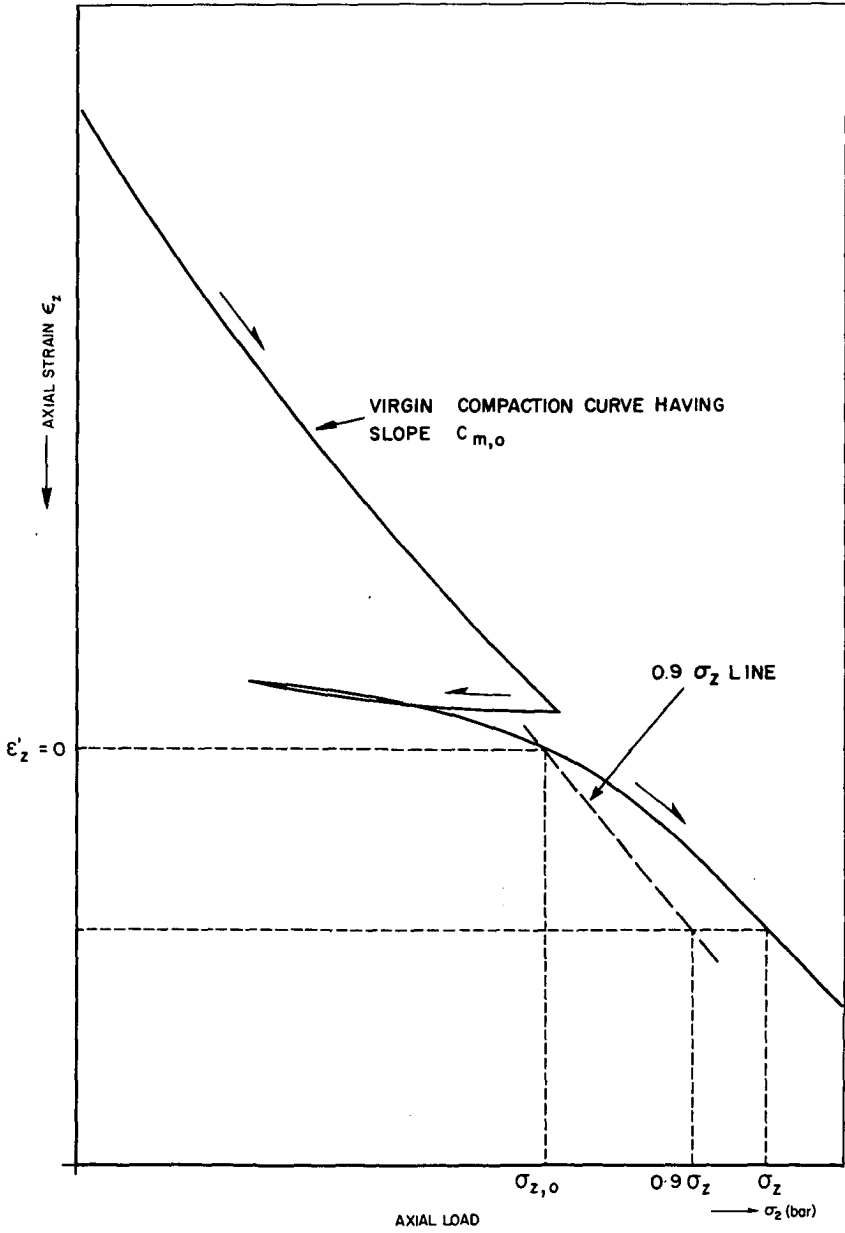
FIG.23 DETERMINATION OF $\sigma_{z,0}$ ON
LABORATORY-MEASURED TRANSITION
CURVE

FIG.24 COMPARISON BETWEEN
GENERAL COMPACTION CURVE AND
LABORATORY DATA (EXPERIMENT 3,
SEE FIG.A4)

FIG.25 COMPARISON BETWEEN
GENERAL COMPACTION CURVE AND
LABORATORY DATA (EXPERIMENT 3,
SEE FIG.A5)

FIG.26 COMPARISON BETWEEN
GENERAL COMPACTION CURVE AND
LABORATORY DATA (EXPERIMENT 3,
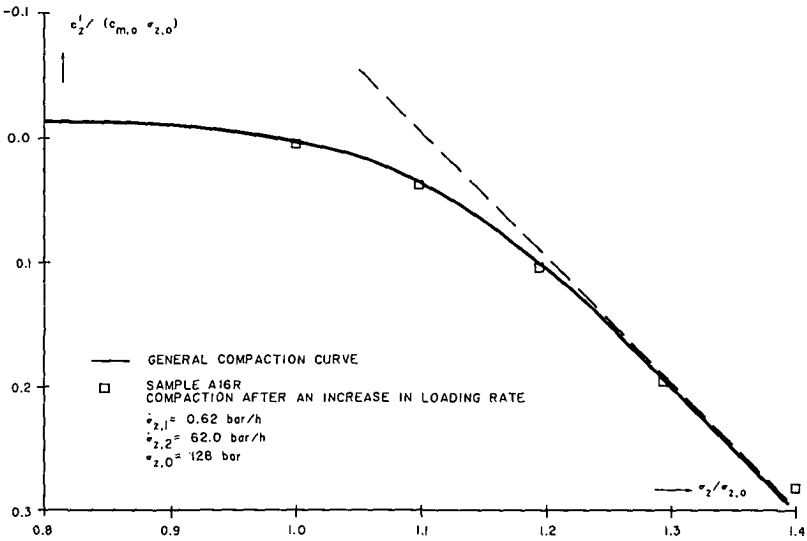SEE FIG.A4)

FIG.27 COMPARISON BETWEEN
GENERAL COMPACTION CURVE AND
LABORATORY DATA (EXPERIMENT 6,
SEE FIG.A7)

FIG.28 COMPARISON BETWEEN
GENERAL COMPACTION CURVE AND
LABORATORY DATA (EXPERIMENT 6,
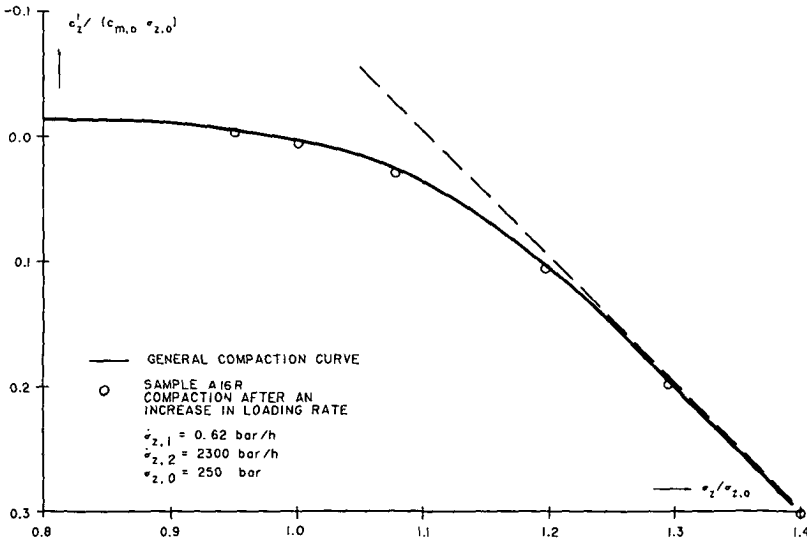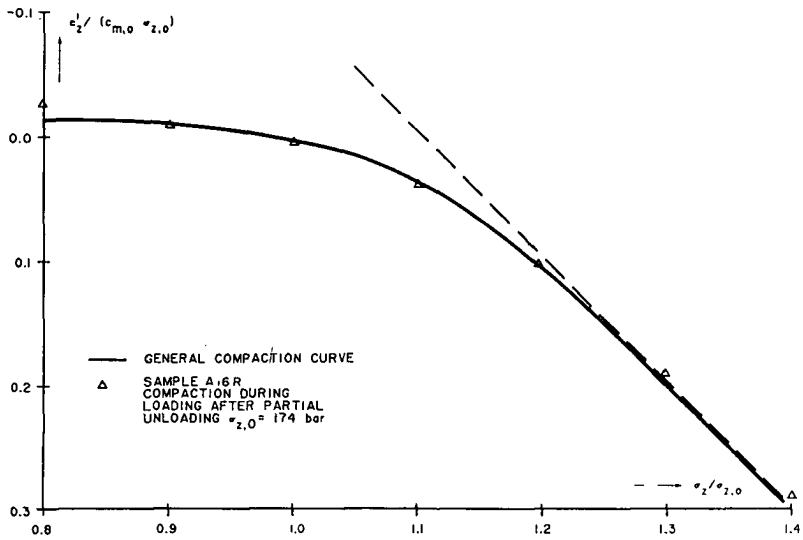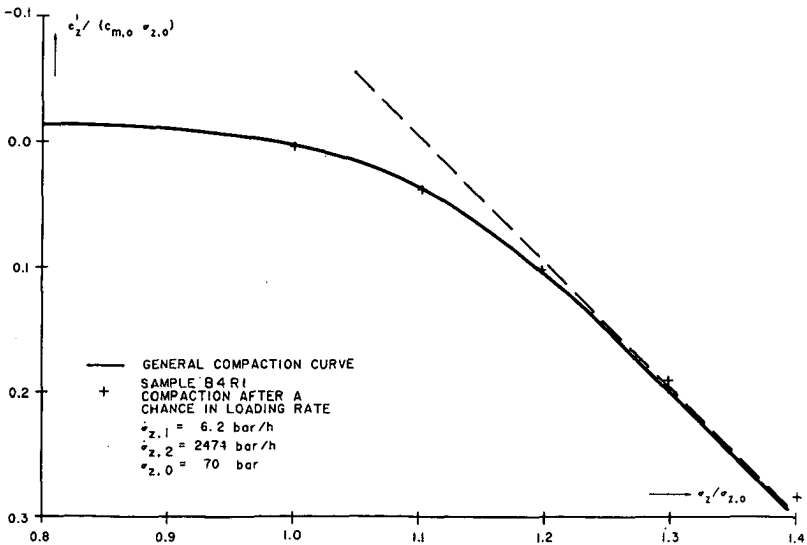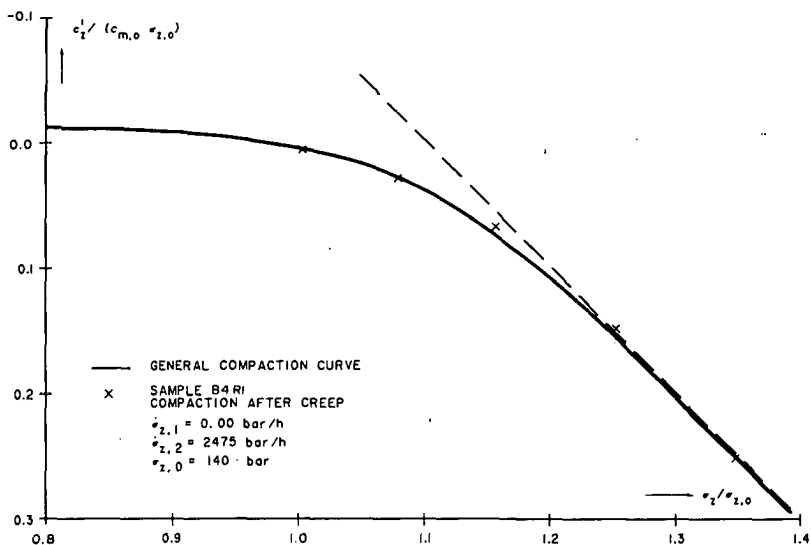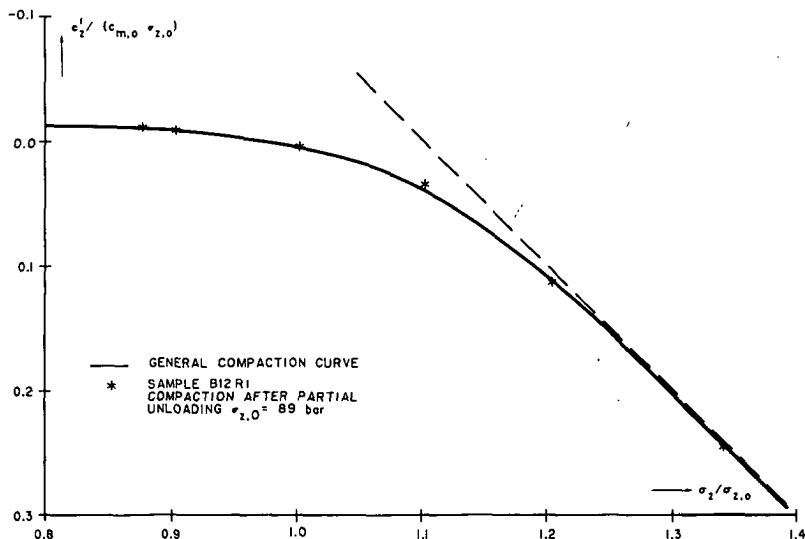SEE FIG.A7)

FIG.29 COMPARISON BETWEEN
GENERAL COMPACTION CURVE AND
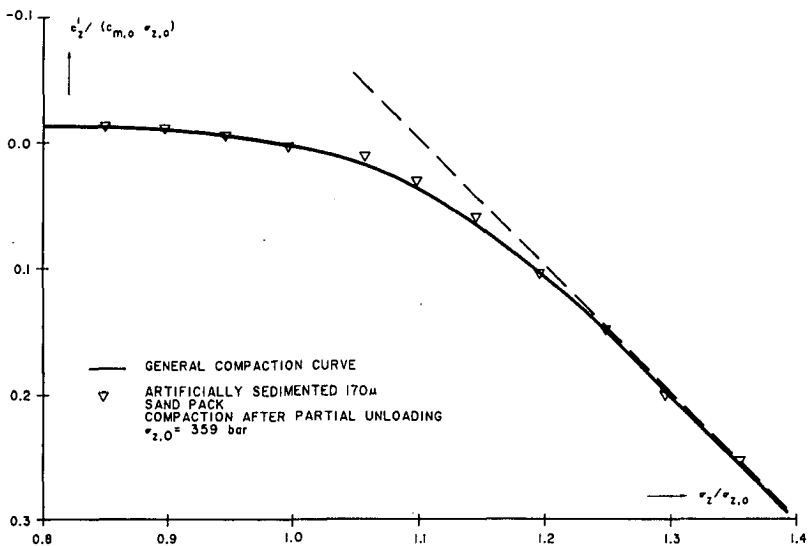LABORATORY DATA (EXPERIMENT 13,
SEE FIG.A8)

FIG.30 COMPARISON BETWEEN GENERAL COMPACTION CURVE AND LABORATORY DATA (EXPERIMENT 22, SEE FIG.A12)
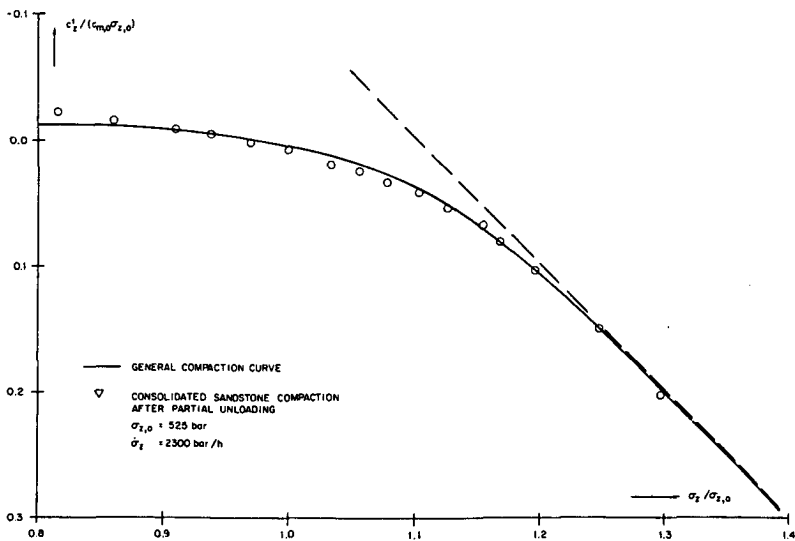

FIG.31 COMPARISON BETWEEN GENERAL COMPACTION CURVE AND LABORATORY DATA

The following algebraic fit describes this general compaction curve with sufficient accuracy:

For x < 0.80: $H(x) = - 0.010$

For x > 0.80: $H(x) = - 0.010 + g(U)*2.969*U^{3.48} +$
$$[1 - g(U)]*(U - 0.30)$$

with: $x = \sigma_z/\sigma_{z,o}$

$U = x - 0.80$

and: $g(U) = e^{-(U/0.43)^{7.58}}$ (7.1)

For a specific experiment, the position of the normalised starting point on this curve is a function of the specific change in loading rate (see equation (6.1)), or of the amount of unloading or creep.

Conversely, this general compaction curve in combination with equation (6.1) can be used to predict the compaction behaviour upon arbitrary increases in loading rate (see sections 9 and 10).

7.2 Conceptual model

The compaction behaviour described in the previous sections resulted in the following conceptual model:

1. When a sample is loaded at a constant loading rate $\dot{\sigma}_z$ starting from an initial point B (see Fig. 32), the compaction behaviour (dashed line) is completely determined by the material constants $c_{m,o}$ and b and the position of B relative to the virgin compaction line corresponding to $\dot{\sigma}_z$. Consequently, it does not matter how point B was arrived at, e.g. as a result of a different loading rate (circles), creep after interruption of loading (squares) or partial unloading (crosses).

2. The position of the virgin compaction line which is finally reached depends only on $\dot{\sigma}_z$, and is independent of the previous stress-strain history. It appears as if this previous history is swept out. This is known in soil mechanics as S.O.M. (Swept Out of Memory, Goldscheider, 1972; Gudehus, 1977).

The above properties are very similar to those of a certain class of
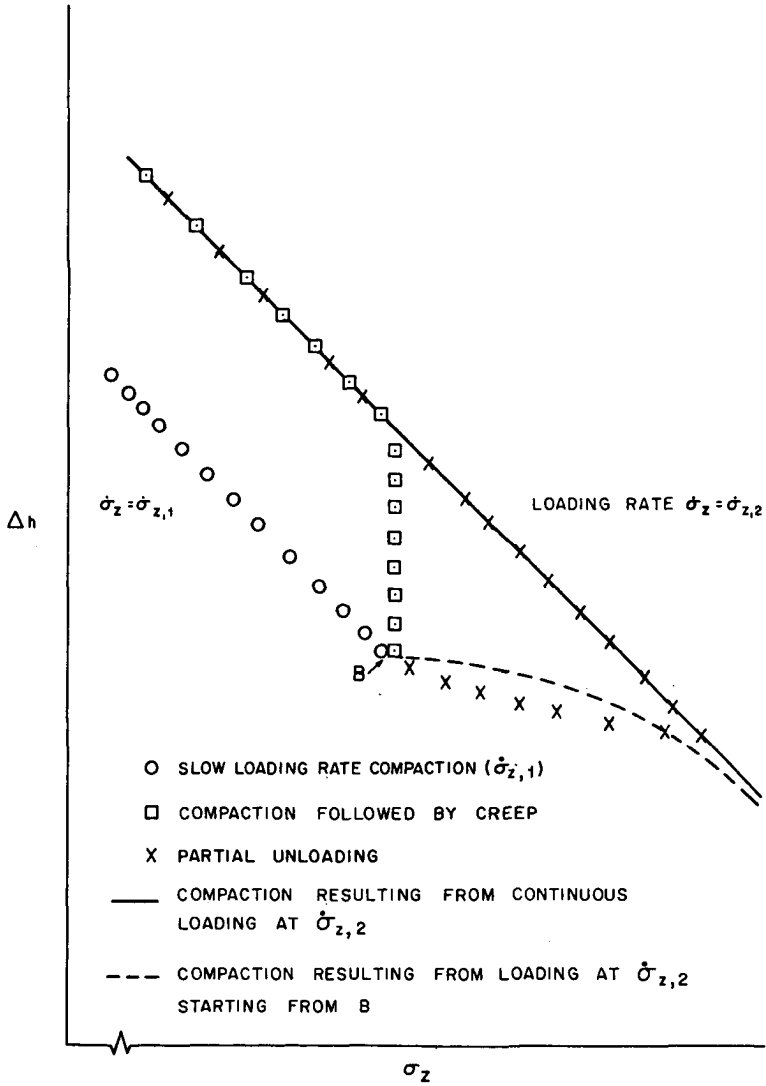
FIG.32 GENERALISED CONCEPTUAL MODEL

materials referred to as being "of the rate type" (Truesdell and Noll, 1965). Examples in the field of soil mechanics are discussed in (Bjerrum, 1967), (Leinenkugel, 1976) and (Leroueil, 1985), while logarithmic creep behaviour of clays was already observed much earlier (Keverling Buisman, 1936). It should be noted that the properties of rate type materials can not be explained by Maxwell models (systems composed of springs, dash pots etc., as for such models the deformation behaviour depends not only on the actual stress/strain state, but also on the previous stress-strain history (Jaeger and Cook, 1969; Kolymbas, 1978). As a result, the latter stress/strain history can not be "swept out" relatively fast by a sufficient amount of constant loading rate stressing.

7.3 Mathematical description

It has been found that mathematical equations properly describing the compaction behaviour discussed in section 6 can be derived from an empirical constitutive equation proposed to describe the stress-strain behaviour of rate type materials (Kolymbas, 1978, 1984; Gudehus and Kolymbas, 1979):

$$\dot{\sigma}_{ij} = h\ (\sigma_{ij},\ \dot{\epsilon}_{ij}) + g\ (\dot{\epsilon}_{ij},\ \dot{\epsilon}_{ij}^{\cdot}) \qquad\qquad (7.2)$$

where

h and g	=	isotropic tensor functions
σ_{ij}	=	stress tensor
ϵ_{ij}	=	strain tensor

The tensor function $h(\sigma_{ij},\ \dot{\epsilon}_{ij})$ describes the loading rate independent part of the material behaviour in terms of σ_{ij} and $\dot{\epsilon}_{ij}$. Rate effects are introduced only by $g(\dot{\epsilon}_{ij},\ \dot{\epsilon}_{ij}^{\cdot})$. Kolymbas suggested:

$$g(\dot{\epsilon}_{ij},\ \dot{\epsilon}_{ij}^{\cdot}) = \frac{B}{\sqrt{[\ C_1^{\ 2} + 1/2\ Tr(\dot{\epsilon}_{ij}^{\ 2})]}}\ \dot{\epsilon}_{ij}^{\cdot} \qquad\qquad (7.3)$$

where

$Tr(\dot{\epsilon}_{ij}^2)$ = trace of the tensor $\dot{\epsilon}_{ij}\dot{\epsilon}_{ji}$

C_1 = material constant with the dimension of inverse time

B = material constant with the dimension of stress

In the constitutive equation originally proposed by Kolymbas, the parameter B was assumed independent of stress level. The present experiments suggest:

$$B = b_o \ Tr(\sigma_{ij}) \qquad (7.4)$$

where

b_o = dimensionless material constant

This possibility was already mentioned in (Kolymbas, 1978).

Given a specific loading path and boundary conditions, equation (7.2) can be simplified considerably. Assuming uniaxial compaction ($\epsilon_r = \dot{\epsilon}_r = \dot{\epsilon}_r = 0$) and a constant ratio of axial to confining stress (more or less valid during uniaxial compaction experiments) yields for the axial component:

$$\dot{\sigma}_z = A_1 \ \dot{\epsilon}_z + \frac{b \ \sigma_z \ \dot{\epsilon}_z}{\sqrt{(C_1^2 + 1/2 \ \dot{\epsilon}_z^2)}} \qquad (7.5)$$

where $\quad b \quad = \quad \dfrac{(1 + \upsilon)}{(1 - \upsilon)} \ b_o$

During a constant loading rate experiment when on a virgin compaction curve, $\ddot{\epsilon}_z \simeq 0$ (neglecting the slight non-linearity of the virgin compaction curve) and under such conditions equation (7.5) reduces to:

$$\dot{\sigma}_z = A_1 \ \dot{\epsilon}_z \qquad (7.6)$$

Hence A1 is the inverse of the uniaxial compressibility coefficient along a virgin compaction curve:

$$A_1 = c_{m,o}^{-1} \tag{7.7}$$

Kolymbas introduced the constant C_1 in equation (7.5) to ensure that rate effects disappear at sufficiently low strain rates ($\dot{\epsilon}_z \ll C_1$). As will be shown later (section 10), rate effects are as important at geological strain rates as at laboratory loading rates (which are up to 10^{11} higher). Hence for all practical applications $\dot{\epsilon}_z \gg C_1$ and we can set $C_1 = 0$. Substituting this and equation (7.7) in equation (7.5) yields:

$$\dot{\sigma}_z = \frac{\dot{\epsilon}_z}{c_{m,o}} + b \, \sigma_z \, \frac{\ddot{\epsilon}_z}{\dot{\epsilon}_z} \tag{7.8}$$

Equation (7.8) will be referred to as the rate type compaction equation from here on. Mathematical equations properly describing the compaction behaviour described in section 6 can be derived from it as will be shown in sections 7.3.1-7.3.4. The physical background of equation (7.8) will be discussed in section 8.

7.3.1 General solution of the rate type compaction equation

Given the strain history, equation (7.8) can be integrated straight forward to obtain the resulting stress. The problem of reservoir compaction is essentially stress controlled however and so are the related laboratory experiments. Equation (7.8) therefore has to be solved to obtain the deformation resulting under the corresponding loading conditions. To this end its general solution will first be considered.

By substituting $Y(t) = \dot{\epsilon}_z$ and after some elementary manipulations we obtain from equation (7.8):

$$\dot{Y} + p \, Y = q \, Y^2 \tag{7.9}$$

with:

$$p(t) = -\frac{\dot{\sigma}_z}{b\sigma_z} \quad \text{and} \quad q(t) = -\frac{1}{bc_{m,o}\sigma_z} \tag{7.10}$$

Equation (7.9) is a particular case of the differential equation of Bernoulli. Substitution of our expressions for $p(t)$ and $q(t)$ (equations (7.10)) in the general solution given in (Teller, 1965) yields:

$$Y(t) = \frac{[\sigma_z(t)/\sigma_z(a)]^{1/b}}{1/Y(a) + \int_a^t [(\sigma_z(u)/\sigma_z(a))^{1/b}/(b\,c_{m,o}\sigma_z(u))]du} \qquad (7.11)$$

where:

a = integration constant

The expression for $\epsilon_z(t)$ can then be obtained from the solution of equation (7.11) by:

$$\epsilon_z(t) = \int_{t_o}^t Y(v)\,dv \qquad (7.12)$$

where:

t_o = integration constant, chosen such that $\epsilon_z(t_o) = 0$.

Using equations (7.11) and (7.12), solutions of equation (7.8) for various loading paths can be calculated. This will be done in sections (7.3.3) and (7.3.4), but first the distance between constant loading rate virgin compaction curves will be considered.

7.3.2 Distance between virgin compaction curves

An equation for the width $\Delta\sigma_z$ of the transition zone caused by an increase in axial loading rate from $\dot{\sigma}_{z,1}$ to $\dot{\sigma}_{z,2}$ can be obtained from the rate type compaction equation in the following way:

For infinitesimal stress changes multiplication of equation (7.8) by dt yields:

$$d\sigma_z = \frac{d\epsilon_z}{c_{m,o}} + b\,\sigma_z d(\ln \dot{\epsilon}_z) \qquad (7.13)$$

The distance between two constant loading rate compaction curves will be determined along an integration path with constant strain ϵ_z as shown in Fig. 22. Hence $\Delta\epsilon_z = 0$ between $\sigma_{z,2}$ and $\sigma_{z,1}$, characterising the stress distance between constant loading rate compaction curves. Thus we obtain from equation (7.13):

$$\sigma_{z,2}/\sigma_{z,1} = (\dot{\epsilon}_{z,2}/\dot{\epsilon}_{z,1})^b \qquad (7.14)$$

For the virgin compaction curves we have approximately (neglecting the non-linearity in the virgin compaction curves for the present purpose):

$$\dot{\epsilon}_z = c_{m,o}\dot{\sigma}_z \qquad (7.15)$$

With $\Delta\sigma_z = \sigma_{z,2} - \sigma_{z,1}$, we obtain:

$$\Delta\sigma_z(\dot{\sigma}_{z,2}; \dot{\sigma}_{z,1}) = \sigma_{z,1}[(\frac{c_{m,o}(\dot{\epsilon}_{z,2})\dot{\sigma}_{z,2}}{c_{m,o}(\dot{\sigma}_{z,1})\dot{\sigma}_{z,1}})^b - 1] \qquad (7.16)$$

which can be approximated by:

$$\Delta\sigma_z(\dot{\sigma}_{z,2}; \dot{\sigma}_{z,1}) = \sigma_{z,1}[(\frac{\dot{\sigma}_{z,2}}{\dot{\sigma}_{z,1}})^b - 1] \qquad (7.17)$$

where

$\Delta\sigma_z(\dot{\sigma}_{z,2}; \dot{\sigma}_{z,1}) =$ shift in axial stress between compaction curves resulting from constant axial loading rates $\dot{\sigma}_{z,2}$ and $\dot{\sigma}_{z,1}$ at a given axial stress $\sigma_{z,1}$ (see Fig. 22)

Equation (7.17) equals equation (6.1) which was obtained empirically by

fitting the results of variable loading rate experiments. The value of b can be determined from the compaction behaviour after an increase or decrease in loading rate according to:

$$b = \frac{\ln(\sigma_{z,2}/\sigma_{z,1})}{\ln(\dot{\sigma}_{z,2}/\dot{\sigma}_{z,1})} \tag{7.18}$$

as can be derived from equation (7.17).

An alternative procedure to determine b is to plot the value of $\Delta\sigma_z/\ln(\dot{\sigma}_{z,2}/\dot{\sigma}_{z,1})$, as obtained from changing the loading rate at a number of different stress levels, versus the appropriate values of $\sigma_{z,1}$. This will yield straight lines with slope b as equation (7.17) can be approximated by:

$$\Delta\sigma_z(\dot{\sigma}_{z,2}; \dot{\sigma}_{z,1}) = b\ \sigma_{z,1}\ln(\dot{\sigma}_{z,2}/\dot{\sigma}_{z,1}) = b\ \sigma_{z,1}\Delta(\ln \dot{\sigma}_z) \tag{7.19}$$

up to sufficiently small values of $\dot{\sigma}_{z,2}/\dot{\sigma}_{z,1}$ (approximately up to 10^3). This procedure has been followed for the various materials tested (see Figs. 33 to 37 and Tables A3 and A4), yielding b values as given in Table 6.1. The value of b is around 0.020 for unconsolidated samples, and decreases with increasing degree of cementation. No significant difference was found between the b values derived from the experiments at room temperature and the value of b derived from an experiment at 90 degrees C (Fig. 36).

Given the values of b the approximation of equation (7.16) by equation (7.17) is quite justified. Using equations (7.15) and (7.17) one can also show:

$$c_{m,o}(\dot{\sigma}_{z,2}) = c_{m,o}(\dot{\sigma}_{z,1})\ [(\dot{\sigma}_{z,2}/\dot{\sigma}_{z,1})^b] \tag{7.20}$$

which relates the uniaxial compressibilities on virgin compaction curves corresponding to different loading rates.
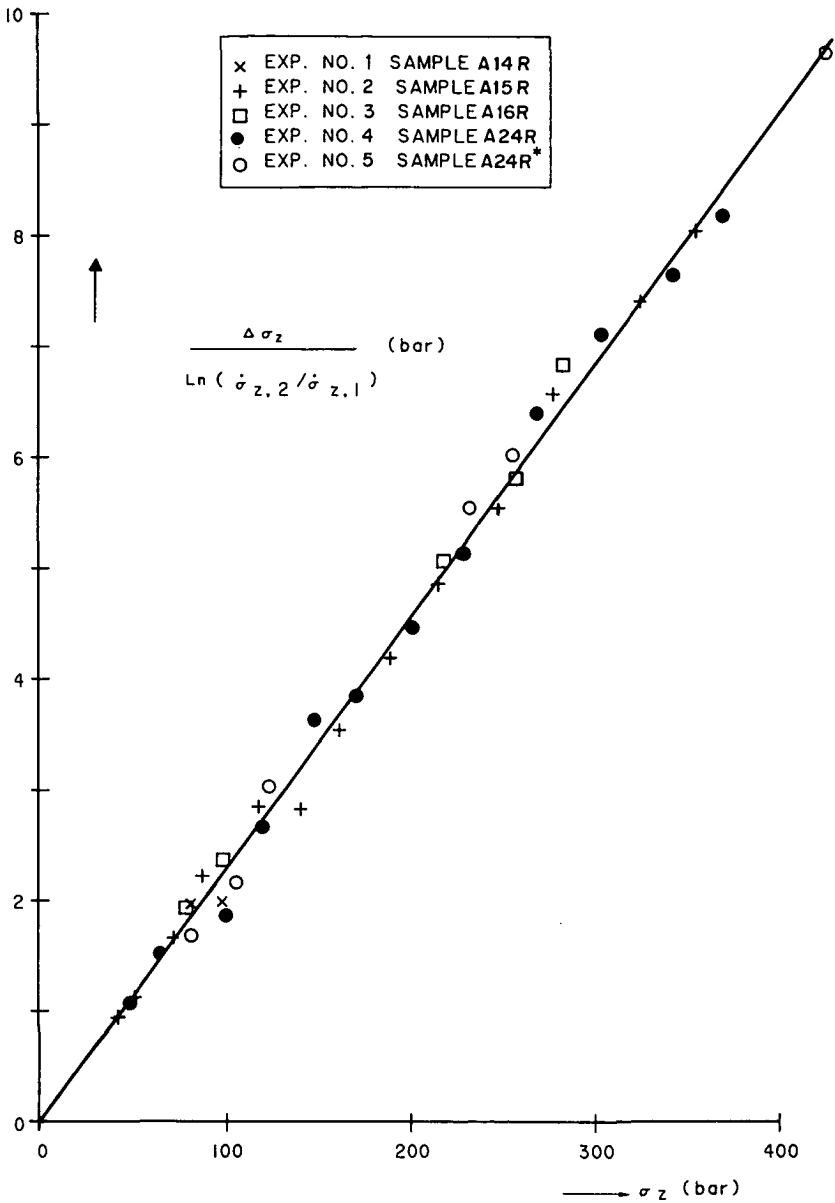
FIG.33 RATE EFFECTS IN THE COMPACTION BEHAVIOUR OF RESERVOIR A SAND AS A FUNCTION OF PRESSURE AND REMOULDING (OEDOMETER TESTS)
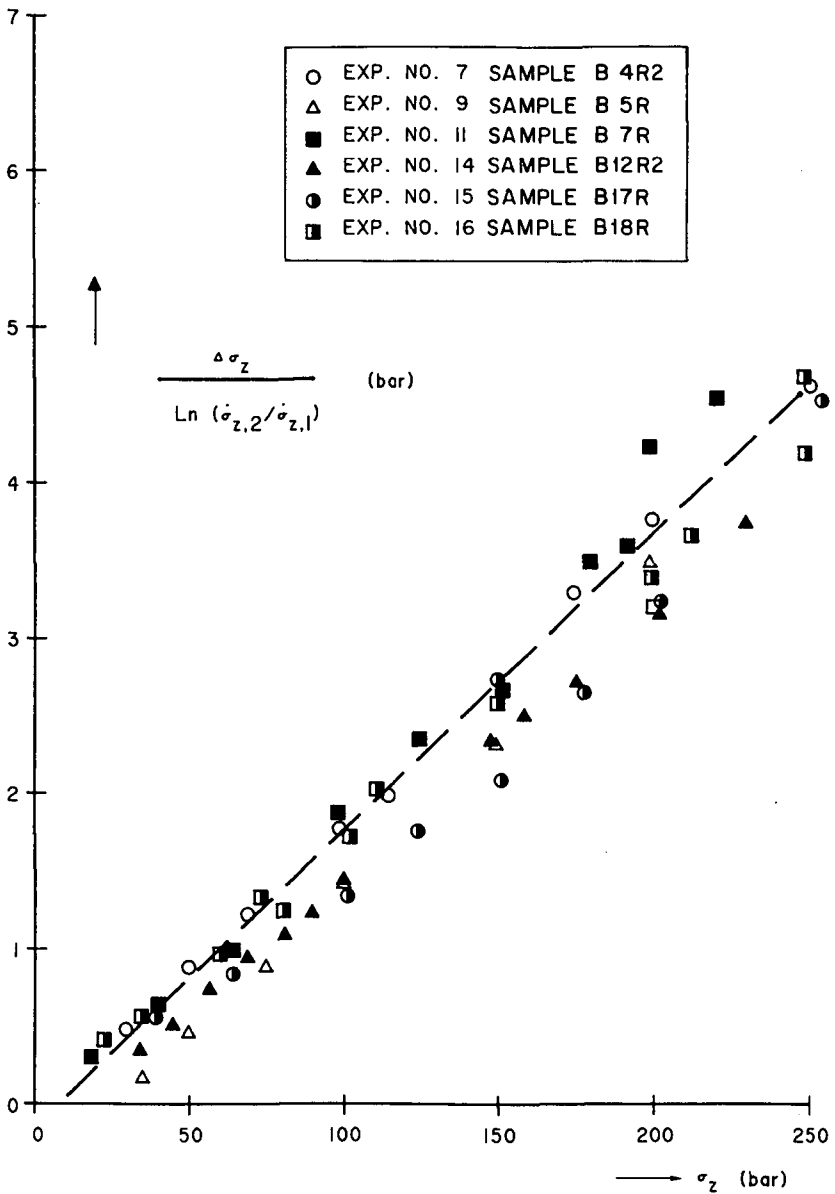
FIG.34 RATE EFFECTS IN THE
COMPACTION BEHAVIOUR OF
RESERVOIR B SAND AND SILT SAMPLES
AS A FUNCTION OF PRESSURE
(OEDOMETER TESTS)
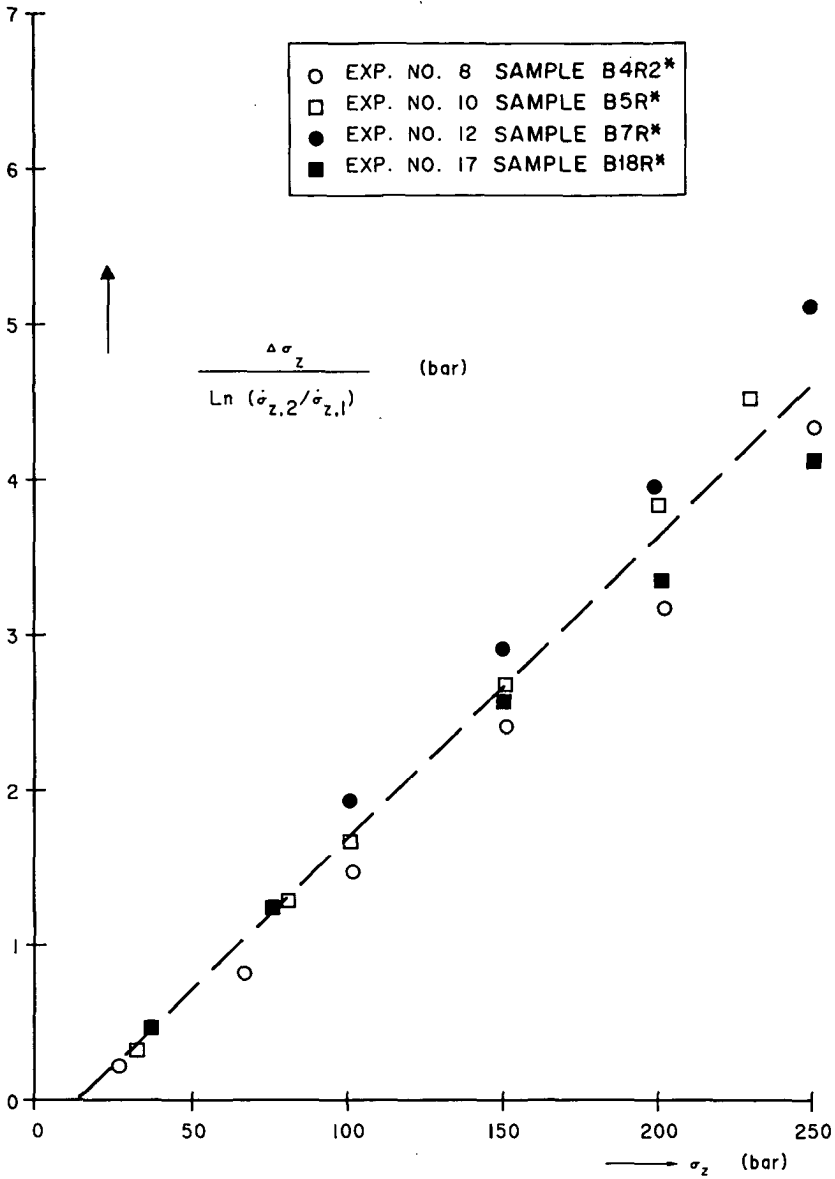
FIG.35 RATE EFFECTS IN THE COMPACTION BEHAVIOUR OF REMOULDED RESERVOIR B SAND AND SILT SAMPLES AS A FUNCTION OF PRESSURE (OEDOMETER TESTS)
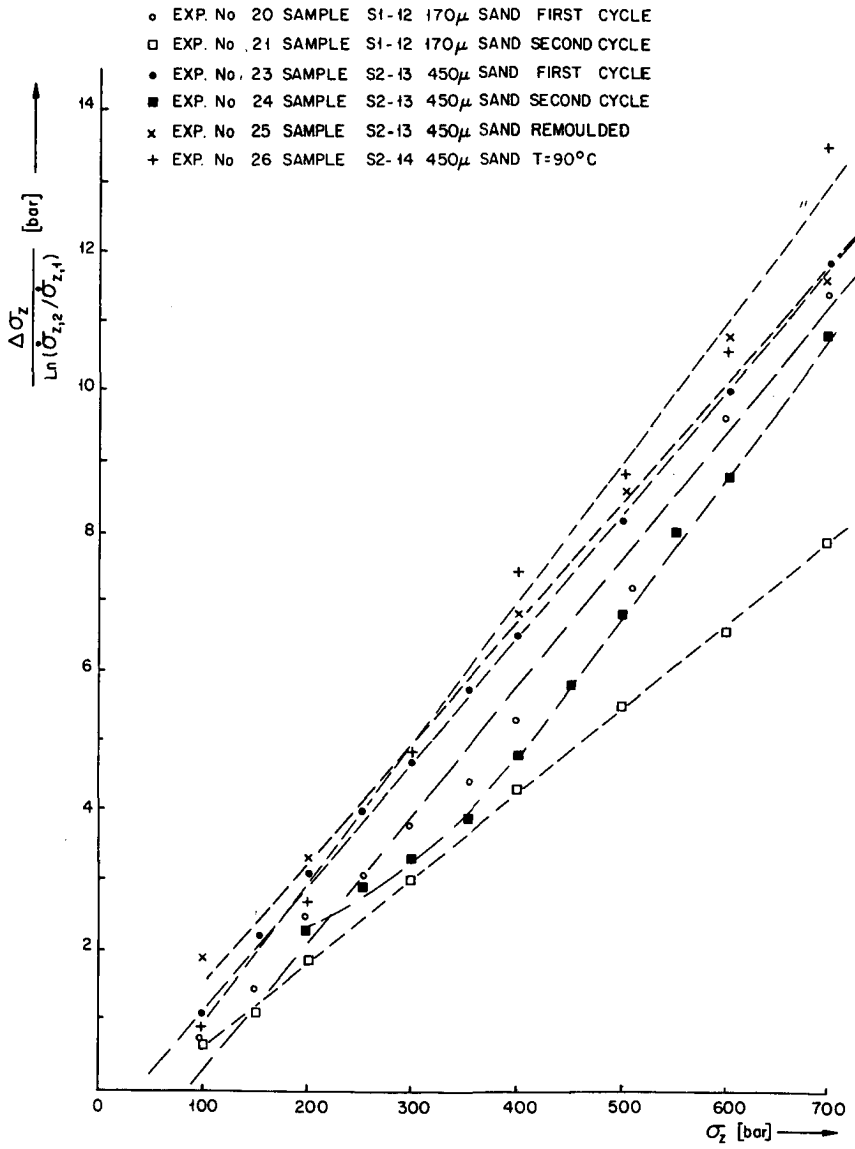
FIG 36 RATE EFFECTS IN THE
COMPACTION BEHAVIOUR OF 170 AND
450μ SAND AS A FUNCTION OF
PRESSURE, REMOULDING AND
TEMPERATURE (OEDOMETER TESTS).

$$\frac{\triangle \sigma_z}{LN\left[\dot{\sigma}_{z,2} / \dot{\sigma}_{z,1}\right]} \quad [bar]$$

O EXP. NO.   27 SAMPLE SB 15 (170 μ STEAL BEADS)

X EXP. NO.   28 SAMPLE AL 16 (ALUMINIUM POWDER)

QUARTZ SAND (EXP.   20 - 26)

σ_z (bar)
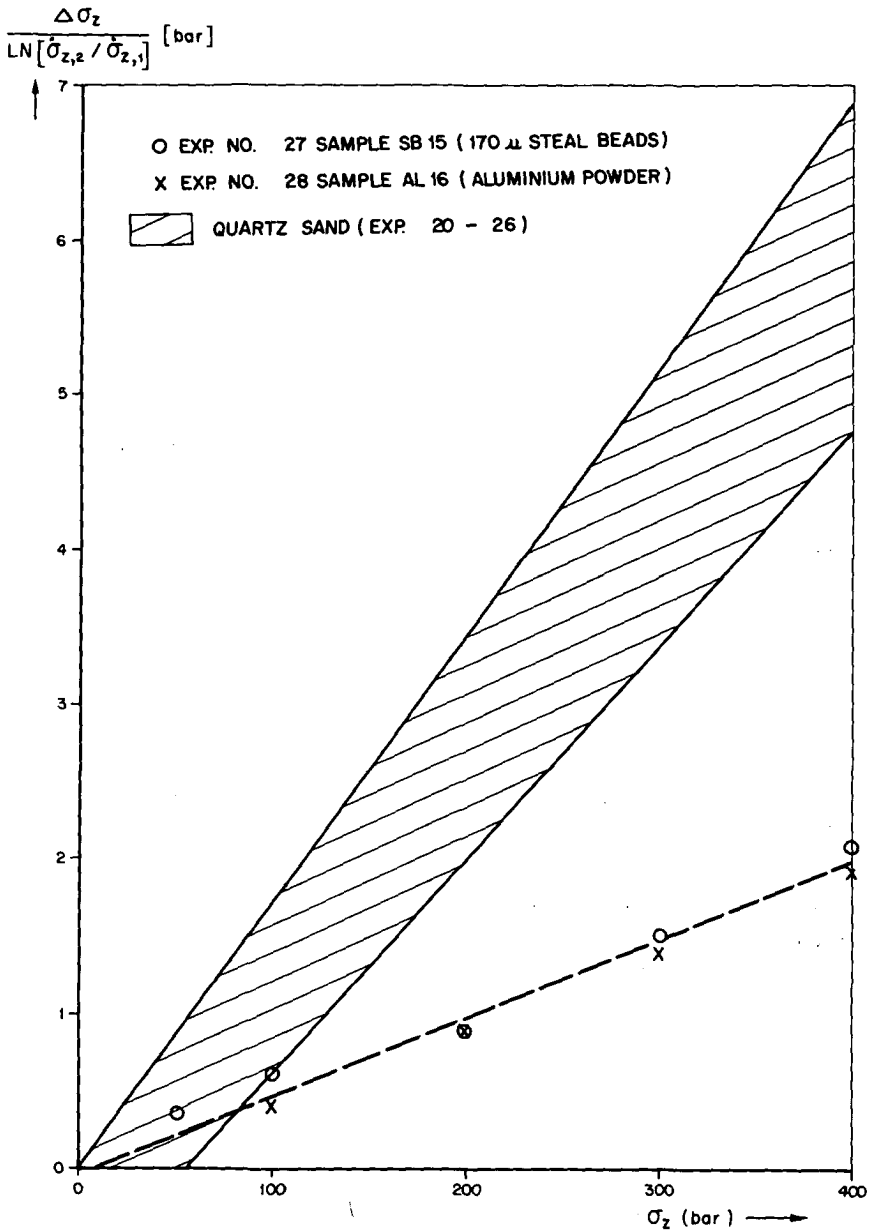
FIG.37 RATE EFFECTS IN THE COMPACTION BEHAVIOUR OF 170 μ STEAL BEADS AND ALUMINIUM POWDER COMPARED TO THOSE FOUND IN PACKS OF QUARTZ SAND.

7.3.3 Creep

In creep experiments we have $\dot{\sigma}_z = 0$; $\sigma_z = \sigma_{z,1} =$ constant. Hence: $\sigma_z(t) = \sigma_z(a)$ for all t. Substituting a = 0 we have from equation (7.11):

$$Y(t) = \frac{Y(0)}{1 + Y(0) \ t/(b \ c_{m,o}\sigma_{z,1})} \qquad (7.21)$$

so that (from equation (7.12)):

$$\epsilon_{z,creep}(t) = b \ c_{m,o}\sigma_{z,1} \ln (1 + \frac{\dot{\epsilon}_z(0) \ t}{b \ c_{m,o}\sigma_{z,1}}) \qquad (7.22)$$

Here t_o = 0 has been taken, so that t = 0 at the start of the creep experiment, while $\dot{\epsilon}_z(0)$ is the initial creep rate after the interruption of loading (at t = 0). The logarithmic type creep behaviour of sandstones as predicted by equation (7.22) is mathematically similar to that observed on clays (Keverling Buisman, 1936) and is indeed observed at constant load (Fig. 38).

However, the experimental data shows that the value of $\dot{\epsilon}_z(0)$ is considerably smaller than the value of $\dot{\epsilon}_z$ just prior to the interruption of loading. which means that $\dot{\epsilon}_z$ is not continuous through changes in loading rate. This will be discussed further in sections 7.3.4 and 7.3.5.

7.3.4 Constant loading rate compaction curves

In the case of constant loading rate we have: $\Delta\sigma_z = \dot{\sigma}_z$ t, with $\dot{\sigma}_z$ = constant. Substituting $Y(t) = \dot{\epsilon}_z = (\frac{d\epsilon_z}{d\sigma_z}) \ \dot{\sigma}_z$ and dt = $d\sigma_z/\dot{\sigma}_z$ in equations (7.11) and (7.12) yields:

$$\epsilon_z = \int_{\dot{\sigma}_z t_o}^{\sigma_z} \frac{u^{1/b}}{C_1 + J} \ du \qquad (7.23)$$

where:

C_1 = integration constant

82

Decrease in sample height (microns)

Observation time
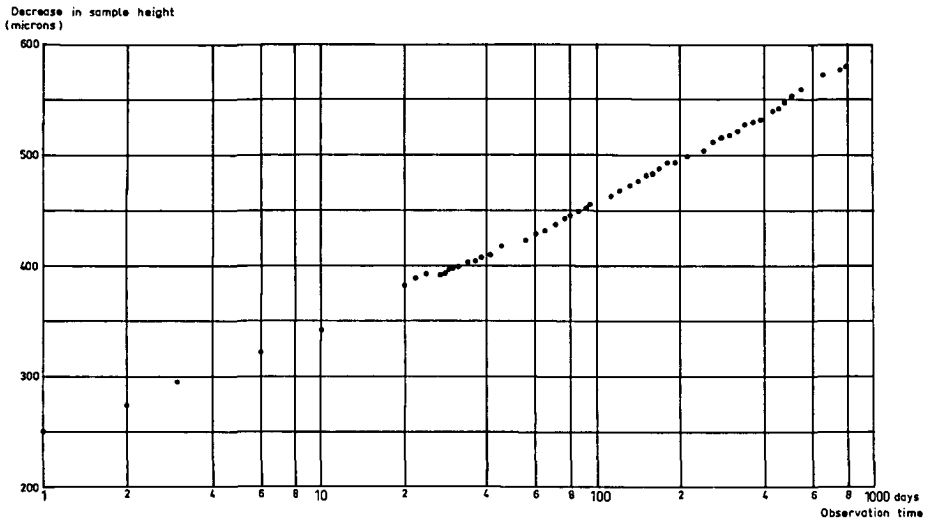
FIG.38 CREEP IN SAND SAMPLE AFTER LOAD INCREASE FROM 150 TO 180 BAR

83

and:

$$J = \int_a^u \frac{v^{-1+1/b}}{b\, c_{m,o}} \; dv = \frac{u^{1/b}}{c_{m,o}} \tag{7.24}$$

Hence:

$$\epsilon_z = c_{m,o} \int_{\dot{o}_z t_o}^{\sigma_z} \frac{1}{1 + C_2\, u^{-1/b}} \; du \tag{7.25}$$

where

$$C_2 \quad = \quad \text{integration constant.}$$

Equation (7.25) can be normalised by defining:

$$z = \frac{\epsilon_z}{c_{m,o}\sigma_{z,o}} \quad \text{and} \quad x = \frac{\sigma_z}{\sigma_{z,o}} \tag{7.26}$$

Then:

$$z = \int_{\dot{o}_z t_o/\sigma_{z,o}}^{\sigma_z/\sigma_{z,o}} \left(\frac{1}{1 + a_1\, x^{-1/b}} \right) dx \tag{7.27}$$

where:

$$\sigma_{z,o} = \text{arbitrarily chosen normalisation stress}$$

while:

$$a_1 \quad = \quad \frac{(1 - c_m(\sigma_{z,o})/c_{m,o})}{c_m(\sigma_{z,o})/c_{m,o}} \quad = \quad \frac{c_{m,o}}{c_m(\sigma_{z,o})} - 1 \tag{7.28}$$

In order to compare equation (7.27) with the general compaction curve derived from the experimental data (equation (7.1), we define $z = 0.0$ at $x = 1.0$ ($t_o = \sigma_{z,o}/\dot{\sigma}_z$). Hence:

$$z = \int_{1}^{\sigma_z/\sigma_{z,o}} \left(\frac{1}{1 + a_1\, x^{-1/b}} \right) dx \qquad (7.29)$$

and

$$c_m/c_{m,o} = \partial z/\partial(\sigma_z/\sigma_{z,o}) = \frac{1}{1 + a_1\, x^{-1/b}} \qquad (7.30)$$

During a conventional constant loading rate experiment $a_1 = 0$, which yields: $\Delta z = \Delta\sigma_z/\sigma_{z,o}$, hence $\Delta\epsilon_z = c_{m,o}\Delta\sigma_z$, which is the normal constant loading-rate solution when linear elasticity applies (although $c_{m,o}$ depends weakly on $\dot{\sigma}_z$ according to equation (7.20)). An excellent fit of equations (7.29) and (7.30) with the experimentally determined general compaction curve (equation 7.1) is obtained with $a_1 = 4.56$ and $b \approx 0.056$ (see Figs. 39 and 40). Hence, the general compaction curve is a constant loading rate solution of the Kolymbas equation.

The b value obtained from fitting equations (7.29) and (7.30) to the general compaction curve differs from that in equation (7.17) which describes the width of the transition zone. This fact indicates that equation (7.8) can not be integrated through changes in loading rate, which suggests that a term containing $\dot{\sigma}_z^*$ is missing from the rate type compaction equation. This is confirmed by experimental evidence: according to equation (7.13), $\dot{\epsilon}_z$ should be continuous through a jump in $\dot{\sigma}_z$, while the laboratory experiments show a discontinuity. A similar observation was made for the initial creep rate after the interruption of loading (see section 7.3.3). As a result, equation (7.29) is only valid for constant loading rate parts of a compaction curve such as virgin compaction curves or constant loading rate transition curves. For the presented laboratory experiments and the in-situ field behaviour during depletion this is not a problem because equation (7.29) (or rather the general compaction curve) is used only to describe the behaviour _after_ a chamge in loading rate. When several loading rates occur,
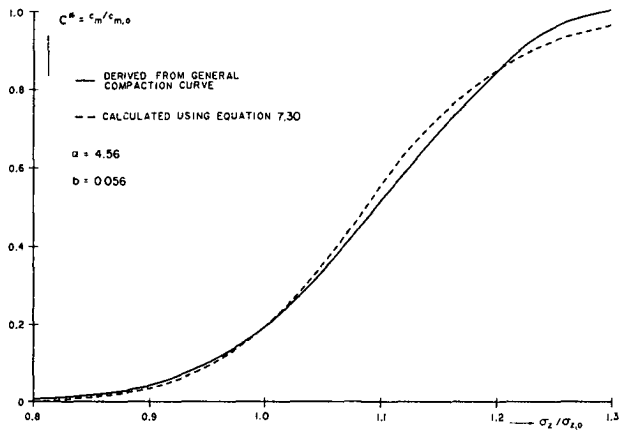
FIG.39 COMPARISON OF NORMALISED COMPRESSIBILITY C*= $c_m/c_{m,o}$ AS DERIVED FROM THE RATE TYPE COMPACTION EQUATION AND FROM THE GENERAL COMPACTION CURVE
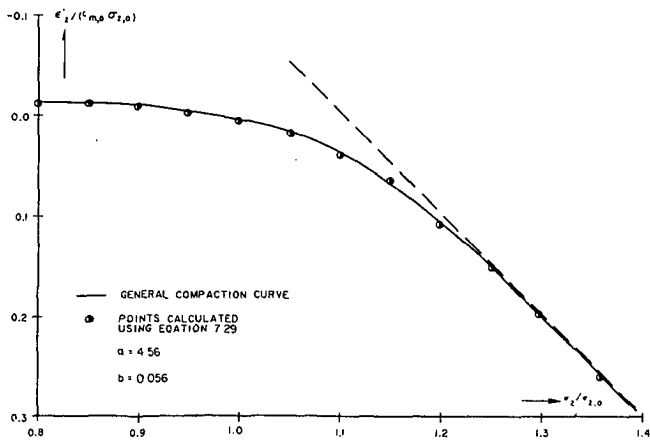
FIG.40 COMPARISON OF NORMALISED COMPACTION AS DERIVED FROM THE RATE TYPE COMPACTION EQUATION AND FROM THE GENERAL COMPACTION CURVE

the resulting compaction curve can be split up into constant loading rate parts, each of which is described by equation (7.29) using the appropriate integration constants.

7.3.5 Extensions of the rate type compaction equation

At first sight, a possible solution for the fact that the rate type compaction equation can not be integrated through a change in loading rate is obtained by adding an additional term to equation (7.8), resulting in:

$$\dot{\sigma}_z + a \, \frac{\sigma_z \ddot{\sigma}_z}{\dot{\sigma}_z} = \frac{\dot{\epsilon}_z}{c_{m,o}} + b \, \frac{\sigma_z \ddot{\epsilon}_z}{\dot{\epsilon}_z} \tag{7.31}$$

where: a   =   material constant

Equation (7.31) reduces to equation (7.29) during loading at a constant rate, as $\ddot{\sigma}_z = 0$ under those conditions. The additional $\ddot{\sigma}_z$ term accounts for the appropriate jump in $\dot{\epsilon}_z$ upon a sudden change in $\dot{\sigma}_z$. Multiplication of equation (7.31) with dt yields:

$$d\sigma_z + a \, \sigma_z d(\ln \dot{\sigma}_z) = 1/c_{m,o} d\epsilon_z + b \, \sigma_z d(\ln \dot{\epsilon}_z) \tag{7.32}$$

During a sudden change in $\dot{\sigma}_z$, $d\sigma_z = d\epsilon_z = 0$ and hence:

$$d(\ln \dot{\epsilon}_z) = \frac{a}{b} \, d(\ln \dot{\sigma}_z) \tag{7.33}$$

Comparison with the experimental data suggests a $\simeq 0.001$. Equations (7.31) and (7.33) properly describe the compaction behaviour resulting after a sudden increase in loading rate. For the specific case of creep (which is actually a decrease in loading rate) there is a problem as equation (7.33) predicts $\dot{\epsilon}_z(0) = 0$ for $\dot{\sigma}_{z,2} = 0$, contrary to the experimental data. This problem and the more general problem of the shape of the compaction curve after a decrease in loading rate is a subject for further research.

8. PHYSICAL BACKGROUND

In this section an attempt will be made to explain the observed rate type compaction behaviour as described in sections 6 and 7 by a physical model. To this end the compaction mechanism of a granular medium will be considered in some detail. Subsequently it will be shown how a simple model based on these considerations and in which the intergranular friction coefficient is taken time dependent, can be used to obtain equation (7.8) (the rate type compaction equation).

It is not claimed that a mathematically rigid and physically well proven description of the compaction process in granular media is obtained. Rather, the model presented is meant to provide more insight into the physical processes underlying the observed rate effects.

8.1 Deformation of a granular medium

The deformation in a granular medium can be due to two mechanisms: 1) deformation of the grains themselves and 2) re-arrangement of the position and orientation of the grains relative to each other. For most reservoir rocks, the latter mechanism is the only relevant one, as the rock bulk compressibility is usually much larger than the rock matrix compressibility. Movement of the grains relative to each other can occur as a result of grain rotation and as a result of sliding of grains over each other (Fig. 41). Sliding will only occur at a contact point if the shear force at that contact point exceeds the maximum friction force which is given by (Jaeger and Cook, 1969: Dieterich, 1978):

$$| \vec{F}_W(max) | = \mu | \vec{F}_N | \qquad (8.1)$$

where

$$| \vec{F}_W(max) | = \text{absolute value of maximum shear stress at an individual contact point}$$

$$| \vec{F}_N | = \text{absolute value of the normal force at an individual contact point}$$
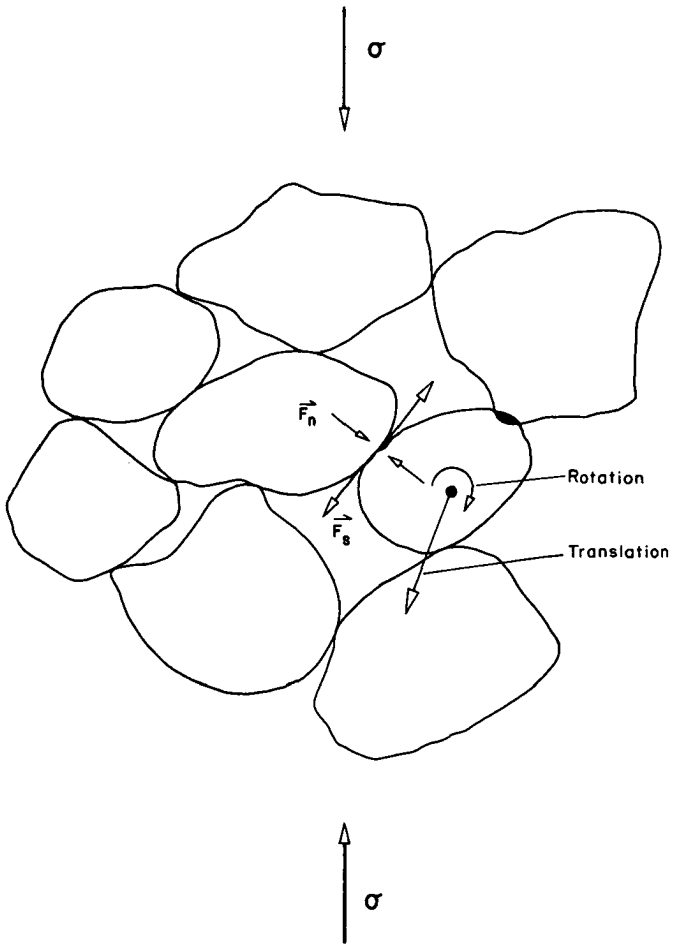
$$\mu = \text{friction coefficient}$$

FIG.41 INTERGRANULAR STRESSES AND DISPLACEMENTS.

As a result, only a limited number of the total number of granular contacts will be "active" simultaneously.

During the loading of unconsolidated sands many grains break under the influence of large stress concentrations at point contacts, allowing large movements of the fragments and the surrounding grains and resulting in large amounts of compaction. In consolidated rocks, the possible deformation is much more limited because many grains are cemented together, reducing stress concentrations and limiting possible movements. Nevertheless in both cases, the basic deformation process will be the frictional sliding of grains, grain fragments or assemblies of grains, relative to each other.

The resulting stress/strain behaviour of a granular medium will be determined by the relationships between external load, intergranular contact forces, grain movements and bulk deformation. Various attempts have been made to model this complicated statistical process, either analytically or numerically, see e.g. (Oda, 1974; Tokue, 1979; Cundall and Strack, 1979,1983; Oda et al, 1982; Cundall et al 1982). Calculated stress and strain patterns in (Cundall and Strack, 1979) are in excellent agreement with earlier experimental work on 2D assemblies of photoelastic discs (Josseling de Jong and Verruijt, 1969). One of the latest developments in this field consists of the computer program TRUEBALL (Cundall, 1985), which can calculate the deformation of a pre-defined 3D assembly of spherical grains under the influence of an external load. Apart from the initial relative position of the grains, the resulting deformation is obviously dependent on the assumed friction law, governing the sliding process between two contacting grains.

For the present purpose, a very simple model will be used to relate macroscopic and microscopic material behaviour. It will be discussed further in section 8.3, after discussing the recent finding that the friction coefficient to be used in such models should be taken time dependent.

8.2 Time dependent friction of mineral surfaces

Because of its importance in understanding earthquake mechanisms, a large amount of scientific effort has been spent recently on the subject of friction between mineral surfaces (Byerlee, 1978). In the friction theory it is now generally accepted that the contact between two mineral grains occurs at a limited number of contact points, called asperities (Bowden and Taybor, 1950, 1964; Bowden, 1954; Scholz and Englander, 1976). Hence, the frictional

sliding between two mineral surfaces (e.g. between two grains) is controlled by the behaviour of these asperities. It has been found experimentally that the friction coefficient μ during mineral sliding processes is logarithmically dependent on the average lifetime t_a of the individual asperities (see Fig. 42, taken from Dieterich, 1978):

$$\mu = \mu_o + A \ln (1 + B t_a) \tag{8.2}$$

where

$$\mu_o = \text{rate independent part of friction coefficient (0.7-0.8)}$$
$$A = \text{material constant (0.016-0.020)}$$
$$B = \text{material constant} \simeq 1.0 \text{ s}^{-1}$$

The increase in friction coefficient is related to an increase in the real area of contact as shown experimentally by Teufel and Logan (1978). This increase in real contact area must be due to growth of the individual asperities or a result of an increase of their number. Various mechanisms have been proposed (Dieterich, 1978; Teufel and Logan, 1978): asperity creep, cataclastic flow, chemical action at the grain boundaries etc., none of which have actually been proven.

For the case of unconsolidated and friable sandstones, the value of the material constant b in equation (7.17), which describes the width of the transition zone resulting after a change in loading rate, is of the same order of magnitude as the material constant A in equation (8.2). This suggests that the observed rate type material behaviour of sandstones and the time dependent friction coefficient are somehow related. It can be expected that the average lifetime t_a of an individual asperity in a compacting granular medium will be coupled to the strain rate tensor $\dot{\epsilon}_{ij}$ according to:

$$t_a = \frac{C}{\sqrt{Tr(\dot{\epsilon}_{ij}\dot{\epsilon}_{ji})}} \tag{8.3}$$

where:
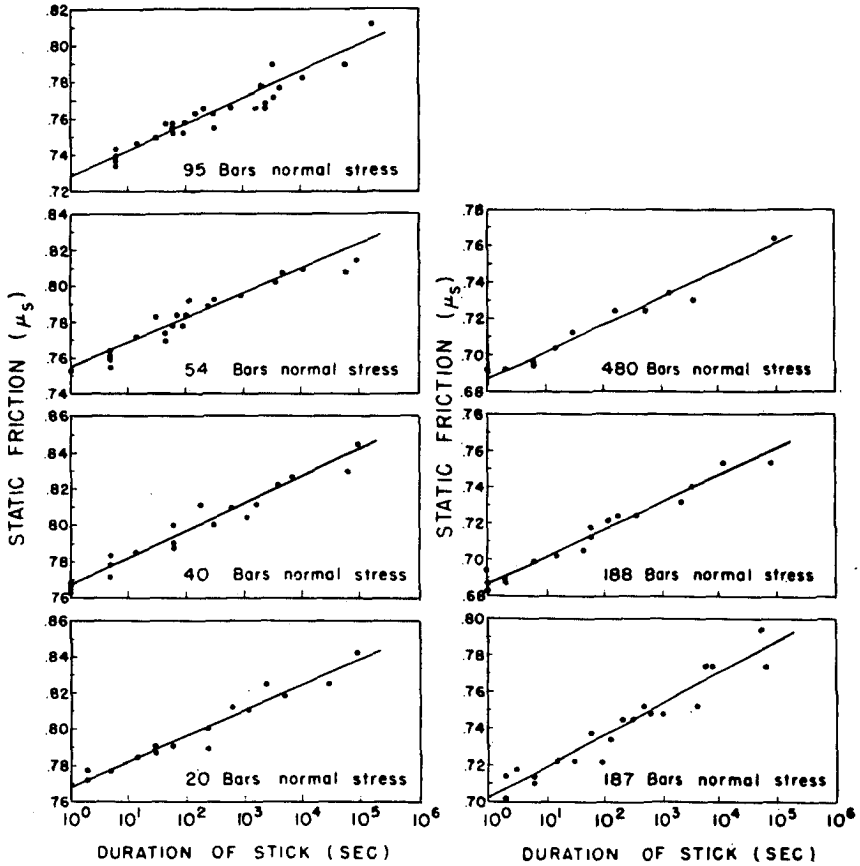
Time-dependence of the coefficient of static friction of quartz sandstone

FIG.42 INTERGRANULAR FRICTION COEFFICIENT AS A FUNCTION OF ASPERITY LIFE-TIME (AFTER DIETERICH 1978)

C = constant, related to the critical movement after which an asperity will break

Substituting equation (8.3) into equation (8.2) results in:

$$\mu = \mu_o + A \ln \left(1 + \frac{C}{\sqrt{Tr(\dot{\epsilon}_{ij}\dot{\epsilon}_{ji})}} \right) \qquad (8.4)$$

For the present purpose, this equation can be approximated by:

$$\mu = \mu_o + A \ln \left(1 + \frac{C}{\dot{e}} \right) \qquad (8.5)$$

This equation will further be referred to as the Dieterich equation. It can be interpretated as follows. When the strain rate is low, it takes a long time for each individual asperity before the critical strain at which it breaks is reached. Meanwhile, new asperities have ample time to develop. Therefore the real area of contact is relatively high, resulting in a larger friction coefficient. Conversely, when the strain rate is high, asperities on average will exist much shorter, resulting in a lower real area of contact and a lower friction coefficient.

8.3 Derivation of the rate type compaction equation

It is assumed that the influence of the complicated statistical grain deformation and grain movement processes during compaction can be described by writing the total compaction as the sum of a matrix compaction component e_n taken proportional to the mean hydrostatic total stress, and a component e_s due to intergranular sliding, taken proportional to the average intergranular maximum shear force. Hence:

$$e_n = D_1 \, \sigma_{ii}/3 \qquad (8.6)$$

where

D_1 = material constant

while:

$$e_s = D_2 \langle \, |\, \vec{F}_w(max)| \, \rangle \qquad\qquad \text{/} \qquad\qquad (8.7)$$

where

$$
\begin{array}{lll}
D_2 & = & \text{material constant} \\
\langle \, |\, \vec{F}_w(max)| \, \rangle & = & \text{average absolute value of the maximum} \\
& & \text{intergranular shear force}
\end{array}
$$

Assuming:

$$\langle \, |\, F_w(max)| \, \rangle = \mu \, \langle \, |\, F_N| \, \rangle \qquad\qquad\qquad (8.8)$$

where

$$
\begin{array}{lll}
\langle \, |\, \dot{F}_N| \, \rangle & = & \text{average absolute value of the maximum} \\
& & \text{intergranular normal force}
\end{array}
$$

and:

$$\langle \, |\, F_N| \, \rangle = D_3 \, (\sigma_{ii}/3 - p) \qquad\qquad (8.9)$$

then yields:

$$e_s = D_2 \, D_3 \, \mu \, (\sigma_{ii}/3 - p) \qquad\qquad (8.10)$$

Substituting equation (8.5) into equation (8.10) yields:

$$e_s = D_4 \, [1 + \frac{A}{\mu_o} \, \ln \, (1 + \frac{C}{\dot{e}} \,)] \, (\sigma_{ii}/3 - p) \qquad\qquad (8.11)$$

where:

$$D_4 = D_2 \, D_3 \, \mu_o$$

Hence we obtain for the total compaction:

$$e = e_n + e_s = [D_1 + D_4(1 + \frac{A}{\mu_o} \, \ln \, (1 + \frac{C}{\dot{e}} \,)] \, (\sigma_{ii}/3 - p) + D_1 p \qquad\qquad (8.12)$$

Differentiation of eq. (8.12) with respect to time yields:

$$\dot{e} = [D_1 + D_4(1 + \frac{A}{\mu_o} \ln(1 + \frac{C}{\dot{e}}))](\dot{\sigma}_{ii}/3 - \dot{p}) - \frac{D_4 A}{\mu_o} \frac{C \ddot{e}(\sigma_{ii}/3 - p)}{\dot{e}^2 + C\dot{e}} + D_1\dot{p}$$

$$(8.13)$$

In (Dieterich, 1978) the value $C = 10^{-4}$ is mentioned for a specific example. Characteristic values for $\dot{e}$ and related quantities for the situations important for our present purpose are given in the following table:

Table 8.1:

Condition	$\dot{e}$ (s^{-1})	$\dfrac{\dot{e}^2}{C\dot{e}}$	F
Sedimentation	10^{-17}	10^{-13}	1.75
Depletion	10^{-10}	10^{-6}	1.35
Lab. experiment	10^{-5}	10^{-1}	1.06

----

where:

$$F = 1 + \frac{A}{\mu_o} \ln(1 + \frac{C}{\dot{e}})$$

$$(8.14)$$

From this table we conclude that for practical cases $\dot{e}^2 \ll C\dot{e}$. Then equation (8.13) becomes:

$$\dot{e} = [D_1 + D_4 F] (\dot{\sigma}_{ii}/3 - \dot{p}) - \frac{D_4 A}{\mu_o} (\sigma_{ii}/3 - p) \frac{\ddot{e}}{\dot{e}} + D_1\dot{p}$$

$$(8.15)$$

where F depends slowly on $\dot{e}$ (see Table above).

For the virgin compaction curves during constant loading-rate experiments the $\ddot{e}$ term in equation (8.15) is negligible. Hence, for those experiments:

$$\dot{e} = [D_1 + D_4 F](\dot{\sigma}_{ii}/3 - \dot{p}) + D_1 \dot{p} \qquad (8.16)$$

comparison with eq. (4.2) yields:

$$D_1 + D_4 F = c_{b,o} \qquad \text{and} \qquad D_1 = \beta\, c_b = c_r \qquad (8.17)$$

Equations (8.17) reflect our assumption that the constant loading-rate experiments are more or less linear. In practice, this assumption is not really valid (see e.g. Figs. 2 and 3). The model could possibly be extended in the future by incorporation of the non-linearity of the constant loading-rate compaction curve.

Substitution of equations (8.17) in equation (8.15) yields:

$$\dot{e} = c_{b,o}(\dot{\sigma}_{ii}/3 - \dot{p}) + b\,(c_{b,o} - c_r)(\sigma_{ii}/3 - p)(-\frac{\dot{\dot{e}}}{\dot{e}}) + c_r \dot{p} \qquad (8.18)$$

where:

$$b = -\frac{A}{\mu_o F} \qquad (8.19)$$

Hence b is a very slowly varying function of $\dot{e}$. Using the values of A and C given by (Dieterich, 1978) for quartz surfaces yields:

Table 8.2

Condition	$\dot{e}\ (s^{-1})$	b
Sedimentation	10^{-17}	0.014
Depletion	10^{-10}	0.019
Laboratory	10^{-5}	0.024

Comparison of equation (8.18) with equation (7.8) shows that equation (8.18) is a somewhat extended version of the rate type compaction equation, which takes the effects of grain compressibility and pore pressure into account. Therefore the above derivation culminating in equation (8.18) confirms the assumed physical background of equation (7.8). For a uniaxial laboratory compaction experiment with zero pore pressure equation (8.18) reduces to:

$$\dot{\epsilon}_z = (1 - c_r/c_{b,o})^{-1} c_{m,o}\dot{\sigma}_z + c_{m,o}\sigma_z b \frac{\ddot{\epsilon}_z}{\dot{\epsilon}_z} \qquad (8.20)$$

Under uniaxial field conditions $\dot{\sigma}_{ii} = \frac{2(1 - 2\upsilon)}{(1 - \upsilon)} (1 - c_r/c_{b,o}) \dot{p})$, so that equation (8.18) reduces to:

$$\dot{\epsilon}_z = - c_{m,o} \dot{p} - c_{m,o}b [1 + (\frac{2(1 - 2\upsilon)}{(1 + \upsilon)})(1 - c_r/c_{b,o})(c_r/c_{b,o})] \dot{p} (\frac{\ddot{\epsilon}_z}{\dot{\epsilon}_z})$$

$$(8.21)$$

From Table 8.2 in which the value of A given by Dieterich has been used to calculate b, it appears that b should be approximately 0.024 under laboratory conditions. This is in reasonable agreement with the value of b $\simeq$ 0.020 found in the present study for unconsolidated sandstone (see Table 1). Equation (8.20) further suggests that for zero pore pressure compaction experiments on stiff rocks ($\beta > 0$), b should be replaced by:

$$b' = b (1 - c_r/c_b). \qquad (8.22)$$

As a result rate effects will become smaller for stiffer materials, finally disappearing for zero porosity rock (for which $c_{b,o} = c_r$). This is indeed confirmed by the laboratory data as shown in Fig. 43. In addition, the derivation given above suggests that b depends weakly on the strain rate (Table 8.2) and hence on the loading rate.
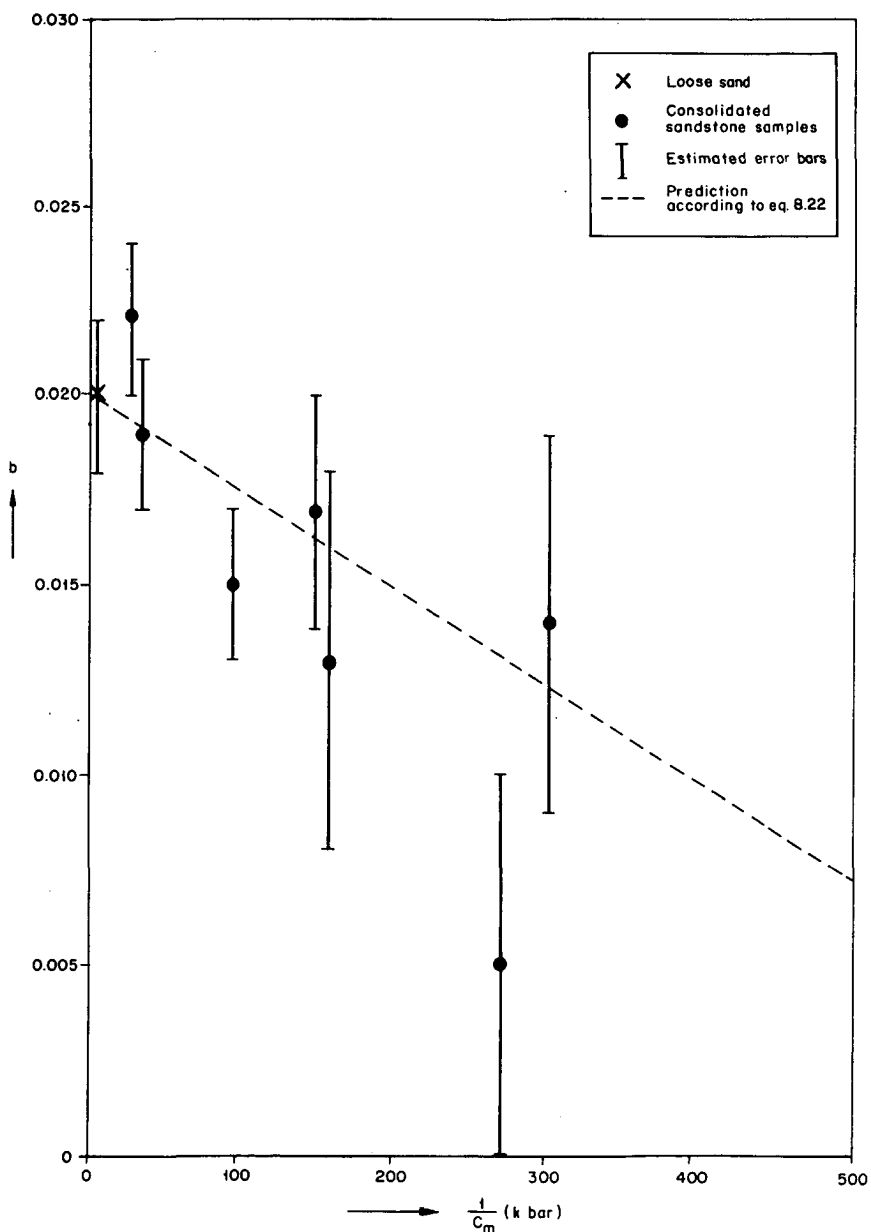
FIG.43 MATERIAL CONSTANT b VERSUS UNIAXIAL COMPRESSION MODULUS FOR CONSOLIDATED SANDSTONE SAMPLES.

9. APPLICATION TO FIELD CONDITIONS

9.1 In-situ conditions

When a reservoir is taken into production, the loading rate of the effective stress exerted on the rock matrix, is suddenly increased from that imposed by the sedimentation process over a geological time span to that induced by the depletion pressure history. The ratio between geological and depletional loading rate is of the order of $10^4 - 10^7$. This will therefore have a large influence on in-situ compaction behaviour if the rate effects observed at laboratory loading rates also occur at geological and depletional loading rates.

The present laboratory experiments have been carried out at loading rates between 0.62 and 4000 bar/h. Whether or not the observed rate effects are also present to the same extent under field conditions, can only be verified by comparing predictions based on the RTCM and laboratory measurements with actual field data. To this end, the problem of simulating changes in loading rate of up to 10^7 in the laboratory (corresponding to the upper limit of the change from geological to depletional loading rate in the field) has to be considered.

9.2 Laboratory simulation of large changes in loading rate

If the observed rate effects upon a sudden increase in loading rate also occur under field conditions, increases in loading rate of up to 10^7 should be applied in the laboratory experiments at the approximate initial in-situ effective stress as discussed in section 9.1. This is experimentally almost impossible. There is a relatively simple solution for this problem however. As discussed in detail in sections 6 and 7, the compaction behaviour after a change in loading rate is completely determined by the (normalised) position of the initial (ϵ_z, σ_z) point relative to the (normalised) virgin compaction curve corresponding to a continuous constant loading at the new loading rate. In addition it does not matter how this initial (ϵ_z, σ_z) point was reached (Fig. 32).

Hence the compaction behaviour caused by a change in loading rate from $\dot{\sigma}_{z,1}$ to $\dot{\sigma}_{z,2}$ can be simulated by a reloading curve after an appropriate
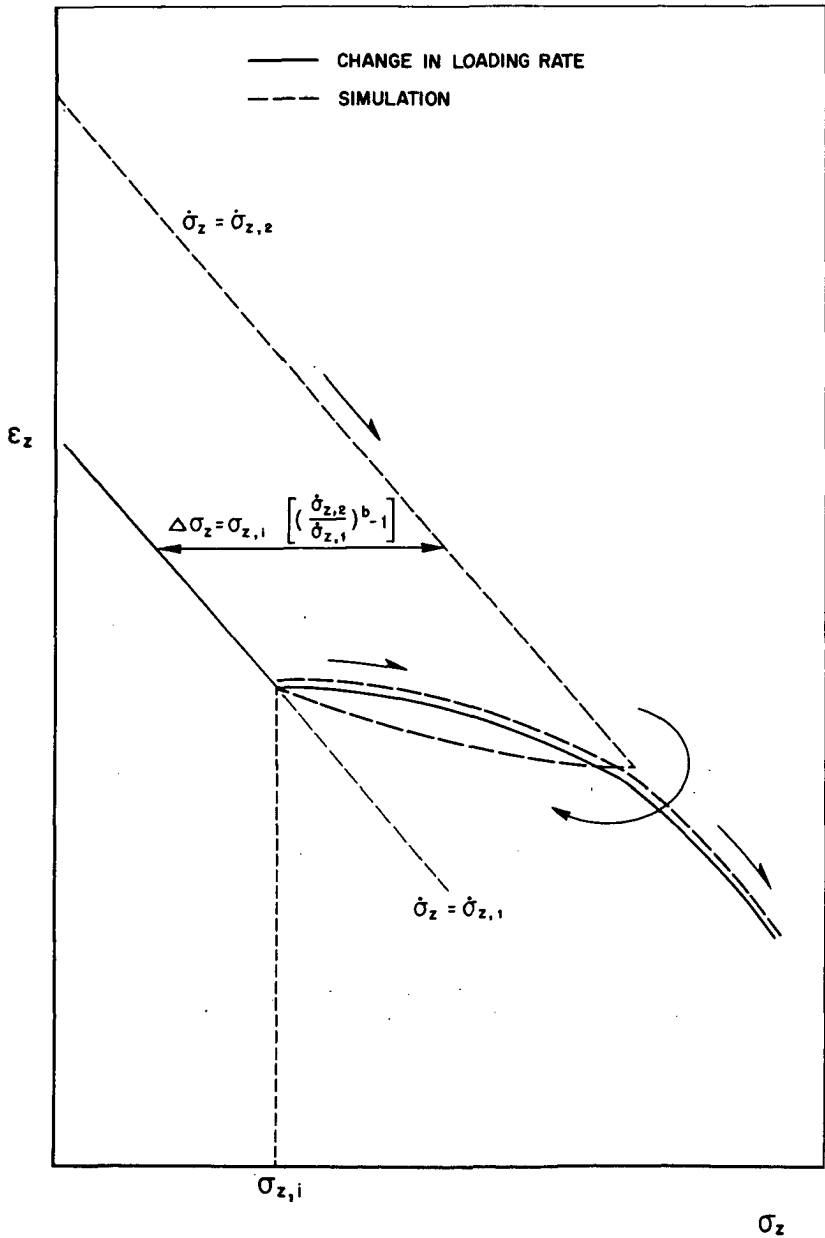
**FIG.44 SIMULATION OF COMPACTION
AFTER AN INCREASE IN LOADING RATE
BY RELOADING AFTER PARTIAL
UNLOADING.**

amount of unloading (Fig. 44). The sample must be unloaded to a pressure $\sigma_{z,i}$ in such a way that the stress difference $\Delta\sigma_z$ between $\sigma_{z,i}$ and the original compaction curve equals that between the continuous loading rate compaction curves at $\dot{\sigma}_{z,1}$ and $\dot{\sigma}_{z,2}$ (Fig. 44). Thus according to equation 7.17:

$$\frac{\Delta\sigma_z}{\sigma_{z,i}} = [\;(\;\frac{\dot{\sigma}_{z,2}}{\dot{\sigma}_{z,1}}\;)^b - 1]\qquad\qquad(9.1)$$

The loading rate of this laboratory experiment is not important, provided it is kept equal before and after partial unloading. From such experiments the part of the general compaction curve corresponding to changes in loading rate larger than a factor of 10^4 has been determined.

The above procedure can be used to determine the shape of the general compaction curve down to values of $\sigma_z/\sigma_{z,o} \simeq 0.8$, corresponding to changes in loading rate of the order of 10^7 (depending on the value of b). For larger amounts of unloading a different compaction behaviour results which is not described by the general compaction curve. This is illustrated in Fig. 45, where the reloading behaviour of a friable sandstone is shown as a function of the degree of unloading. A similar behaviour is observed for unconsolidated sands (see Fig. 11).

9.3 Prediction of field behaviour

For a prediction of field compaction based on the RTCM, we must know the transition zone that will arise upon a change in loading rate from the geological value $\dot{\sigma}_{z,geol}$ to the depletional value $\dot{\sigma}_{z,dep}$. The geological loading rate is roughly equal to the ratio of the initial effective stress and the age of the reservoir. The depletional loading rate is determined by the production plan. Because of the almost logarithmic relation between $\Delta\sigma_z$ and $\dot{\sigma}_{z,2}/\dot{\sigma}_{z,1}$ (see section 7.3.2), fluctuations in the depletional loading rate are not important. For the same reason several fold differences between the estimated and the actual geological loading rate will only have a small influence on the prediction.

The normalised field compaction behaviour is given by the general compaction curve between the normalised vertical stress values $(\sigma_{z,i}/\sigma_{z,o})$ and $(\sigma_{z,f}/\sigma_{z,o})$ (Fig. 46), where $\sigma_{z,f}$ corresponds to the final in-situ

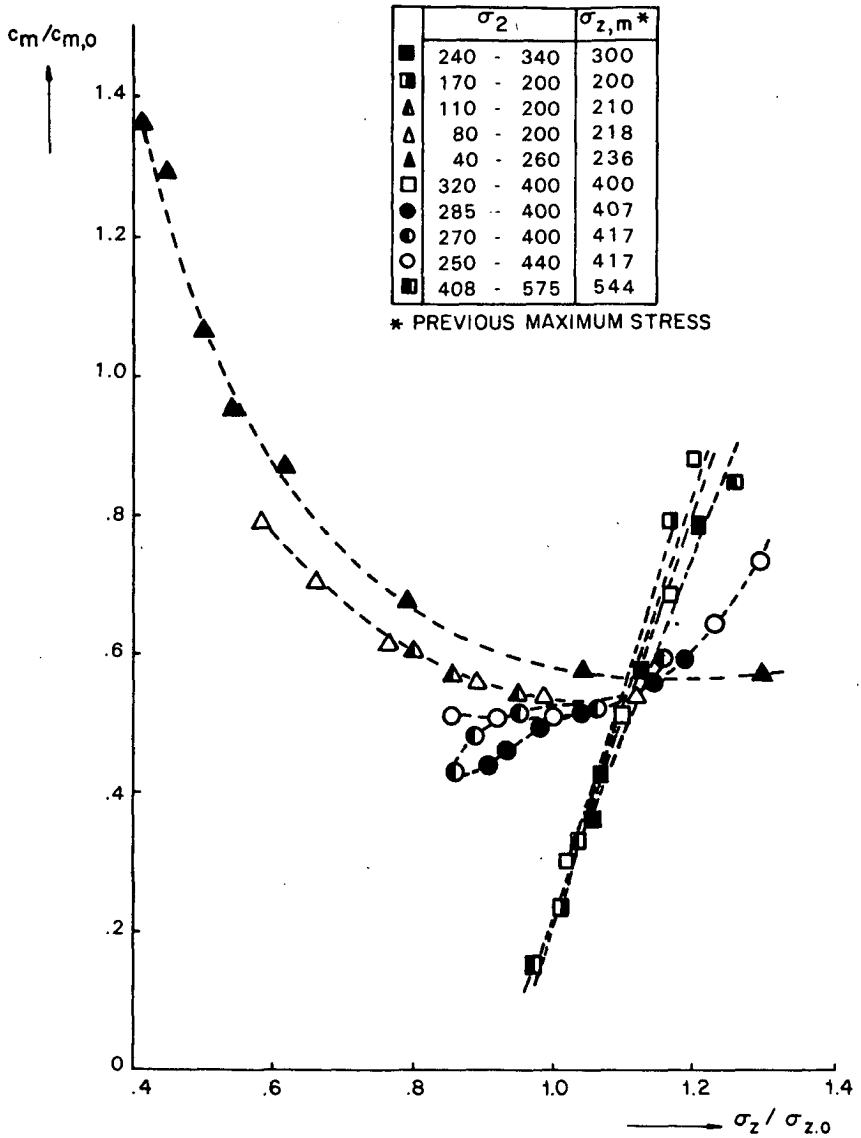|	σ_2		$\sigma_{z,m}$ *
■	240	- 340	300
◨	170	- 200	200
▲	110	- 200	210
△	80	- 200	218
▲	40	- 260	236
□	320	- 400	400
●	285	- 400	407
◐	270	- 400	417
○	250	- 440	417
▣	408	- 575	544

* PREVIOUS MAXIMUM STRESS

FIG.45 DIMENSIONLESS RELOADING
COMPRESSIBILITY OF FRIABLE
SANDSTONE VERSUS DIMENSIONLESS
RELOADING PRESSURE FOR VARIOUS
DEGREES OF UNLOADING

vertical effective stress (after depletion). The non-normalised prediction is obtained by multiplying the normalised compaction and normalised vertical stress axes by the appropriate values of $(c_{m,o}\sigma_{z,o})$ and $\sigma_{z,o}$ respectively.

Hence, the reservoir compaction at a certain value of the reservoir pressure drop Δp is given by:

$$\frac{\Delta h}{h} = c_{m,o}(\text{field})\ \sigma_{z,o}\ [H(x) - H(x_i)] \qquad\qquad (9.2)$$

where $x = \sigma_z/\sigma_{z,o}$, $x_i = \sigma_{z,i}/\sigma_{z,o}$, $\sigma_z = \sigma_{z,i} + \Delta p$, and $H(x) =$ the general compaction curve given by Fig. 46, for which an algebraic fit has been given in equation (7.1). The determination of b, $c_{m,o}$ and $\sigma_{z,o}$ is discussed below.

9.3.1 Determination of the material constant b

As discussed in section (7.3.2), the value of the material constant b, which characterises the relative width $\Delta\sigma_z/\sigma_{z,1}$ of the transition zone, and which is required for the calculation of $c_{m,o}(\text{field})$ and $\sigma_{z,o}$, can be determined from the compaction behaviour in laboratory experiments after an increase or decrease in loading rate. In practice, the loading rate is usually switched between two values, differing by one to two orders of magnitude, allowing the determination of the corresponding two virgin compaction curves (see Figs. A6, A11 and A13-A15).

9.3.2 Determination of the virgin field compressibility

For $c_{m,o}$ the virgin field compressibility must be used. Owing to the difference in loading rate between reservoir depletion and laboratory measurement, the value of $c_{m,o}$ measured in the laboratory must be corrected according to:

$$c_{m,o}(\text{field}) = (\dot\sigma_{z,\text{lab}}/\dot\sigma_{z,\text{dep}})^b\ c_{m,o}(\text{lab}) \qquad\qquad (9.3)$$

which is based on equation (7.20).

From the experiments discussed in section 4.3 it can be concluded that the value of $c_{m,o}$, measured during the first laboratory loading cycle on relatively undisturbed core samples, should be used in equation (9.3). This has been further confirmed by comparison of actual field compaction behaviour and predictions based on the RTCM (see section 10).

9.3.3 Determination of the normalisation stress

The normalisation stress $\sigma_{z,o}$ is determined in the following way. The normalised stress $\sigma_{z,i}/\sigma_{z,o}$ corresponding to the initial in-situ state must satisfy equation (7.17), hence:

$$\frac{(\Delta\sigma_z/\sigma_{z,o})}{(\sigma_{z,i}/\sigma_{z,o})} = \left[\left(\frac{\dot{\sigma}_{z,dep}}{\dot{\sigma}_{z,geol}}\right)^b - 1\right] \tag{9.4}$$

For a given point A on the general compaction curve, the denominator and the numerator of the left hand side of equation (9.4) are indicated in Fig. 46. Hence, the right hand side of equation (9.4) can be calculated. This calculation has been made for every point of the general compaction curve. The result is shown in Fig. 47 and can be approximated by the following algebraic fit:

$$\sigma_{z,o} = \frac{\sigma_{z,i}}{1.4 - 0.804 \, y^{0.314}} \tag{9.5}$$

with: $y = (\dot{\sigma}_{z,dep}/\dot{\sigma}_{z,geol})^b - 1$

9.3.4 The effect of previous deeper burial

Some reservoirs have been buried deeper in the past than they are at present. According to the conceptual model the effects of this previous deeper burial ("overconsolidation") and rate effects will accumulate. The situation is depicted in Fig. 48. The appropriate initial point in the normalised compaction curve in such a case should be determined graphically, using the laboratory compaction curves, as the position of this point is influenced by the unloading behaviour of the material. In addition there will be an influence of rate effects on its position if the loading rate during the overconsolidation period is considerably different from the average geological loading rate (e.g. overconsolidation resulting from ice coverage during ice ages). The effect of overconsolidation can in first approximation be taken into account by replacing $\sigma_{z,i}$ in equation (9.5) by $\sigma_{z,i} + \Delta\sigma_{z,oc}$.
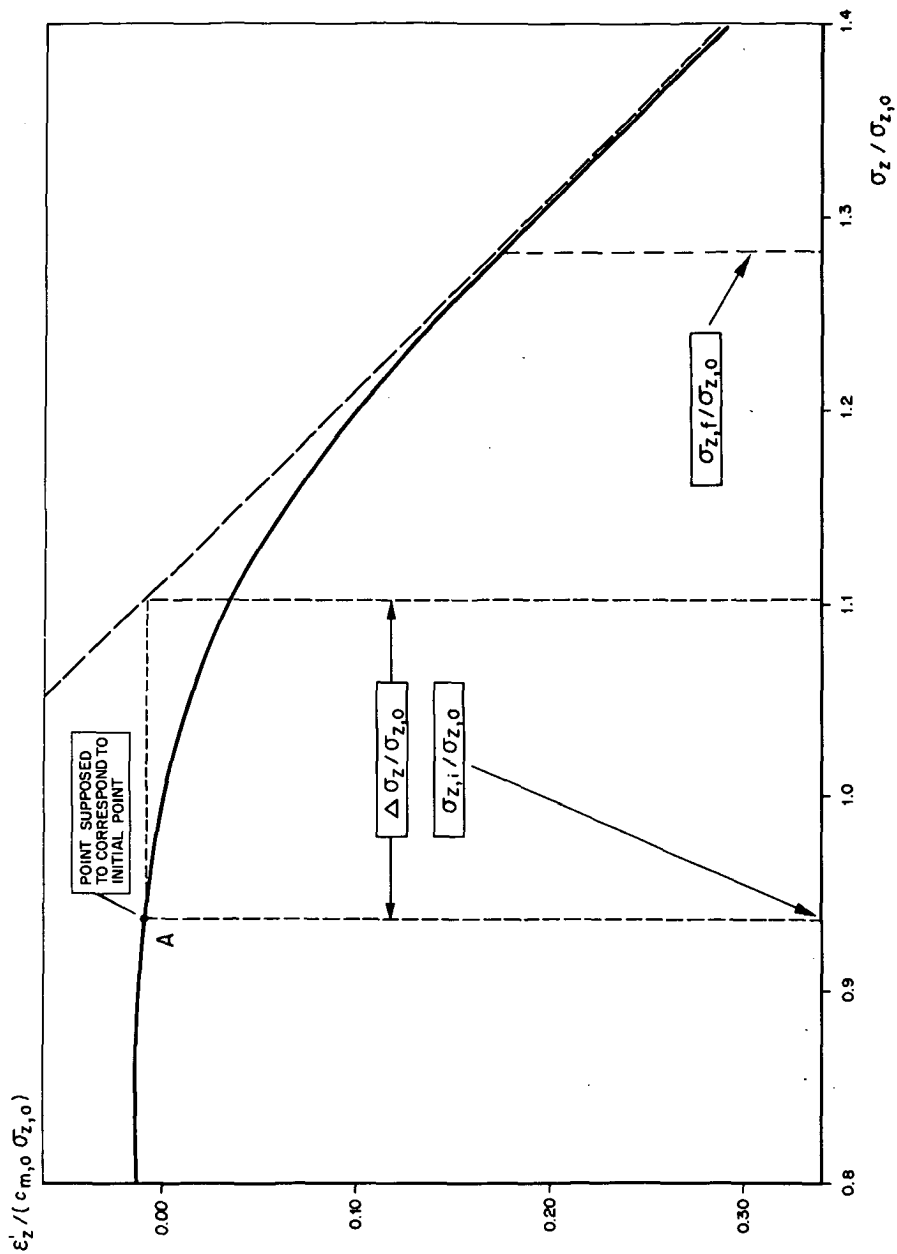
FIG.46 PREDICTION OF FIELD BEHAVIOUR USING THE GENERAL COMPACTION CURVE
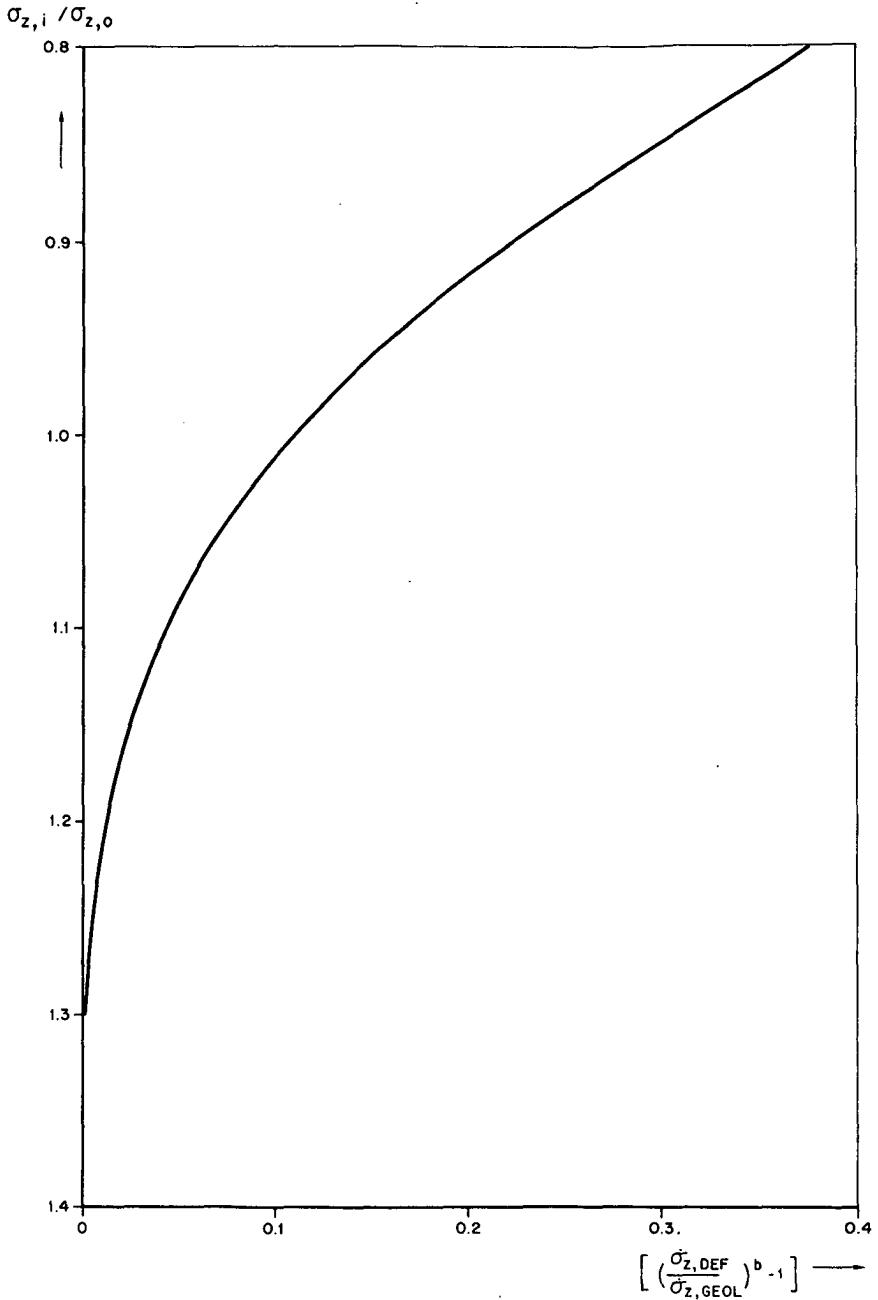
FIG.47 $\sigma_{z,i}/\sigma_{z,o}$ AS A FUNCTION OF $\Delta\,\sigma_z/$
$\sigma_{z,i}$ DETERMINED GRAPHICALLY FROM
THE GENERAL COMPACTION CURVE.

$\dot{\sigma}_z = \dot{\sigma}_{z,2}$

$\dot{\sigma}_z = \dot{\sigma}_{z,1}$

$\Delta \sigma_z$

$\Delta \sigma_{z,oc}$

ϵ_z

$\sigma_{z,i}$ $\sigma_{z,i} + \Delta\sigma_{z,oc}$ σ_z

FIG.48 EFFECT OF OVERCONSOLIDATION

9.4 Relation between reservoir compaction and surface subsidence

The observed non-linear compaction behaviour will have an influence on the relation between reservoir compaction and surface subsidence. To fully evaluate this, a 3-D rate type compaction equation would be required, but such an equation is not available at present. The magnitude of the effect is expected to be limited, as most deformation will only occur in the reservoir and its immediate surroundings. This suggests that elastic models based e.g. on the nucleus of strain approach as discussed in section 2.1.2, can still be used to calculate subsidence from compaction. This assumption is confirmed by the field evidence discussed in section 10.

9.5 Comparison between the RTCM and the linear compaction model

The new compaction model is more complex than the linear compaction model. For a worst case prediction the linear model is still applicable because it appears in practice that the compaction according to the new model is less than that predicted on the basis of the linear model (using first cycle laboratory compressibilities). This is caused by the relatively small amount of compaction in the transition zone. A schematic comparison of an old and a new prediction is given in Fig. 49. In that figure, also the extrapolation of early compaction or subsidence measurements is sketched. It is clear that such an extrapolation would lead to an under-estimation of ultimate compaction and subsidence. Use of the linear model on the other hand would lead to a too pessimistic estimate. For an accurate prediction, therefore, application of the new model, although more elaborate, is essential.

PACTION

START OF DEPLETION

ABANDONMENT
CONDITION

LINEAR EXTRAPOLATION
OF EARLY FIELD
MEASUREMENTS

REAL FIELD BEHAVIOUR
(RTCM)

PREDICTION ACCORDING TO CLASSICAL LINEAR
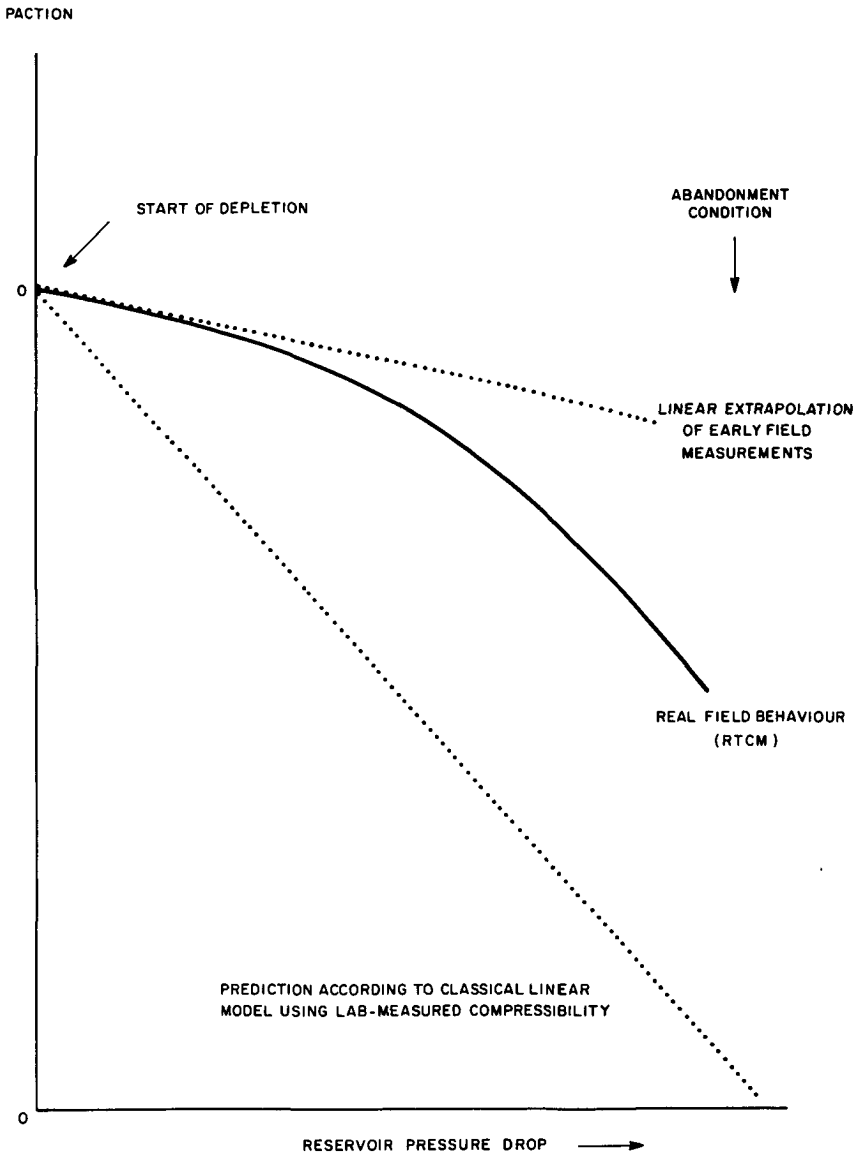MODEL USING LAB-MEASURED COMPRESSIBILITY

RESERVOIR PRESSURE DROP ⟶

FIG.49 CONSEQUENCES OF NON-
LINEARITY DUE TO STRESS-RATE
EFFECTS FOR THE PREDICTION OF
FIELD COMPACTION

10. COMPARISON WITH ACTUAL FIELD DATA

To accurately test the applicability of the RTCM under field conditions, data on the earliest stages of field development are required. For Bachaquero, Tia Juana, Wilmington and Groningen such data are available and for these fields a detailed comparison has been made between the observed field behaviour and that predicted by the RTCM. The following criteria were used:

1. Comparison of the observed (normalised) field data with the laboratory derived general compaction curve.

2. Comparison of actual and predicted subsidence bowl volume.

3. Comparison of actual and predicted transition zone width.

4. Comparison of predicted and field derived uniaxial compressibility $c_{m,o}$.

The obtained results, fully confirming the applicability of the RTCM under field conditions, are discussed in detail in the following paragraphs.

10.1 Bolivar Coast

Several studies have been undertaken to investigate the compaction behaviour of the Bolivar Coast oil reservoirs (v.d. Knaap and v.d. Vlis, 1967; Merle et al, 1975; Nunez and Escojido, 1977; Schenk and Puig, 1983; Perez and Toscaz, 1984). Recently a complete re-analysis has been made of all available Bachaquero field data, resulting in a more consistent description of the reservoir compaction. Two anomalies remained however as mentioned in section 3:

1. The occurrence of transition zones in which the compressibility increased during the initial stage of reservoir depletion (Fig. 7).

2. In-situ compaction calculations based on the 1972 subsidence and pressure data show a strong compressibility contrast between depleted (oil-bearing) and less depleted (partially water-bearing) sands in Bachaquero (Fig. 8).

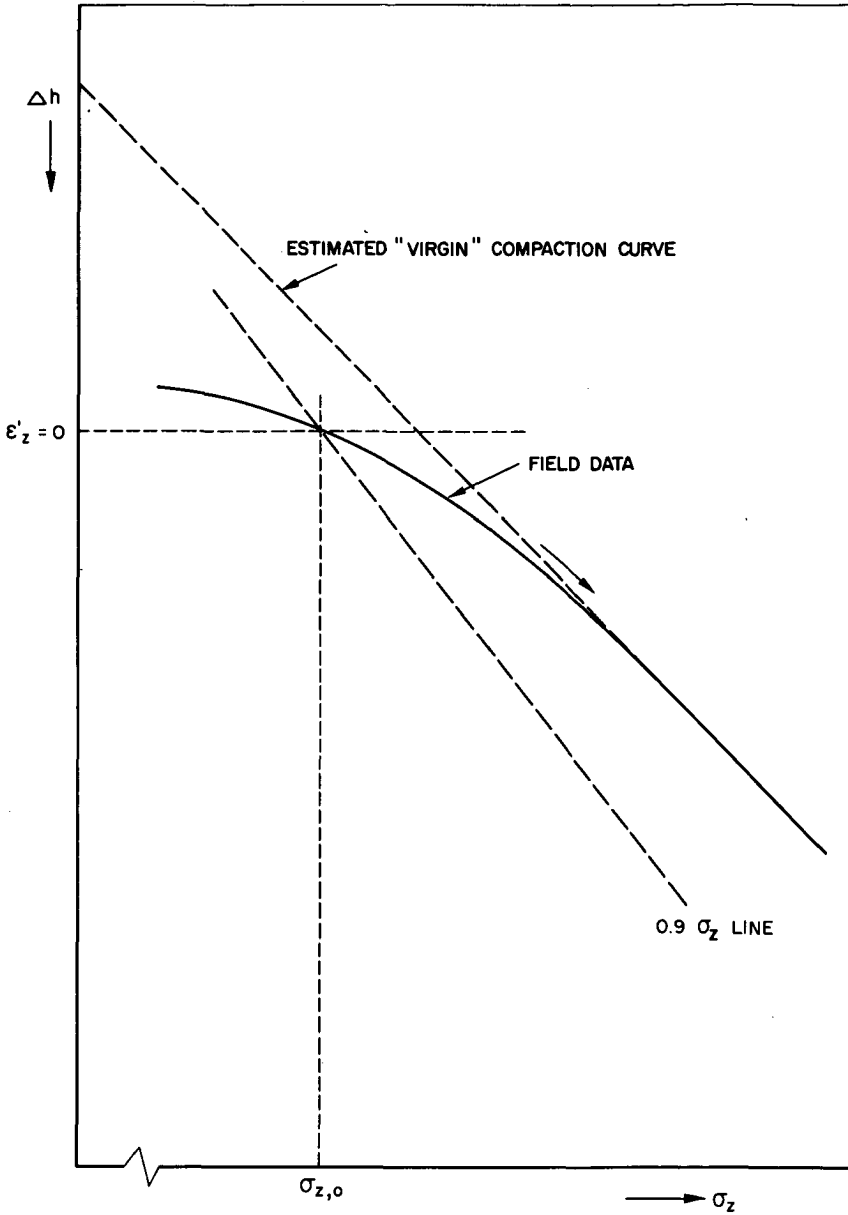Both these anomalies are explained by the RTCM as will be shown below.

FIG.50 DETERMINATION OF $\sigma_{z,o}$ FROM FIELD DATA

10.1.1 Transition zones

The compaction behaviour in the transition zones as shown in Fig. 7 is similar to that observed in the laboratory experiments upon suddenly increasing the loading rate. For example, when normalising and plotting the Bachaquero compaction behaviour of block PP6 (Fig. 7), according to the procedure described in section 7.1 (see Fig. 50), good agreement with the laboratory derived general compaction curve is obtained (Fig. 51). A similar result was obtained for Tia Juana (Fig. 52).

In Bachaquero, the observed width of the transition zone increases linearly with increasing depth, i.e. with the initial effective vertical stress as shown in Fig. 53. Also shown is the theoretical line calculated with equation (7.17) assuming a b value of 0.020 and using the value of 5×10^4 for the ratio of depletional over geological loading rate (considered to be applicable for Bachaquero).

10.1.2 Compressibility contrast between oil and water sands

The compressibility contrast between the oil-bearing and the water-bearing sands observed in 1972 can be explained with the new model, when taking the variation of relative depletion with depth at that time into account. In the shallower oil-bearing blocks, the effective stress ratio $\sigma_z/\sigma_{z,i}$ at that time was 1.4 to 1.6. In the deeper, partly water-bearing blocks near the oil water contact, $\sigma_z/\sigma_{z,i}$ dropped rapidly to unity (Fig. 54). Low $\sigma_z/\sigma_{z,i}$ values were also present in some very shallow blocks, but as no subsidence data are available for these blocks, these data could not be used for further analysis.

First consider the consequences for a shallow block ($\sigma_z/\sigma_{z,i}$= 1.5). The 1972 state of such a block is represented by point B in Fig. 55. According to the new RTCM, the intermediate stress/strain path is given by the segmented line A-D-B. Future compaction will proceed along B-C. As a result, compressibilities for the shallow blocks in 1972 were of the same order of magnitude as predicted on the basis of conventional laboratory experiments. In fact, in Bachaquero the intermediate stress/strain path was assumed to be represented by the dotted line A-B'.

Next consider the situation for a deeper block near the oil-water contact. The 1972 state of such a block is represented by point D in Fig. 55 ($\sigma_z/\sigma_{z,i}$= 1.2). Therefore, its 1972 compressibility is much less than expected on the basis of the conventional laboratory experiments.

The change in compressibility with stress for a given block as predicted by the RTCM is shown in Fig. 56. The final compressibility has

been taken equal to the average first cycle laboratory measured $c_{m,o}$ value for Bachaquero, corrected for the difference between the laboratory and the field loading rates (equation 9.3).

The 1972 compressibility as a function of depth (or initial vertical effective stress) as calculated with the RTCM is shown in Fig. 57. Also shown are the field derived compressibilities for that date. From the excellent agreement between calculated and observed compressibilities it can be concluded that the inferred compressibility contrast between oil-bearing and water-bearing sands did exist in 1972 but also that it was only a result of the fact that the blocks near the oil water contact were less depleted at that time.

10.2 Wilmington

As discussed in section 3, the field subsidence behaviour of Wilmington is strongly non-linear (Helm, 1984). Application of a linear compaction model resulted in a too large subsidence prediction. Furthermore, the observed subsidence bowl is much more restricted to the central region of the field than was predicted. A non-linear model of the cap-type had to be introduced to properly describe the observed subsidence behaviour (Kossloff and Scott, 1980b).

The cap-type material behaviour is fully explained by the RTCM. The width of the transition zone taken in the cap-model appears to lie in the same order of magnitude as the value predicted by the RTCM (for most blocks approximately 0.3 times the initial effective stress). Moreover the RTCM predicts that the outer region of the field, which is less depleted than the center, will be compacted much less because of the non-linear form of the general compaction curve. As in the Bolivar Coast, the observed field compressibility after the transition zone became more or less equal to the laboratory measured first cycle uniaxial compressibility (Kossloff and Scott, 1984b).

Finally, excellent agreement exists between the normalised subsidence behaviour of a typical benchmark (derived from Lee, 1978) and the general compaction curve of the RTCM as shown in Fig. 58.

10.3 Groningen

Application of a linear compaction model for the Groningen gas field,
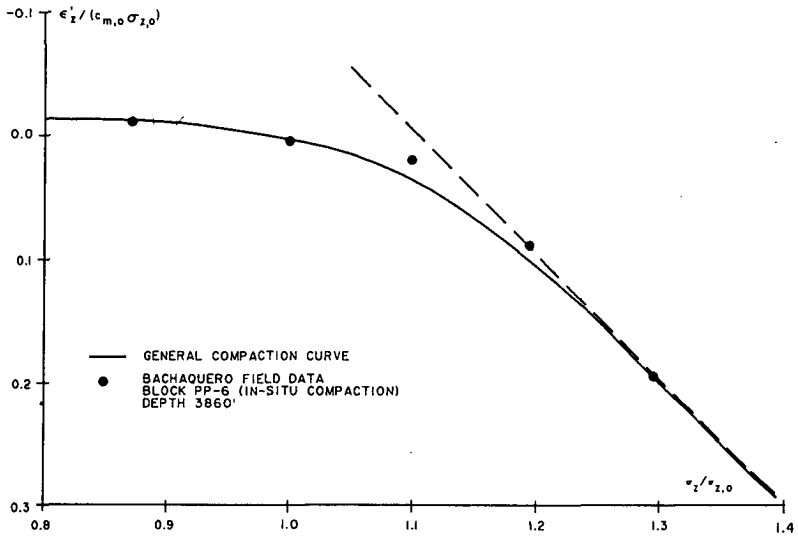
FIG.51 COMPARISON BETWEEN
GENERAL COMPACTION CURVE AND
BACHAQUERO FIELD DATA
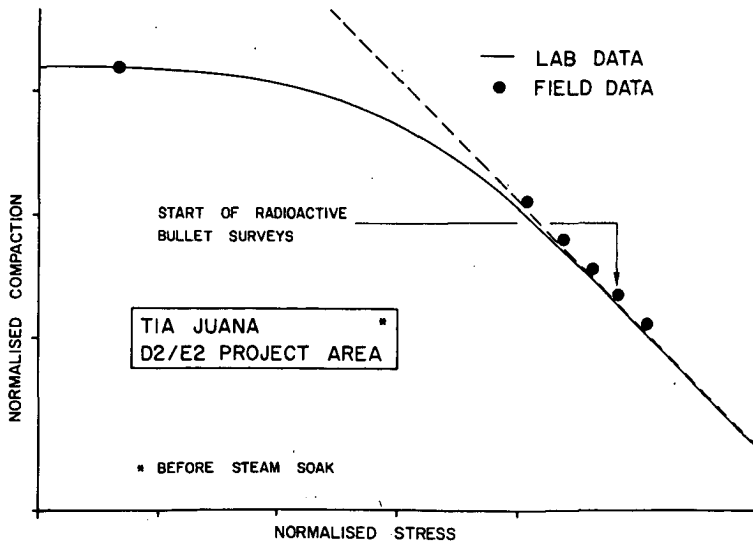
FIG.52 COMPARISON BETWEEN
GENERAL COMPACTION CURVE AND
THE TIA JUANA FIELD DATA
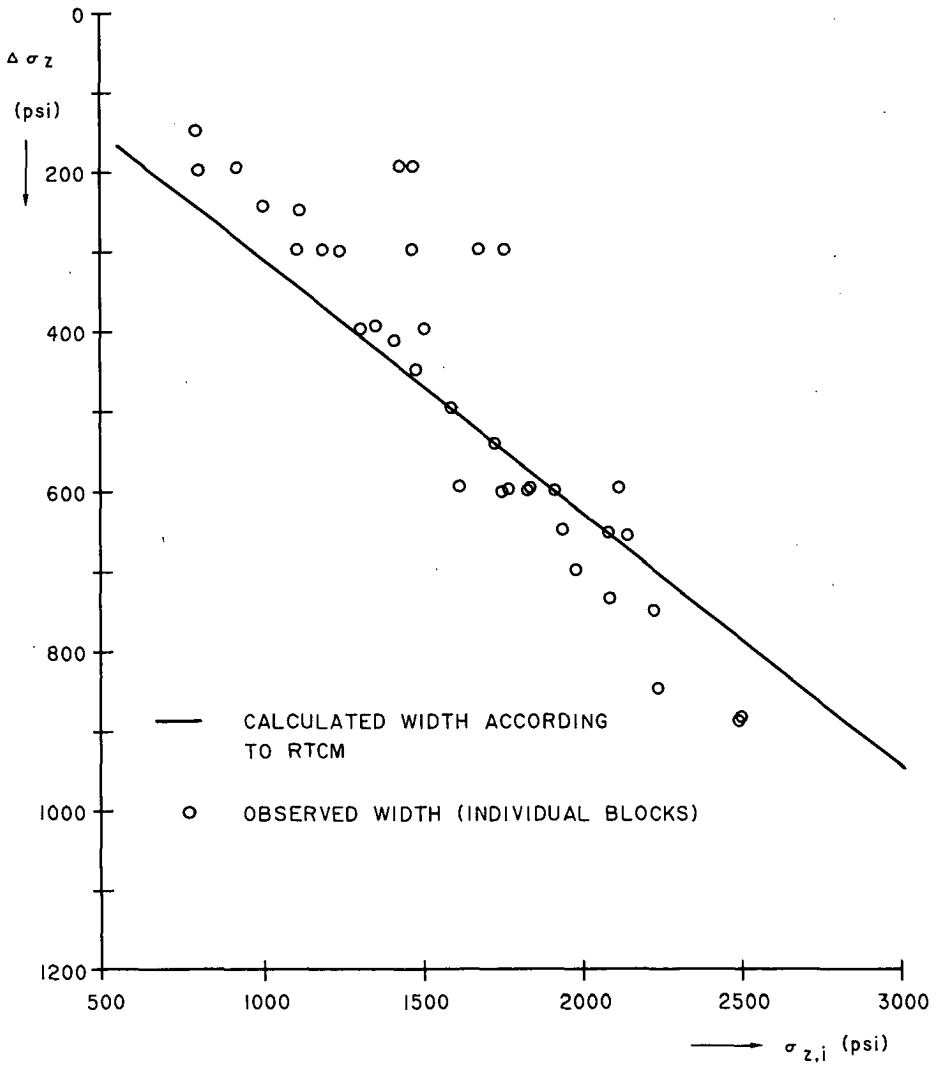
FIG.53 BACHAQUERO: CALCULATED AND OBSERVED WIDTH OF TRANSITION ZONE AS A FUNCTION OF INITIAL EFFECTIVE STRESS
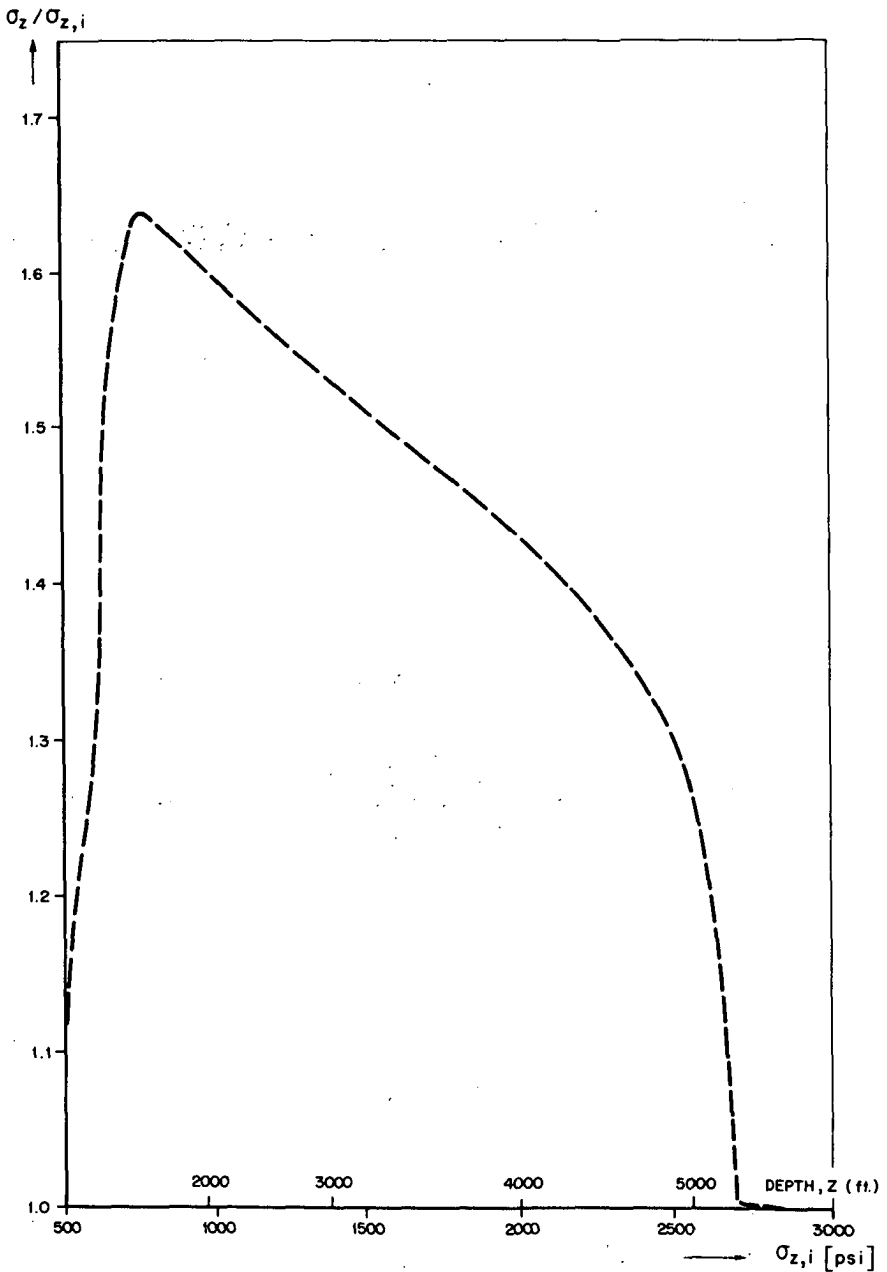
FIG.54 BACHAQUERO: RATIO OF
EFFECTIVE STRESS IN 1972 AND
INITIAL EFFECTIVE STRESS ($\sigma_z/\sigma_{z,i}$)
VERSUS INITIAL EFFECTIVE STRESS ($\sigma_{z,i}$)
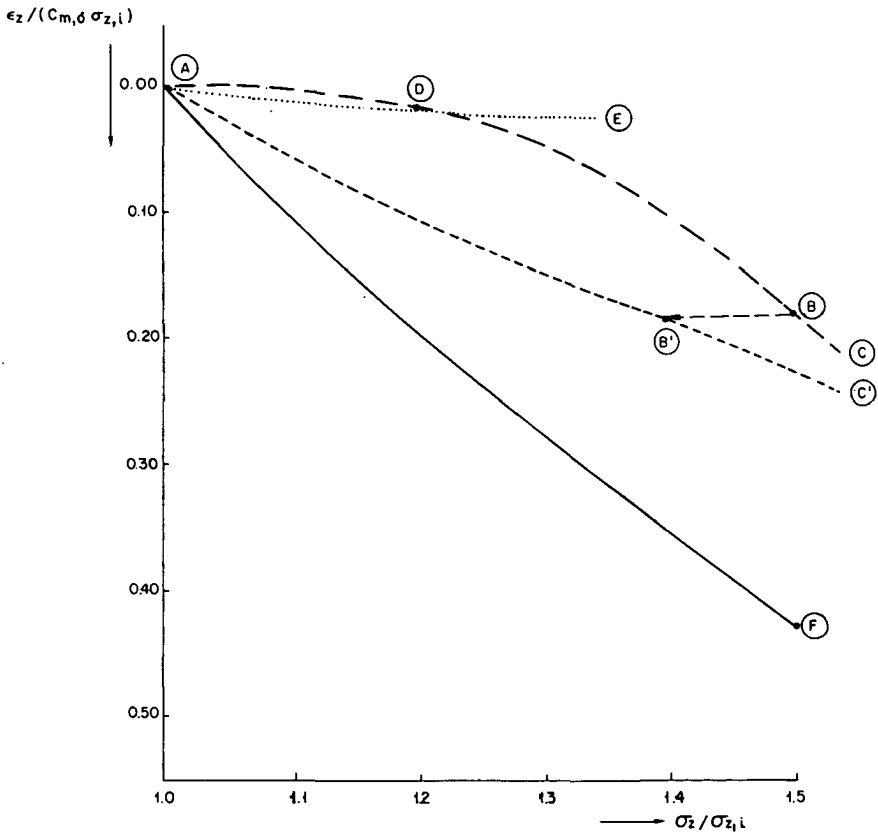
FIG.55 BACHAQUERO: COMPARISON
BETWEEN REAL AND APPARENT FIELD
BEHAVIOUR
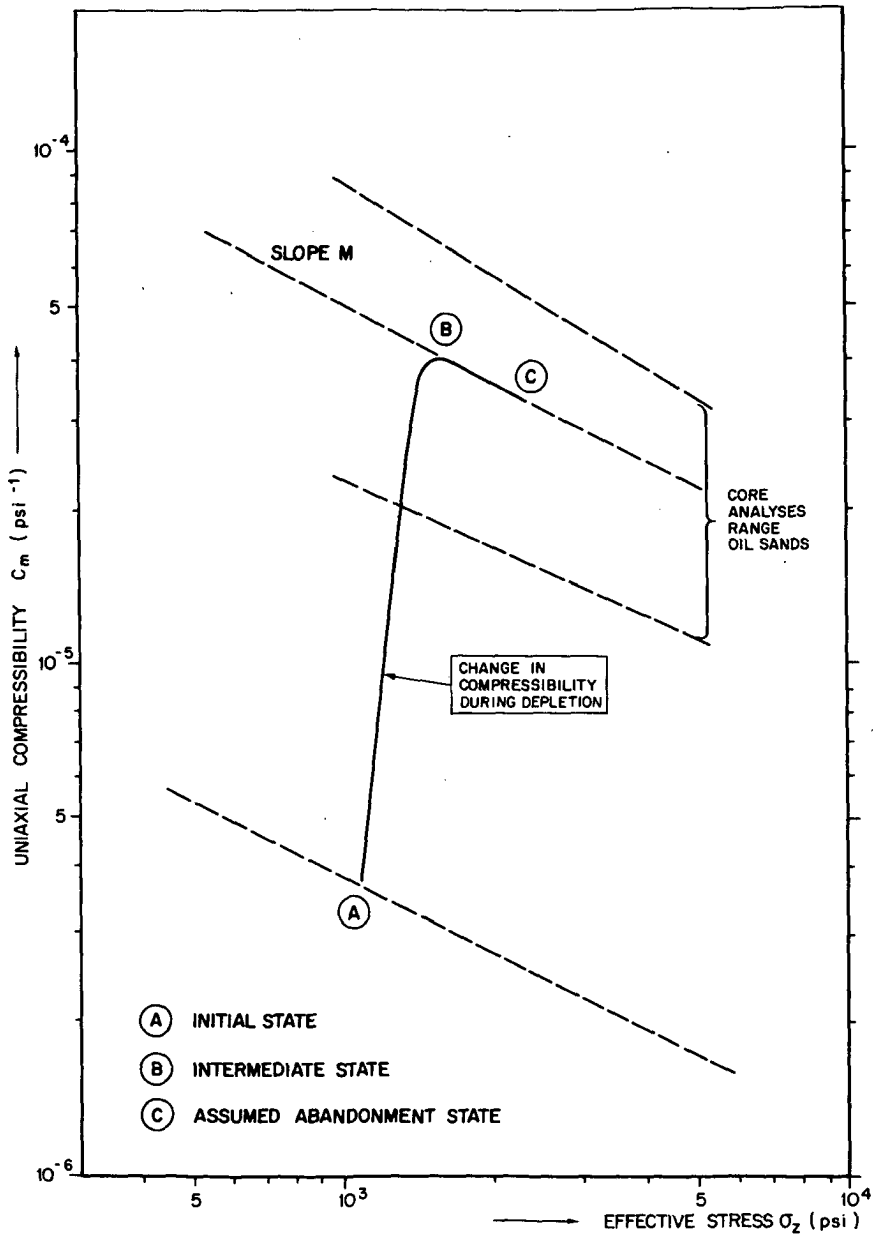
FIG.56 BACHAQUERO: EXAMPLE OF
CHANGE IN COMPRESSIBILITY DURING
DEPLETION (AT A GIVEN DEPTH)
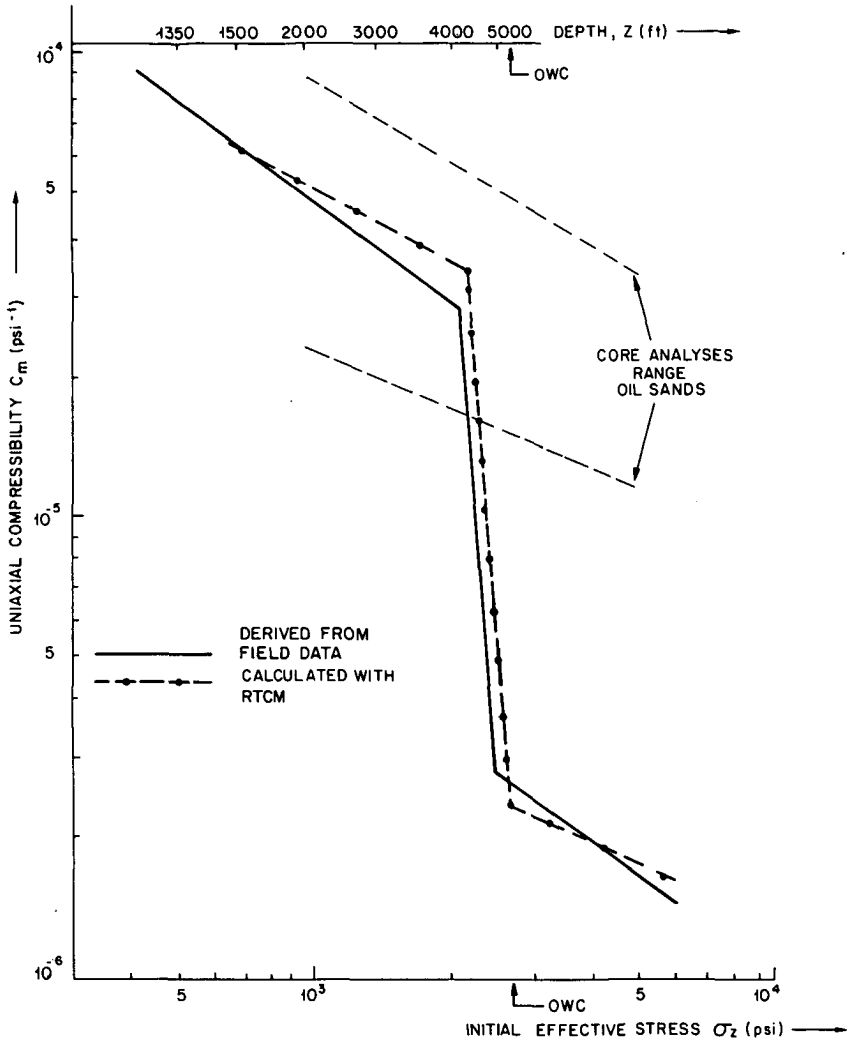
FIG.57 BACHAQUERO: COMPARISON OF
OBSERVED 1972 COMPRESSIBILITIES
WITH THOSE PREDICTED BY THE RTCM
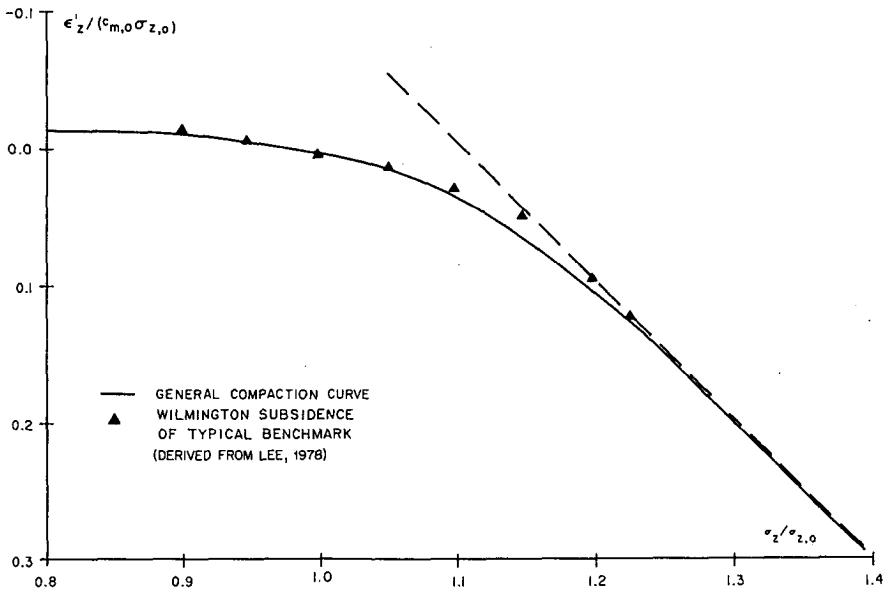
FIG.58 COMPARISON BETWEEN
GENERAL COMPACTION CURVE AND
WILMINGTON FIELD DATA

resulted in a predicted maximum subsidence of approximately 100 cm at the end of the production period (Geertsma and van Opstal, 1973). In 1974 this prediction was modified because linear extrapolation of early field subsidence measurements appeared to indicate a maximum subsidence of 30 cm only (Schoonbeek, 1976). The discrepancy was attributed to sample disturbance. Recently, the actual subsidence started to deviate again, resulting in 1984 in an actual subsidence some 15% larger than predicted on the basis of the linear extrapolation of the early field data.

By that time the RTCM had been developed at KSEPL for unconsolidated sands. During 1983 and 1984, its applicability could be tested on consolidated sandstone samples from new cores taken from the Groningen reservoir in 1983, using the improved triaxial compaction equipment described in section 5.4. The results obtained confirmed the applicability of the RTCM for the Groningen reservoir rock under laboratory conditions. In addition they confirmed the previously established porosity-constant loading rate compressibility relationship (van Kesteren, 1973) as shown in Fig. 59. Subsequently the RTCM was used to predict the Groningen field behaviour.

To this end the RTCM was built into the existing program to calculate the surface subsidence above the Groningen reservoir (which is based on the stiff basement nucleus of strain approach, see section 2.1.2). Obtained results show an excellent agreement between the observed field behaviour and that calculated straightforward on the basis of the laboratory measurements and the RTCM (without the need to introduce any adjustments):

1. The discrepancies between the observed field behaviour and the previous predictions (Geertsma and van Opstal, 1973; Schoonbeek, 1976) are fully explained by the RTCM.
2. An excellent fit is obtained between calculated and observed subsidence bowl volume as shown in Fig. 60 (data prior to 1980 is not used as the data scatter becomes too large before that date).
3. The calculated 1984 contour lines are in good agreement with those observed. This becomes even more clear when comparing calculated and (smoothed) observed subsidence along a north-south and an east-west cross section through the field as shown in Fig. 61. Remaining differences can be fully explained from the expected inaccuracy in the levelings (5 - 10 mm) and remaining uncertainties in the prediction.

Based on the RTCM a maximum subsidence between 60 and 70 cm is now predicted at the end of the production period.

GRONINGEN

R = 0.73   95 % CONF. LIMITS

A = $-8.70 * 10^{-1}$ N = 65

B = $1.41 * 10^{-1}$

○   TEEUW

×   EKL-12

△   ZDP-12

■   AVERAGE VALUE FOR THE SAMPLES MEASURED BY TEEUW

+   AVERAGE VALUE FOR EKL-12

●   AVERAGE VALUE FOR ZDP-12

UNIAXIAL COMPRESSIBILITY (10^{-5} bar^{-1})

ATMOSPHERIC POROSITY (%)
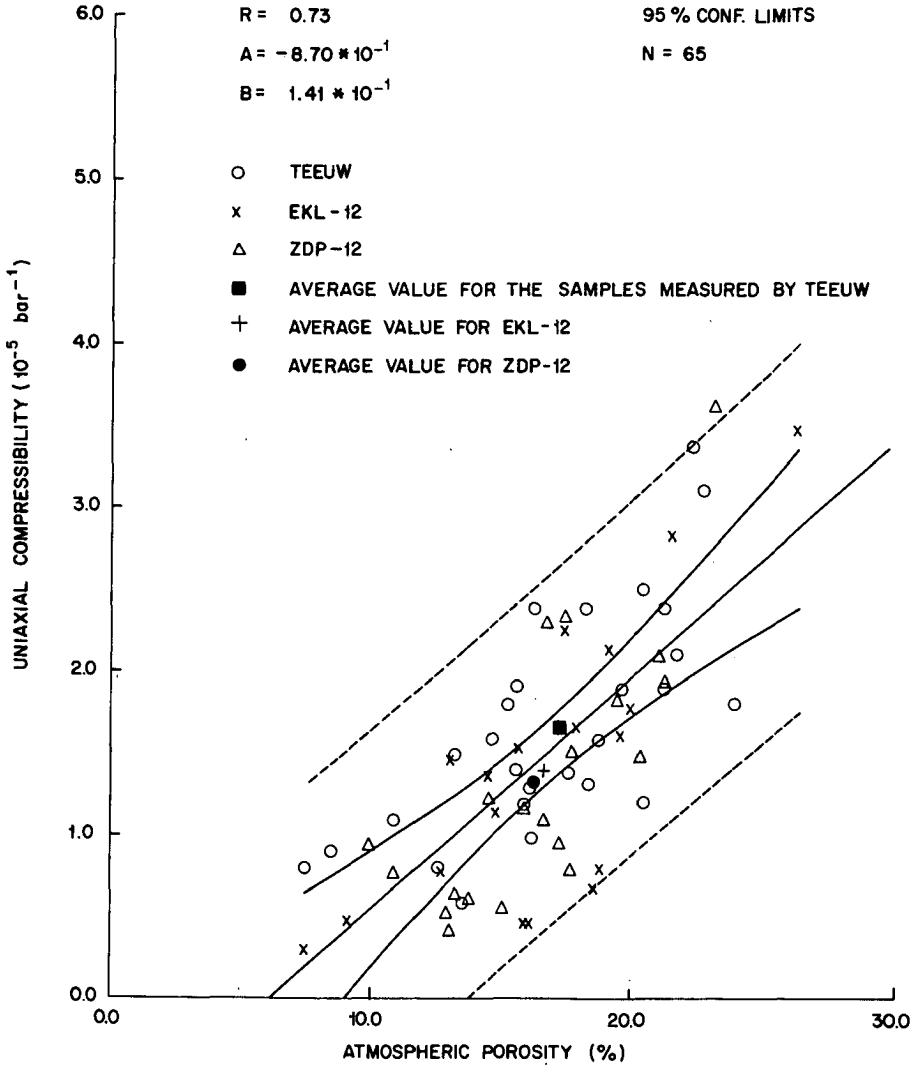
FIG.59 UNIAXIAL COMPRESSIBILITY VERSUS ATMOSPHERIC POROSITY FOR THE ZDP-12, EKL-12 AND PREVIOUS GRONINGEN SAMPLES

VOLUME OF SUBSIDENCE BOWL
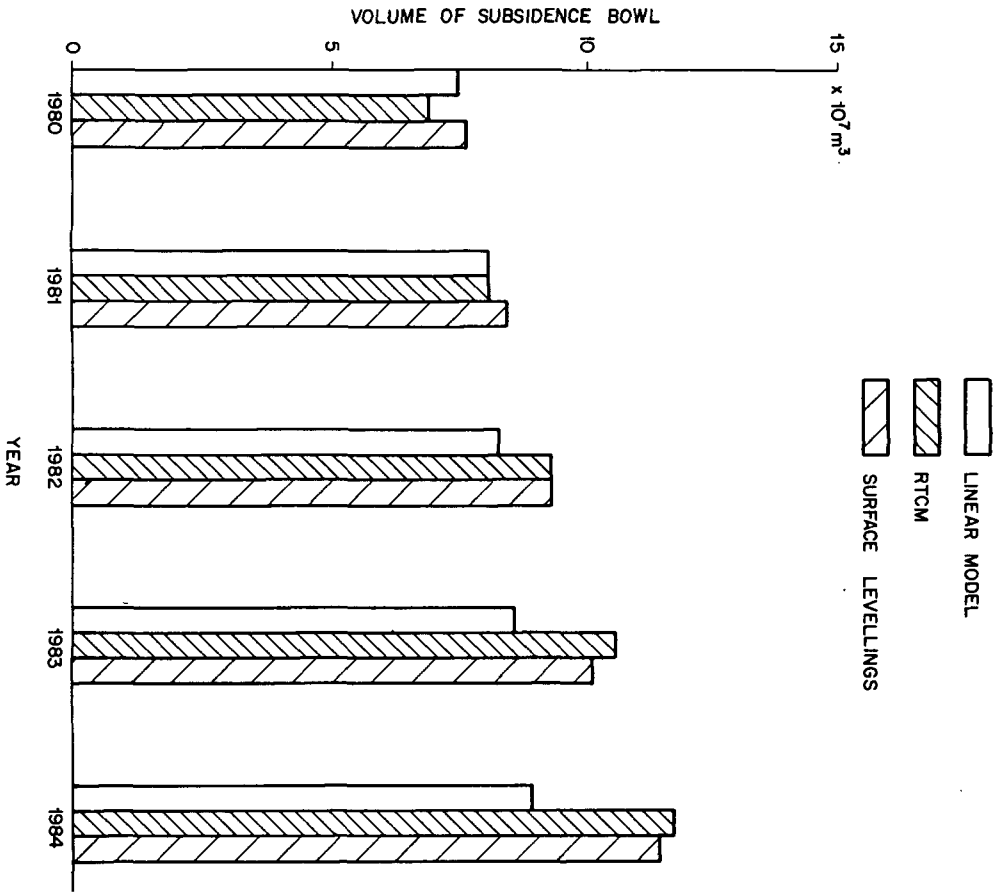
FIG.60 MEASURED AND CALCULATED
VOLUMES OF THE SUBSIDENCE BOWL
OF THE GRONINGEN GAS FIELD.

LINEAR MODEL

RTCM

SURFACE LEVELLINGS
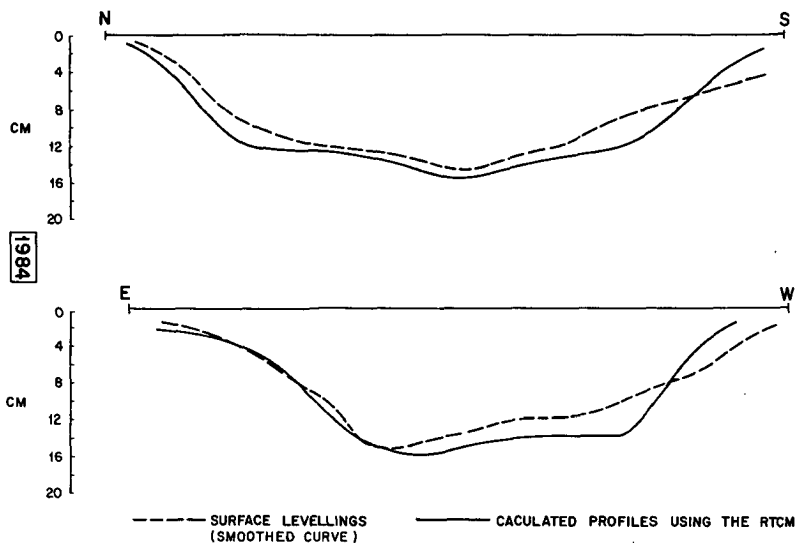
FIG.61 NORTH-SOUTH AND EAST-WEST
PROFILES OF MEASURED AND
CALCULATED SURFACE SUBSIDENCE
OF THE GRONINGEN GAS FIELD

10.4 Consequences

From the above field data it can be concluded that rate effects under field conditions are both qualitatively and quantitatively equal to those observed in the laboratory. The RTCM in combination with laboratory measurements of b and $c_{m,o}$ should therefore be used to obtain accurate predictions of reservoir compaction and surface subsidence. The field data also show that first cycle laboratory compressibility values should be used.

In addition, the RTCM should be used to evaluate the influence of compaction on production, for which it has too be built into existing reservoir simulators. In fact, further confirmation of the applicability of the RTCM under field conditions has recently been obtained from a comparison of reservoir simulation data and actual reservoir pressures in a Middle East sandstone reservoir.

CONCLUSIONS

1. The present work demonstrates that rate effects in the compaction behaviour of sandstone reservoir rock are far more important than has previously been recognised.

2. Changes in loading rate within a loading cycle, creep and partial unloading strongly influence the compaction behaviour.

3. The influence of creep, partial unloading and changes in loading rate on the compaction behaviour can be interrelated in a simple conceptual model. This shows that sandstone reservoir rock behaves as a rate type material.

4. By applying an appropriate normalisation procedure, the compaction behaviour after changes in loading rate, creep or partial unloading for various sandstone rock types and at various stress levels can be described with one general normalised compaction curve. Conversely this curve can be used to predict the strongly non-linear field behaviour which results from the sudden change from geological loading rate to depletional loading rate at the start of production.

5. The observed rate type effects are described properly by a constitutive equation of the rate type. This equation was derived from a simple model in which time-dependent intergranular friction as reported by Dieterich is taken into account. This equation appears to be a special case of a constitutive equation of the rate type postulated earlier by Kolymbas on empirical grounds.

6. Available field data strongly support the applicability of the rate type compaction model at in-situ conditions. The model also explains the apparent discrepancies observed in the past.

NOMENCLATURE

a	Constant used in the extended rate type compaction equation (7.31)
A	Constant used in Dieterich's friction equation (8.5)
b	Material constant describing the influence of loading rate effects on compaction: see equation (7.17)
b'	Modified version of b, taking into account the effect of grain compressibility: see equation (8.22)
c	Reservoir depth of burial, m
C	Constant used in Dieterich's friction equation (8.5), s^{-1}
c_b	Bulk volume compressibility, bar^{-1}
$c_{b,o}$	Bulk volume compressibility along virgin compaction curve, bar^{-1}
c_m	Uniaxial compressibility, bar^{-1}
$c_{m,o}$	Uniaxial compressibility along virgin compaction curve, bar^{-1}
$c_{m,o}(field)$	Uniaxial compressibility finally reached in the field, bar^{-1}
$c_{m,o}(lab)$	Uniaxial compressibility on virgin compaction curve in constant loading rate laboratory compaction experiments, bar^{-1}
c_r	Rock matrix volume compressibility, bar^{-1}
C_1	Constant used in the loading rate dependent part of the Kolymbas equation (7.3)
D_1, D_2, D_3, D_4	Constants used in section 8.3, D_1 and D_4 are in bar^{-1}, D_2 is in N^{-1}, D_3 is in m^2
e	Total compaction, i.e. bulk strain (see section 8.3)
ė	Time derivative of e, s^{-1}
ė'	Time derivative of ė, s^{-2}
e_n	Matrix compaction component (see section 8.3)
e_s	Compaction component due to intergranular sliding (see section 8.3)
F	Function of ė: equation (8.14)
g	Auxiliary function used in the algebraic fit of the general compaction curve, (see section 7.1)
G	Bulk shear or rigidity modulus, bar
h	Sample height (laboratory) or reservoir thickness (field), m
Δh	Change in sample height (laboratory) or change in reservoir thickness (field), m
H	Algebraic fit of the general compaction curve (equation 7.1)
k	unit vector in z direction
p	Pore pressure, bar
ṗ	Time derivative of p, bar/s
Δp	Change in pore pressure, bar
P	Potential energy, J
R	Reservoir radius, m
$\vec{R}_1, \vec{R}_2, \vec{R}_3$	Distance vectors used in equation (2.5), m
t	Time, s
T	Temperature, K
u	Displacement vector
u	Integration variable used in equation (7.11)
U	Auxiliary variable (see section 7.1)
V_b	Bulk volume, m^3
V_p	Pore volume, m^3
x	Normalised stress σ_z/σ_z^o
x_f	Value of x at the end of depletion

x_i	value of x at the start of depletion
y	Auxiliary variable: see equation (9.5)
Y	$\dot{\epsilon}_z$, s^{-1}
α	Coefficient of linear thermal expansion
a_1	Parameter in equation (7.27)
β	Ratio of rock matrix over rock bulk compressibility
δ_{ij}	Kronecker delta
ϵ_z	Vertical strain due to compaction $= \Delta h/h$
ϵ'_z	Translation of ϵ_z, such that $\epsilon'_z = 0$ at $\sigma_z = \sigma_{z,o}$
$\dot{\epsilon}_z$	Time derivative of ϵ_z , s^{-1}
$\ddot{\epsilon}_z$	Time derivative of $\dot{\epsilon}_z$, s^{-2}
$\epsilon_{z,creep}$	Vertical strain due to creep
$\Delta\epsilon_z$	Change in ϵ_z
μ	Intergranular friction coefficient
μ_o	Rate independent part of the intergranular friction coefficient
υ	Poisson's ratio
σ	Externally applied hydrostatic stress, bar
σ_{ii}	Trace of stress tensor, bar
σ_{ij}	Bulk stress tensor, bar
σ_r	Radial effective stress, bar
σ_z	Vertical effective stress, bar
$\sigma_{z,f}$	Vertical effective stress at the end of depletion, bar
$\sigma_{z,i}$	Vertical effective stress at the start of depletion, bar
$\sigma_{z,o}$	Normalisation stress, bar
$\sigma_{z,1}$	Vertical effective stress at which the loading rate is increased, bar
$\sigma_{z,2}$	$\sigma_{z,1} + \Delta\sigma_z$, bar
$\Delta\sigma_z$	Distance between constant loading rate compaction curves, given by equation (7.17), bar
$\dot{\sigma}_z$	Loading rate (time derivative of σ_z), bar/s
$\dot{\sigma}_{z,1}$	Value of $\dot{\sigma}_z$ before increase in loading rate, bar/s
$\dot{\sigma}_{z,2}$	Value of $\dot{\sigma}_z$ after increase in loading rate, bar/s
$\dot{\sigma}_{z,dep}$	Depletional loading rate, bar/s
$\dot{\sigma}_{z,geol}$	Geological loading rate, bar/s
$\dot{\sigma}_{z,lab}$	Laboratory loading rate, bar/s
$\ddot{\sigma}_z$	Time derivative of $\dot{\sigma}_z$, bar/s^2

REFERENCES

Adams, S.H. and Williamson, E.D., 1923, The Compressibility of Minerals and Rocks at High Pressures, Journal of the Franklin Inst., 195, p 475.

Allen, D.R., 1968, Physical Changes of Reservoir Properties Caused by Subsidence and Repressurizing Operations, Wilmington field, California, J. Pet. Tech. Jan, pp 23-29.

Allen, D.R., 1969, Collar and Radioactive Bullet Logging for Subsidence Monitoring, Dept. of Oil Properties, City of Long Beach, Cal., paper presented at the SPWLA 20th Annual Logging Symp.

Allen D.R. and Mayuga, M.N., 1970, The Mechanics of Compaction and Rebound, Wilmington Oil Field, Long Beach, California, U.S.A. in: Proceedings of the 1st International Symposium on Land Subsidence, 1969, Publication 88 and 89 of the International Association of Hydrologic Science and UNESCO, pp 410-423.

Abou-Sayed, A.S., 1982, Elastic/plastic Compaction Model Applicable to Low Cohesion Oil Sands Reservoirs, in: Proceedings of 1982 Forum on Subsidence due to Fluid Withdrawals, November 14-17, 1982, Fountainhead State Resort, Checotah, Oklahoma, pp 15-24.

Beyerlee, J.D. and Wyss, M., 1978, Rock Friction and Earthquake Prediction, Pure and Applied Geophysics (Pageoph), Special Issue, Vol. 116, No. 4-5.

Byerlee, J., 1978, Friction of Rocks, in: Rock Friction and Earthquake Prediction, Pageoph, Special Issue, Vol. 116, No. 4-5, pp 615-626.

Biot, M.A., 1935, Le Probleme de la Consolidation des Matieres Argileuses Sous une Charge, Ann. Soc. Sci. Brux., B55, pp 110-113.

Biot, M.A., 1941, General Theory of Three-Dimensional Consolidation, J. Appl. Phys., Vol. 12 pp 155-164.

Biot, M.A., 1955, Theory of Elasticity and Consolidation of a Porous Anisotropic Solid, J. of Appl. Phys., 26, pp 182-185.

Biot, M.A., 1956, General Solution of the Equations of Elasticity and Consolidation for a Porous Material, J. of Appl. Mech., Vol 78, pp 91-96.

Biot, M.A., 1957, The Elastic Coefficients of the Theory of Consolidation, J. of Appl. Mech., Vol. 24, pp 594-601.

Bjerrum, L., 1967, Engineering Geology of Norwegian Normally Consolidated Marine Clays as Related to the Settlements of Buildings, Geotechnique, 17, pp 81-118.

Blanton, B.L., 1981, Deformation of Chalk Under Confining Pressure and Pore Pressure, Soc. of Petr. Eng. J., v. 21, no. 1, February, pp 43-50.

Boot, R., 1973, Level Control Surveys in the Groningen Gas Field, Verh. Kon. Ned. Geol. Mijnbouwkundig Genootschap, 28, pp 105-109.

Bowden, F.P., 1954, The Friction of Non-Metallic Solids, J. Inst. Petrol., 40, pp 89-103.

Bowden, F.P. and Tabor, D., 1950, The Friction and Lubrication of Solids, vol. 1, Oxford, Clarendon Press.

Bowden, F.P. and Tabor, D., 1964, The Friction and Lubrication of Solids, vol. 2, Oxford, Clarendon Press.

Breckels, I.M. and Eekelen, H.A.M. van, 1981, Relationship Between Horizontal Stress and Depth in Sedimentary Basins, SPE 10336.

Brighenti, G., 1967, Influence of Pore Pressure Decline on the Behaviour of Petroleum Reservoir Rocks, Proc. 7th World Petr. Congr., Vol. 3, pp 97-105.

Casagrande, A., 1936, Proceedings 1st Int. Conf. on Soil Mech. and Found. Eng., 3, pp 60-64.

Chilingarian, G.V. and Wolf, K.H., 1975-1976 Compaction of Coarse Grained Sediments, Volumes 1 and 2, Amsterdam.

Chilingar, G.V., Yen, T.F. and Fertl, W.H., 1983, Compressibilities of Sands and Clays, in: Proceedings of the 1st International Symposium on Land Subsidence, 1969, Publication 88 and 89 of the International Association of Hydrologic Science and UNESCO, pp 25-32.

Christian, J.T. and Hirschfield, R.C., 1974, Subsidence of Venice: Predictive Difficulties, Science, vol. 185, p 1185.

Ciabatti, M. 1963, Giorn. Geol. Bologna 1956-57, Vol. 27, pp 31-101, abstract in: Bibliography and Index of Geology exclusive of North America, Publ. by Geol. Soc. Amer., 1964.

Corapcioglu, M.Y., 1984, Land Subsidence - A. A State of the Art Review, in: Proceedings of the NATO Advanced Study Institute on Mechanics of Fluids in Porous Media, Newark, Delaware, USA, July 18-27, pp 371-444.

Corapcioglu, M.Y. and Bear, J., 1984, Land Subsidence - B. A Regional Mathematical Model, in: Proceedings of the NATO Advanced Study Institute on Mechanics of Fluids in Porous Media, Newark, Delaware, USA, July 18-27, pp 445-498.

Cundall, P.A. and Strack, O., 1979, A Discrete Numerical Model for Granular Assemblies, Geotechnique 39, No. 1 pp 47-65.

Cundall, P.A., Drescher, A. and Strack, O., 1982, Numerical Experiments on Granular Assemblies: Measurements and Observations, IUTAM Symposium on Deformation and Failure of Granular Materials, Delft, pp 355-370

Cundall, P.A. and Strack, O., 1983, Modeling of Microscopic Mechanisms in Granular Material, Mechanics of Granular Materials: New Models and Constitutive Equations, edited by Jenkins, J.T. and Satake, Elsevier Science Publishers B.V. Amsterdam.

Cundall, P.A., 1985, personal communication.

Dárcy, H.J., 1856, Determination of the Law of Flow of Water Through Sand, in: Les Fontaines Publiques de la Ville de Dijon, Libraire de Corps Imperiaux des Pont et Chaussees et des Mines, Paris, pp 590-594.

Dasseault, M.B., 1980, Sample Disturbance in Athabasca Oil Sands, J. of Canadian Petr. Techn., 18(2), pp 85-92.

Dasseault, M.B., and Domselaar, H.R. van, 1982, Unconsolidated Sand Sampling in Canadian and Venezuelan Oil Sands, Revista Technica Intevep (Venezuela) 2,2 pp 165-174.

Dieterich, J.H., 1978, Time-Dependent Friction and the Mechanics of Stick-Slip, Pageoph, vol. 116, No. 4-5, pp 790-806.

Ditzhuizen, P.J.D. van, and Waal, J.A. de, 1984, Reservoir Compaction and Surface Subsidence in the Central Luconia Gas Bearing Carbonates, Offshore Sarawak, East Malaysia, in: Proceedings 5th Offshore South East Asia, Singapore, 21-24 February.

Domenico, P.A. and Mifflin, M.D., 1965, Water From Low Permeability Sediments and Land Subsidence, Water Resources Research, 1, pp 563-576.

Evangelisti, G. and Poggi, B., 1970, Sopra i Fenomini di Deformazione dei Terreni da Variazione della Pressione di Strato, Atti. Accad. Sci. Inst. Bologna, Mem, Ser., II(6). 124 pp.

Fatt, I. and Davies, D., 1952, Reduction in Permeability With Overburden Pressure, Trans. AIME, Vol 195, p 329.

Fatt, I., 1953, The Effect of Overburden Pressure on Relative Permeability, J. of Petr. Tech., Oct., pp 325-326.

Fatt, I., 1958, Compressibility of Sandstone at Low to Moderate Pressures, Am. Ass. Pet. Geol., 42(8) pp 1924-1957.

Finol, A., 1975, Numerical Simulation of Oil Production With Simultaneous Ground Subsidence, Soc. of Petr. Eng. J., October, pp 411-424.

Fung, Y.C., 1965, Foundations of Soil Mechanics, Prentice-Hall.

Gambolati, G., 1972, A Three-dimensional Model to Compute Land Subsidence, Bull. Int. Assoc. Hydrological Sciences, Vol 17, pp 219-226

Gambolati, G. and Freeze, R.A., 1973, Mathematical Simulation of the Subsidence of Venice, 1. Theory, Water Resources Research, 9, pp 721-733.

Gabrysch, R.K. and Bonnet, C.W., 1975, Land subsidence in the Houston-Galveston region, Texas Water Development Board Report, Austin, Texas, 188.

Gassmann, F., 1951, Über die Elastizität poröser Medien, Vierteljahrsschrift der Naturforschenden Gesellschaft in Zurich, March, 96, I, Sec. 1-52. I; Mitteilungen aus dem Institut fur Geophysik, 17, p 1.

Geertsma, J., 1957a, The Effect of Fluid Pressure Decline on Volumetric Changes of Porous Rocks, Trans. AIME, 210, pp 331-338.

Geertsma, J., 1957b, A Remark on the Analogy Between Thermoelasticity and Elasticity of Saturated Porous Media, J. Mech. Phys. Solids, 6, pp 13-16.

Geertsma, J., 1966, Problems of Rock Mechanics in Petroleum Production Engineering, Proc. First Cong. of the Int. Soc. of Rock Mechanics, Lisbon.

Geertsma, J., 1973a, Land Subsidence Above Compacting Oil and Gas Reservoirs, SPE 3730, Trans. 255.

Geertsma, J., 1973b, A Basic Theory of Subsidence Due to Reservoir Compaction: the homogeneous case, Verh. Kon. Ned. Geol. Mijnbouwkundig Genootschap, 28, pp 43-62.

Geertsma, J. and Opstal, G. van, 1973, A Numerical Technique For Predicting Subsidence Above Compacting Reservoirs Based on the Nucleus of Strain Concept, Verh. Kon. Ned. Geol. Mijnbouwkundig Genootschap, 28, pp 63-78.

Gilluly, J. and Grant, U.S., 1949, Subsidence in the Long Beach Harbor Area, California, Bull. GSA, 60, p 461.

Goldscheider, M., 1972, Spannungen im Sand bei Raumlicher, Monotoner Verformung, Thesis, Institutes fur Bodenmechanik der Universitat Fridericiana in Karlsruhe.

Goodier, J.N., 1937, On the Integration of the Thermoelastic Equations, Phil. Mag., 7, p 107.

Gudehus, G., Goldscheider, M., and Winter, H., 1977, Mechanical Properties of Sand and Clay and Numerical Integration Methods: Some Scources of Errors and Bounds of Accuracy, Finite Elements in Geomechanics, edited by G. Gudehus, Wiley, London, pp 121-150.

Gudehus, G. and Kolymbas, D., 1979, A Constitutive Law of the Rate Type for Soils, Proc. 3rd Int. Conf. on Num. Meth. in Geomech., Aachen, 2-6 April, edited by Wittke, W., Balkema Rotterdam.

Hall, H.N., 1953, Compressibility of Reservoir Rocks, J. of Petr. Tech., Jan., pp 309-314.

Helm, D.C., 1975, One-dimensional Simulation of Aquifer System Compaction Near Pixley, California, 1. Constant Parameters, Water Resour. Res., 11, pp 465-578.

Helm, D.C., 1976, One-dimensional Simulation of Aquifer System Compaction Near Pixley, California, 2. Stress-Dependent Parameters, Water Resour. Res., 12, pp 375-391.

Helm, D.C., 1984, Field Based Computational Techniques for Predicting Subsidence Due to Fluid Withdrawal, Geological Society of America, Reviews in Engineering Geology, Volume VI, pp 1-22.

Hirono, T., 1969, Niigata Ground Water Subsidence and Ground Water Change, in: Proceedings of the 1st International Symposium on Land Subsidence, 1969, Publication 88 and 89 of the International Association of Hydrologic Science and UNESCO, I, p 144.

Holzer T.L., 1981, Preconsolidation Stress of Aquifer Systems in Areas of Induced Land Subsidence, Water Resources Research, 17, pp 693-704.

Holzer, T.L., and Pampeyan, E.H., 1981, Earth Fissures and Localised Differential Subsidence, Water Resources Research, Vol. 17, pp 223-227.

Holzer, T.L., 1984, Ground Failure Induced by Ground-Water Withdrawal From Unconsolidated Sediment, Geological Society of America, Reviews in Engineering Geology, Volume VI, pp 67-105.

Jaeger, J.C. and Cook, N.G.W., 1969, Fundamentals of Rock Mechanics, John Wiley & Sons, Inc. New York.

Jones, O.J., 1975, A Laboratory Study of the Effects of Confining Pressure on Fracture Flow and Storage Capacity of Carbonate Rocks, J. of Petr. Tech., Jan., pp 21-27.

Josselin de Jong, G. and Verruijt, A., 1969, Etude Photo Elastique d'un Depilement de Disques, Cah. Grpe. Fr. Etud. Rheol, 2 pp 73-86.

Kennedy, D.J.L., 1961, A Study of Failure of Liners for Oil Wells Associated with the Compaction of Oil Producing Strata, PhD thesis, University of Illinois, Urbana, Illinois, 251 p.

Kesteren, J. van, 1973, Estimate of Compaction Data Representative of the Groningen Field, Verh. Kon. Ned. Geol. Mijnbouwkundig Genootschap, 28, pp 33-42.

Keverling Buisman, A.S., 1936, Results of a Long Duration Settlement Test, Proc. 1st. Int. Conf. Soil Mech. and Found. Eng., Cambridge (Mass.).

Knaap, W. van der, 1958, Nonlinear Behaviour of Elastic Porous Media, Petroleum Transactions AIME, vol. 216, pp 179-187.

Knaap, W. van der & Vlis, A.C. van der, 1967, On the Cause of Subsidence in Oil Producing Areas, 7th World Petroleum Congress, V. 13, Mexico City, pp 85-95.

Knutsen, C.F. and Bohor, B.F., 1963, Reservoir Rock Behaviour Under Moderate Confining Pressure, Proc. 5th Rock Mech. Symp., Univ. of Minesota, Macmillan, New York.

Kolymbas, D., 1978, Ein Nichtlineares Viscoplastisches Stoffgestetz für Boden, Thesis, Institutes für Bodenmechanik der Universitat Fridericiana in Karlsruhe.

Kolymbas, D., 1984, Anelastic Deformation of Porous Media, in: Proceedings of the NATO Advanced Study Institute on Mechanics of Fluids in Porous Media, Newark, Delaware, USA, July 18-27, pp 499-524.

Kosloff, D. and Scott., R.F., 1980a, Finite Element Simulation of Wilmington Oil Field Subsidence: I Linear Modelling, Tectonophysics, 65, pp 339-368.

Kosloff, D. and Scott, R.F., 1980b, Finite Element Simulation of Wilmington Oil Field Subsidence: II Nonlinear Modelling, Tectonophysics, 70, pp 159-183.

Lachange, D.P. and Andersen, M.A., 1983, Comparison of Uniaxial Strain and Hydrostatic Stress Pore Volume Compressibilities in the Nugger Sandstone, SPE 11971.

Lee, K.L., 1978, Subsidence Earthquake at a California Oil Field, Proc. Int. Conf. on Evaluation and Prediction of Subsidence, Casino Hotel, Pensacola Beach, Florida, U.S.A., pp. 549-564.

Leinenkugel, H.J., 1976, Deformations und Festigkeitsverhalten Bindiger Erdstoffe. Experimentelle Ergebnisse und ihre Physikalischen Bedeutung, Thesis, Institut fur Bodenmechanik und Felsmechanik der Universitat Fridericiana in Karlsruhe, Heft 66.

Leroueil, S., Kabbaj, M., Tavenas, E. and Bouchard, R., 1985, Stress-Strain-Strain Rate Relation for the Compressibility of Sensitive Natural Clays, Geotechnique, 35, No. 2, pp 159-180.

Lofgren, B.E., 1961, Measurement of Compaction of Aquifer Systems in Areas of Land Subsidence, California Department of Water Resources, Paper 24, published in Geological Survey Research.

Lofgren, B.E., 1974, Measuring Ground Movement in Geothermal Areas of Imperial Valley, California, U.S. paper presented at Geothermal Energy Conference, Pasadena, C0l., Sept. 23-25.

Loos, J.M. de, 1973, Compaction Measurements in Groningen Observation Wells, Verh. Kon. Ned. Geol. Mijnbouwkundig Genootschap, 28, pp 79-104.

Lubinski, A., 1954, The Theory of Elasticity for Porous Bodies Displaying a Strong Porous Structure, Proc. U.S. Nat. Congr. Appl. Mech., 2nd, pp 247-256.

Martin, J.C. and Serdengecti, S., 1984, Subsidence over Oil and Gas Fields, Geological Society of America, Reviews in Engineering Geology, Volume VI, pp 23-35.

Mattax, C.C., McKinley, and Clothier, A.T., 1975, Core Analysis of Unconsolidated and Friable Sands, J. of Petr. Techn., December, p 1423.

Mayuga, M.N. and Allen, D., 1969, Subsidence in the Wilmington Oil field, Long Beach, California, in: Proceedings of the 1st International Symposium on Land Subsidence, 1969, Publication 88 and 89 of the International Association of Hydrologic Science and UNESCO.

McLatchie, A.S., Henstock, R.S. and Young, J.W., 1958, Effective Compressibility of Reservoir Rock, its Effect on Permeability, J. of Petr. Tech. June, pp 49-51.

McCann, G.D. and Wilts, C.H., Nov. 1951, A Mathematical Analysis of the Subsidence in the Long Beach-San Pedro Area, internal report, California Institute of Technology.

Merle, H.A., Kenthie, C.J.P., Opstal, G.H.C. van and Schneider, G.M.H., 1975, The Bachaquero Study - a Composite Analysis of the Behaviour of a Compaction Drive/Solution Gas Drive Reservoir, J. of Petr. Techn. 27, pp 1107-1114, SPE 5529.

Mess, K.W., 1978, On the Interpretation of Core Compaction Behaviour, Proc. Int. Conf. on Evaluation and Prediction of Subsidence, Casino Hotel, Pensacola Beach, Florida, U.S.A., pp. 76-79.

Mindlin, R.D. and Cheng, D.H., 1950, Thermoelastic Stress in the Semi-Infinite Solid, J. Appl. Phys., 21, pp 931-933.

Mitchell, R.F. and Goodman, M.A., 1978, Permafrost Thaw Subsidence Casing Design, J. of Petr. Tech., March, pp p 455-460.

Morita, N. and Gray, K.E., 1984, Rock Property Change During Reservoir Compaction, SPE 13099.

Newman, G.H., 1973, Pore Volume Compressibility of Consolidated, Friable and Unconsolidated Reservoir Rocks under Hydrostatic Loading, J. of Petr. Tech., vol. 25, p 129.

Newman, G.H. and Martin, J.C., 1977, Equipment and Experimental Methods for Obtaining Laboratory Characteristics of Reservoir Rock under Various Stress and Pressure Conditions, SPE 6855.

Nowacki, W. 1962, Thermoelasticity, Addison Wesly, Mass./Pergamon Press, Oxford/Polish Scientific Publishers, Warszawa, 628 p.

Nunez, O. and Escojido, D., 1977, Subsidence in the Bolivar Coast, in: Proc. of the 2nd Int. Symp. on Land Subsidence, Anaheim, California, Int. Ass. of Hydr. Sc., Publ. 121, pp 257-266.

Oda, M., 1974, A Mechanical and Statistical Model of Granular Material, Soils and Foundations, Vol. 14, No. 1, pp 13-17.

Oda, M., Nemat-Nasser, S. and Mehrabadi, 1982, A Statistical Study of Fabric in a Random Assembly of Spherical Granules, Int. J. Num. Anal. Meth. Geomechanics, 6, pp 77-94.

Okumara, T., 1969, Analysis of Land Subsidence in Niigata, in: Proceedings of the 1st International Symposium on Land Subsidence, 1969, Publication 88 and 89 of the International Association of Hydrologic Science and UNESCO, I, p 130.

Opstal, G. van, 1974, The Effect of Base Rock Rigidity on Subsidence Due to Compaction, Proceedings of the Third Congress of the International Society of Rock Mechanics, Denver, Colorado, September 1-7, 1974, Volume II, part B, National Academy of Sciences, Washington, D.C.

Patillo, D.P. and Smith, B., 1982, The Effect of Formation Flow on the Integrity of Perforated Casing, SPE 11123.

Perez, A.A.S. and Toscas, C., 1984, Analysis of Reservoir Compaction and Surface Subsidence Using an Elastoplastic Critical State Model, Revista Technica Intevep 4 (1): 35-40 enero 1964/35.

Philip, J.R., 1968, Sorption and Volume Change in Colloid Pastes, Aust. J. Soil Res., Vol. 6, pp 249-267.

Poland, J.G. and Davis, G.H., 1969, Land Subsidence Due to Withdrawals of Fluids, in Reviews in Engineering Geology II, Boulder, Colo. Geol. Soc. Am. pp 187-269.

Pratt, W.E. and Johnson, D.W., 1926, Local Subsidence of the Goose Creek Field, J. of Geology, 34, p 577.

Proceedings of the 1st International Symposium on Land Subsidence, 1969, Publication 88 and 89 of the International Association of Hydrologic Science and UNESCO.

Proceedings of the 2nd International Symposium on Land Subsidence, 1977, International Association of Hydrologic Science, Anaheim, California, Publication 121, 670 p.

Proceedings International Conference on Evaluation and Prediction of Subsidence, 1979, Casino Hotel, Pensacola Beach, Florida, U.S.A, edited by: Saxena, S.K., Am. Soc. of Civil Eng.

Proceedings of 1982 Forum on Subsidence due to Fluid Withdrawals, November 14-17, 1982, Fountainhead State Resort, Checotah, Oklahoma.

Proceedings of the NATO Advanced Study Institute of Fluids in Porous Media, 1984, Fundamentals of Transport Phenomena in Porous Media, edited by: Bear, J. and Corapcioglu, U.S.A., Newark, Delaware, July 18-27, NATO ASI Series, Series E: Applied Sciences - No. 82.

Propkovitch, N.P., 1983, Tectonic Framework and Detection of Aquifers Susceptible to Subsidence, in: Proceedings of 1982 Forum on Subsidence due to Fluid Withdrawals, November 14-17, 1982, Fountainhead State Resort, Checotah, Oklahoma, pp 33-44.

Richter, C.F., 1958, Elementary Seismology, W.H. Freeman Company.

Rieke, H.H., Chilingarian, G.V. and Fertl, H., 1978, A Review of the Importance of Gravitational Sediment Compaction in Oil Producing Areas, Energy Sources, Vol. 4, Number 2, pp 165-193.

Roberts, J.E. and Souza, de, J.M., 1958, The Compressibility of Sands, Proc. Am. Soc. Test. Mat., p 1269.

Roscoe, K.H. and Poorooshasb, H.B., 1963, A Theoretical and Experimental Study of Strains in Triaxial Compression Tests on Normally Consolidated Clays, Geotechnique, XIII, pp 12-38.

Sandhu, R.S., 1968, Fluid Flow in Saturated Porous Elastic Media, Ph.D. Thesis, Univ. of California at Berkeley, California.

Sandhu, R.S., 1982, Finite Element Analysis Of Subsidence Due to Fluid Withdrawal, Proceedings of 1982 Forum on Subsidence due to Fluid Withdrawals, November 14-17, 1982, Fountainhead State Resort, Checotah, Oklahoma., pp. 97-107.

Saxena, S.K., 1981, A Revieuw of The Theories Used In Investigation of Subsidence, Indian Geotech. J., 11, No. 1, pp 75-91.

Schenk, L. and Puig, F., 1983, Aspects of Compaction/Subsidence in the Bolivar Coast Heavy Oil Fields, Highlighted by Performance Data of the M-6 Project Area, in: Proceedings of 1982 Forum on Subsidence due to Fluid Withdrawals, November 14-17, 1982, Fountainhead State Resort, Checotah, Oklahoma, pp 109-120.

Schiffman, R.L., 1984, A Bibliography of Consolidation, in: Proceedings of the NATO Advanced Study Institute on Mechanics of Fluids in Porous Media, Newark, Delaware, USA, July 18-27, pp 617-670.

Scholz, C.H. and Englander, J.T., 1976, The Role of Asperity Indentation and Ploughing in Rock Friction, I - Asperity Creep and Stick-Slip, Int. Rock Mech. Min. Sci., 13, pp 149-154.

Schoonbeek, J.B., 1976, Land Subsidence as a Result of Natural Gas Extraction in the Province of Groningen, SPE 5751.

Sen, B., 1950, Note on the Stresses Produced by Nuclei of Thermoelastic Strain in a Semi-Infinite Elastic Solid, Q. J. Appl. Math., 8, pp 365-369.

Sharma, 1956, Stresses in an Infinite Slab Due to a Nucleus of Thermoelastic Strain in it, Zeitschrift angew. Math. Mech., Bd 36, Nr. 1/2, Jan./Febr.

Smits, R.M.M. and Waal, J.A. de , The Influence of Pressure-Lags in Clay Layers on Reservoir Compaction and Subsidence. Behaviour. Article to be published.

Smits, R.M.M. and Waal, J.A. de, Prediction of Reservoir Compaction in Carbonates Showing Pore Collapse, article to be published.

Snider, L.C., 1927, A Suggested Explanation for the Surface Subsidence in the Goose Creek Oil and Gas Field, Texas, Bull., AAPG, II, 729.

Taylor, D.W. and Merchant, W., 1940, A Theory of Clay Consolidation Accounting for Secondary Compression, J. of Math. Phys., Vol. 19, pp 167-185.

Teeuw, D., 1971, Prediction of Reservoir Compaction from Laboratory Compressibility Data, SPE Journal, September, p 263.

Teeuw, D., 1973, Laboratory Measurements of Groningen Reservoir Rock, Trans. Royal Dutch Soc. of Geologists and Mining Engineers, 28, pp 19-32.

Teller, O., 1965, Taschenbuch der Mathematik, Munchen (Lindauer Verlag).

Teufel, L.W. & Logan, J.M., 1978, Effect of Displacement Rate on the Real Area of Contact and Temperatures Generated During Frictional Sliding of Tennessee Sandstone. Pageoph, vol. 116.

Terzaghi, K., 1923, Die Berechnung der Durchlässigkeitsziffer des Tones aus dem Verlauf der Hydrodynamischen Spannungserscheinungen, Sitzungsb. Akad. Wiss., Wien, 132, pp 125-138.

Terzaghi, K., 1943, Theoretical Soil Mechanics, Wiley, N.Y. 510 pp.

Tokue, T., 1979, A Stress Dilatancy Model of Granular Material under General Stress Condition, Soils and Foundations, Vol. 19, No. 1, pp 63-80.

Truesdell, C. & Noll, W., 1965, The Non-Linear Field Theories of Mechanics, Handbuch der Physik Bd IIIc, par. 36, Springer Verlag.

Verhandelingen van het Koninklijk Nederlands Geologisch Mijnbouwkundig Genootschap, 1973, The analysis of surface subsidence resulting from gas production in the Groningen area, the Netherlands, edited by Nederlandse Aardolie Maatschappij B.V., vol 28.

Verruijt, A., 1969, Elastic Storage of Aquifer Flow Through Porous Media, Edited by R.J.M. DeWiest, Academic Press N.Y., pp 331-375.

Verruijt, A., 1979, Generation and Dissipation of Pore Water Pressures, in: Finite Elements in Geomechanics, edited by Gudehus, G., London, Wiley, pp 293-317.

Verruijt, A., 1984, The Theory of Consolidation, in: Proceedings of the NATO Advanced Study Institute on Mechanics of Fluids in Porous Media, Newark, Delaware, USA, July 18-27, pp 349-368.

Waal, J.A. de and Smits, R.M.M., 1985, Prediction of Reservoir Compaction and Surface Subsidence - Field Application of a New Model, SPE 14214.

Williamson, A.S., 1974, Volumetric Subsidence - Compaction Ratio for a Layered Elastic Half Space, Proceedings of the Third Congress of the International Society of Rock Mechanics, Denver, Colorado, September 1-7, 1974, Volume II, part B, National Academy of Sciences, Washington, D.C.

Wooley, G.R., 1984, Reservoir Compaction Loads in Casings and Liners, SPE 13088.

Wroth, C.P., 1977, The Predicted Performance of Soft Clay Under a Triaxial Embankment Loading Based on the Cam Clay Model, in: Finite Elements in Geomechanics, edited by G. Gudehus, J. Wiley.

Wygall, R.J., 1963, Construction of Models That Simulate Oil Reservoirs, SPE Journal, 3, p 281.

Yerkes, R.F. and Castle, R.O., 1969, Surface Deformation Associated With Oil and Gas Field Operations in the United States, in: Proceedings of the 1st International Symposium on Land Subsidence, 1969, Publication 88 and 89 of the International Association of Hydrologic Science and UNESCO, I, p 55.

Zienkiewicz, O.C., 1971, The Finite Element Method in Engineering Science, McGraw-Hill Publishing Company, London.

Zienkiewicz, O.C. and Naylor, D.J., 1973, Finite Element Studies of Soils and Porous Media, in: Lectures in Finite Element Methods in Continuum Mechanics, edited by Oden and Oliveira, Univ. of Alabama, Huntsville, pp 459-493.

APPENDIX A
DETAILED EXPERIMENTALL RESULTS

Table A1   Unconsolidated samples

LEGEND

S1 Artificially sedimented 170μ sand
S2 Artificially sedimented 450μ sand
SB Artificially sedimented 170μ steel beads
AL Artificially sedimented aluminium powder
A Unconsolidated core samples from reservoir A
B Unconsolidated core samples from reservoir B
* Remoulded samples

Exp. No.	Sample No.	Depth (ft)	ϕ at $\sigma_z = 0$	Description	Figs.
1	A14R	907.7	0.34	Changes in loading rate (first cycle)	33,A1
2	A15R	909.7	0.34	Changes in loading rate (first cycle)	33,A2,A3
3	A16R	909.9	0.34	Changes in loading rate and reloadings after partial unloadings (first cycle)	24,25,26, A4,A5
4	A24R	918.0	0.35	Determination of stress dependence of rate effects (first cycle)	33,A6
5	A24R*	918.0	0.42	Same as exp.4 but on remoulded sample (first cycle)	33,A6
6	B4R1	511.3	0.40	Comparison of compaction behaviour after a change in loading rate, partial unloading and creep (first cycle)	27,28,A7
7	B4R2	511.4	0.40	Determination of stress dependence of rate effects (first cycle)	34
8	B4R2*	511.4	0.46	Same as exp. 7 but on remoulded sample (first cycle)	35
9	B5R	550.2	0.38	Determination of stress dependence of rate effects (first cycle)	34
10	B5R*	550.2	0.41	Same as exp.9 but on remoulded sample (first cycle)	35

11	B7R	564.6	0.35	Determination of stress dependence of rate effects (first cycle)	34
12	B7R*	564.6	0.35	Same as exp.11 but on remoulded sample (first cycle)	35
13	B12R1	624.6	0.38	Compaction after partial unloading (first cycle)	29,A8
14	B12R2	624.7	0.38	Determination of stress dependence of rate effects (first cycle)	34
15	B17R	689.9	0.26	Determination of stress dependence of rate effects (first cycle)	34
16	B18R	694.5	0.31	Determination of stress dependence of rate effects (first cycle)	34
17	B18R*	694.5	0.36	Same as exp.16 but on remoulded sample (first cycle)	35
18	S1-10	–	0.36	Comparison of compaction behaviour after a change in loading rate, partial unloading and creep (first cycle, sample sedimented with particle distributor (Wygall))	A9
19	S1-11	–	0.34	Comparison of compaction behaviour after a change in loading rate, partial unloading and creep (first cycle, sample sedimented with funnel)	A10
20	S1-12	–	0.36	Determination of stress dependence of rate effects (first cycle, sample preparation Wygall)	36,A11
21	S1-12	–	–	Same as 20, but second loading cycle	36
22	S1-13	–	–	Compaction after partial unloading at higher stress (first cycle)	30,A12
23	S2-13	–	–	Determination of stress dependence of rate effects (first cycle, sample preparation Wygall)	36
24	S2-13	–	–	Same as exp.23, but second loading cycle	36

25	S2-13*	-	-	Same as exp.23 but on remoulded sample (first cycle)	36
26	S2-14	-	-	Same as exp.23, but at T=90°C to study the influence of temperature on rate effects	36
27	SB-1	-	-	Changes in loading rate at various stress levels.	37,A13
28	AL-1	_	-	Same as exp.27	37,A14

Table A2 Consolidated sandstones from well EKL-12 selected for
compaction experiments

Sample	Depth (m)	Atmospheric porosity (%)	Grain density (g/cc)
E001	2903.75		
E003	2954.10	26.5	2.65
E004	3001.25	21.6	2.66
E005	3012.30	14.5	2.69
E006	3071.58	7.5	2.68
E007	3072.52	15.9	2.68
E008	3074.36	18.6	2.72
E009	2968.48	17.5	2.68
E010	3017.11	14.8	2.68
E011	3026.19	12.7	2.70
E012	3072.42	16.1	2.68
E013	2974.35	20.1	2.66
E014	3074.26	18.8	2.72
E015	2982.57		
E016	2997.94	9.1	2.71
E019	3015.08	15.7	2.68
E023	2924.95	19.6	2.69
E024	2951.88	18.0	2.67
E025	3010.64	13.1	2.69
E026	3027.07	19.2	2.67

Indicated depth is drillers depth.

Table A3 Results of the compaction experiments performed on EKL-12
         samples

Sample	depth (m)	h_0 (mm)	Type of exp.	c_m (10^{-5} bar^{-1})	b
E001	2903.75	30.25	C	3.50	
E003	2954.10	29.80	SR	3.47	0.022 ± 0.002
E004	3001.25	29.50	SR	2.82	0.019 ± 0.002
E005	3012.30	29.75	C	1.35	
E006	3071.58	29.85	C	0.29	
E007	3072.58	29.95	SR	0.45	0.014 ± 0.005
E008	3074.36	29.85	SR	0.67	
E009	2968.48	30.10	SR	2.25	0.012 ± 0.002
E010	3017.11	30.00	SR	1.13	0.015 ± 0.002
E011	3026.19	29.80	SR	0.77	0.017 ± 0.003
E012	3072.42	99.80	SR	0.45	0.009 ± 0.002
E013	2974.35	100.00	SR	1.77	0.015 ± 0.002
E014	3074.26	99.90	SR	0.79	0.006 ± 0.002
E015	2982.57	99.80	SR	1.57	0.010 ± 0.002
E016	2997.94	29.90	SR	0.47	0.020 ± 0.002
E019	3015.08	29.60	SR	1.53	0.017 ± 0.002
E023	2924.95	30.10	SR	1.60	0.019 ± 0.002
E024	2951.88	30.10	SR	1.66	0.017 ± 0.002
E025	3010.64	29.75	SR	1.46	0.015 ± 0.002
E026	3027.07	29.55	SR	2.13	0.019 ± 0.002

C: constant loading rate
SR: stress rate variation experiment

Table A4   Results of the compaction experiments on samples from well ZDP-12

Sample no.	Depth (m)	h_0 (mm)	ϕ_{atm} (%)	$c_{m,o}$ (10^{-5}/bar)	b (-)
ZDP-1	2904.4	30.45	21.3	1.93	0.020
ZDP-2	2907.2	29.80	15.1	0.55	0.014
ZDP-3	2908.2	30.30	17.7	1.51	0.016
ZDP-4	2908.5	30.00	16.6	1.09	0.014
ZDP-6	2913.7	29.30	16.8	2.30	0.018
ZDP-7	2920.6	29.85	12.9	0.52	0.014
ZDP-9	2940.7	30.40	19.5	1.82	0.014
ZDP-10	2944.6	25.95	21.1	2.09	0.016
ZDP-12	2947.3	30.25	13.2	0.63	0.014
ZDP-13	2962.6	30.05	13.8	0.61	0.014
ZDP-14	2960.3	30.00	23.3	3.62	0.014
ZDP-15	2965.4	30.10	17.7	0.78	0.016
ZDP-16	2966.6	30.20	17.3	0.95	0.016
ZDP-17	2967.3	30.05	13.0	0.41	0.014
ZDP-18	2973.6	30.05	20.4	1.48	0.020
ZDP-20	2978.0	30.00	15.	9.16	0.010
ZDP-22	2982.2	30.25	10.9	0.76	0.014
ZDP-23	2993.1	30.10	17.5	2.34	0.014
ZDP-24	2997.7	30.00	9.9	0.93	0.007
ZDP-26	3004.3	30.15	14.6	1.23	0.010
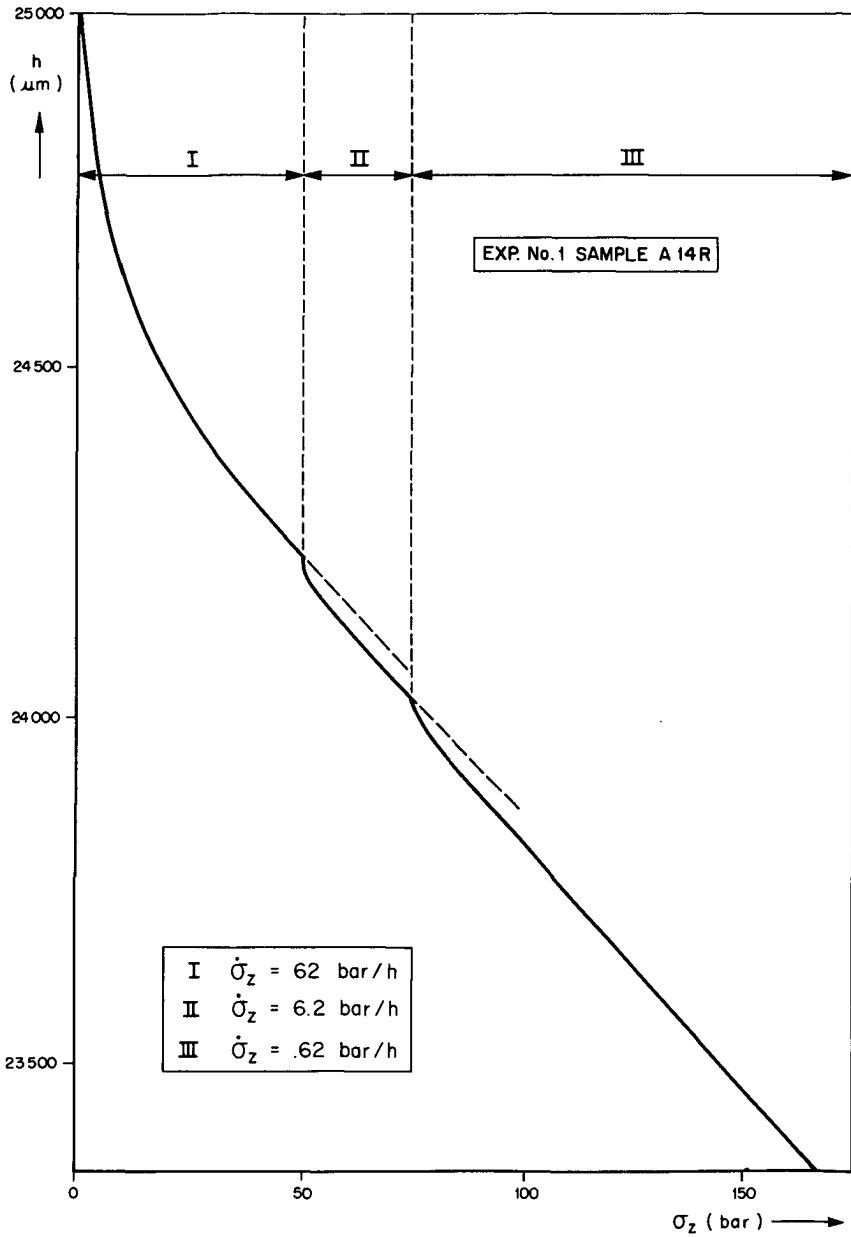
FIG.A1 INFLUENCE OF DECREASING LOADING RATE ON THE COMPACTION BEHAVIOUR OF AN UNCONSOLIDATED RESERVOIR SAND. (RESERVOIR A, OEDOMETER TEST)
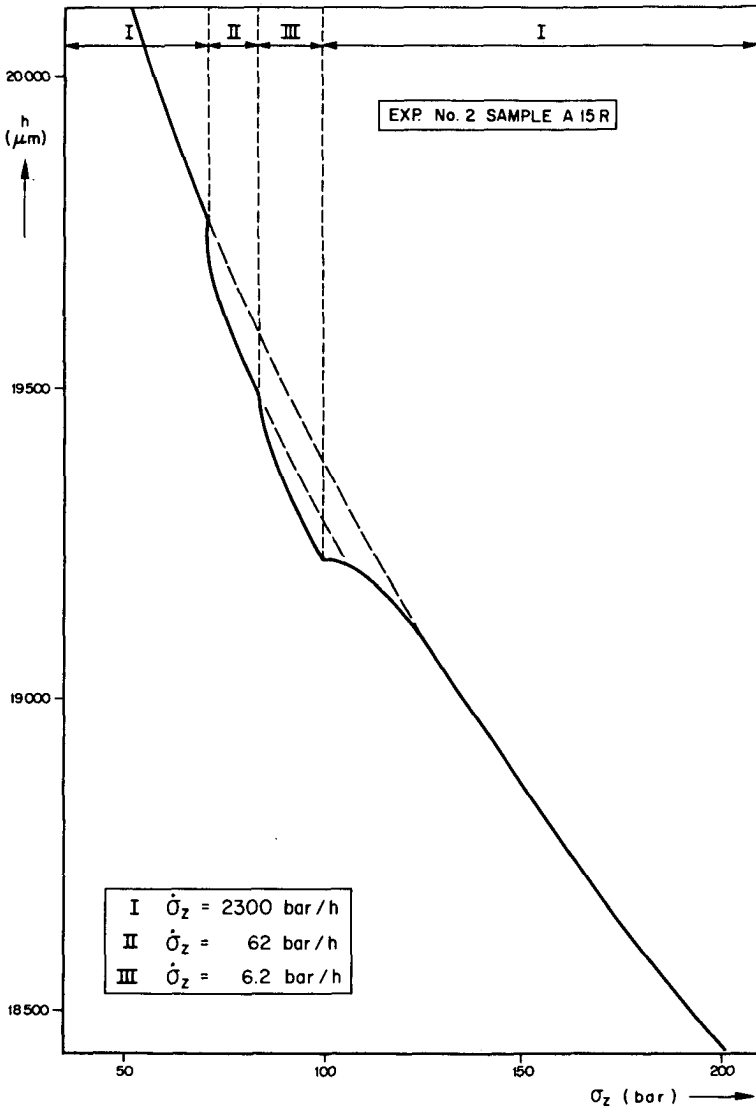
FIG.A2 INFLUENCE OF CHANGES IN
LOADING RATE ON THE COMPACTION
BEHAVIOUR OF AN UNCONSOLIDATED
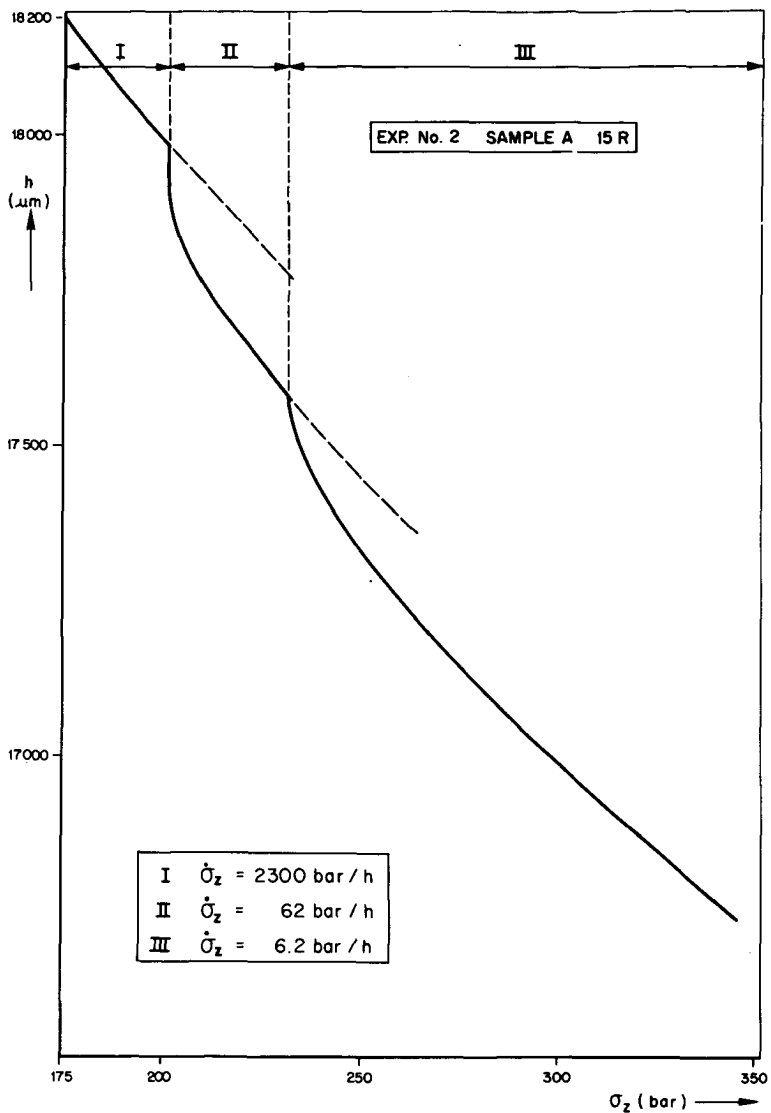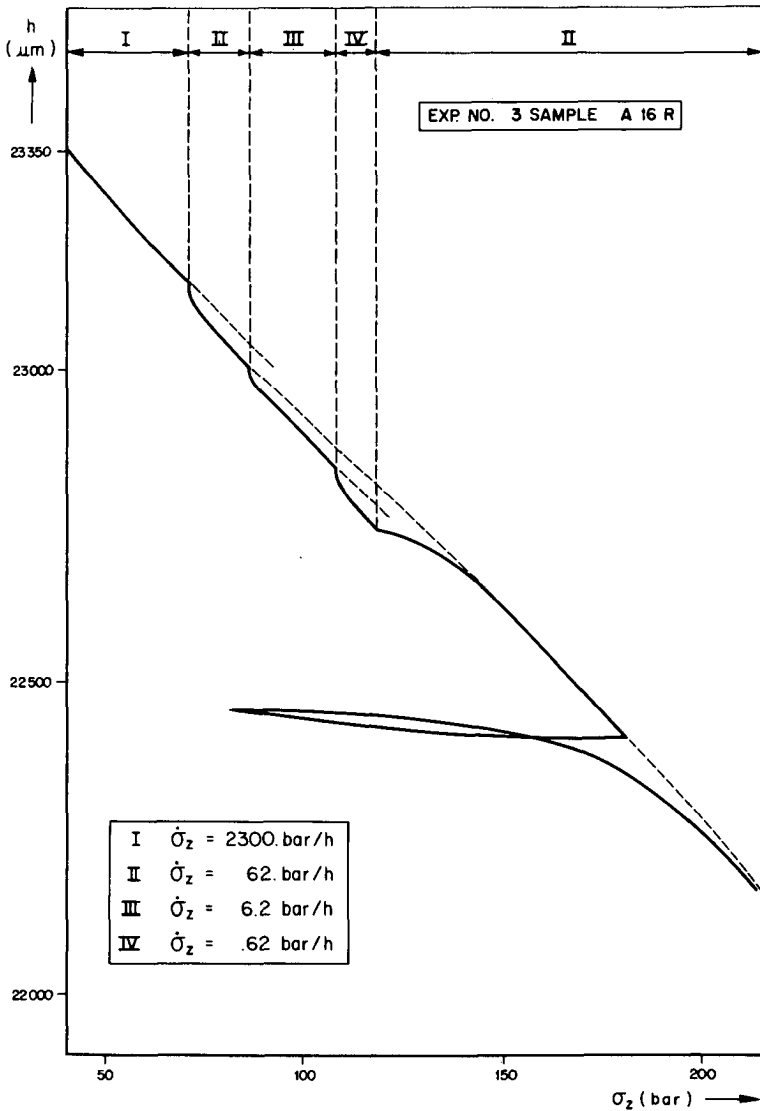RESERVOIR SAND AT LOWER
STRESSES. (RESERVOIR A,
OEDOMETER TEST)

FIG.A3 INFLUENCE OF CHANGES IN LOADING RATE ON THE COMPACTION BEHAVIOUR OF AN UNCONSOLIDATED RESERVOIR SAND AT HIGHER STRESSES. (RESERVOIR A, OEDOMETER TEST)
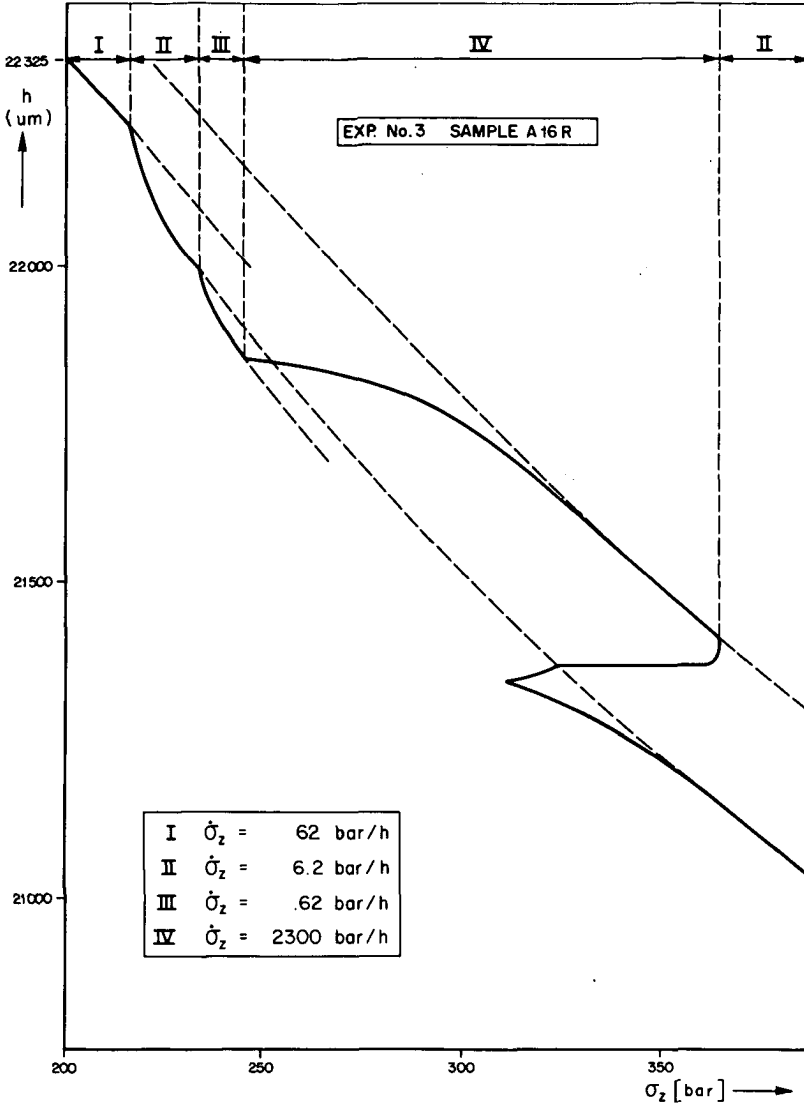
FIG.A4 INFLUENCE OF CHANGES IN
LOADING RATE AND PARTIAL
UNLOADING ON THE COMPACTION
BEHAVIOUR OF AN UNCONSOLIDATED
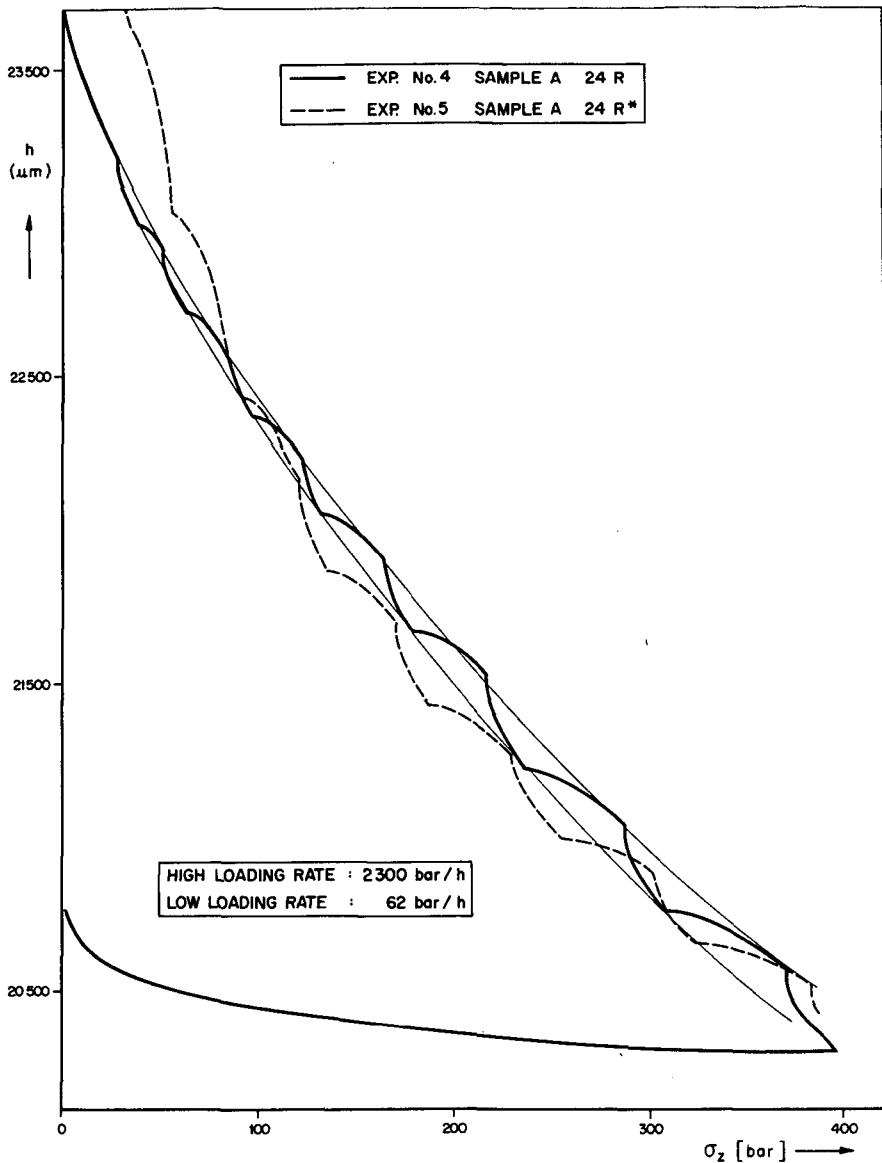RESERVOIR SAND AT LOWER
STRESSES. (RESERVOIR A,
OEDOMETER TEST)

I $\dot{\sigma}_z$ =   62 bar/h
II $\dot{\sigma}_z$ =   6.2 bar/h
III $\dot{\sigma}_z$ =   .62 bar/h
IV $\dot{\sigma}_z$ =   2300 bar/h

EXP. No.3   SAMPLE A 16 R

FIG.A5 INFLUENCE OF CHANGES IN LOADING RATE AND PARTIAL UNLOADING ON THE COMPACTION BEHAVIOUR OF AN UNCONSOLIDATED RESERVOIR SAND AT HIGHER STRESSES. (RESERVOIR A, OEDOMETER TEST)

FIG.A6 INFLUENCE OF CHANGES IN
LOADING RATE AT VARIOUS STRESS
LEVELS ON THE COMPACTION
BEHAVIOUR OF AN UNCONSOLIDATED
RESERVOIR SAND (RESERVOIR A,
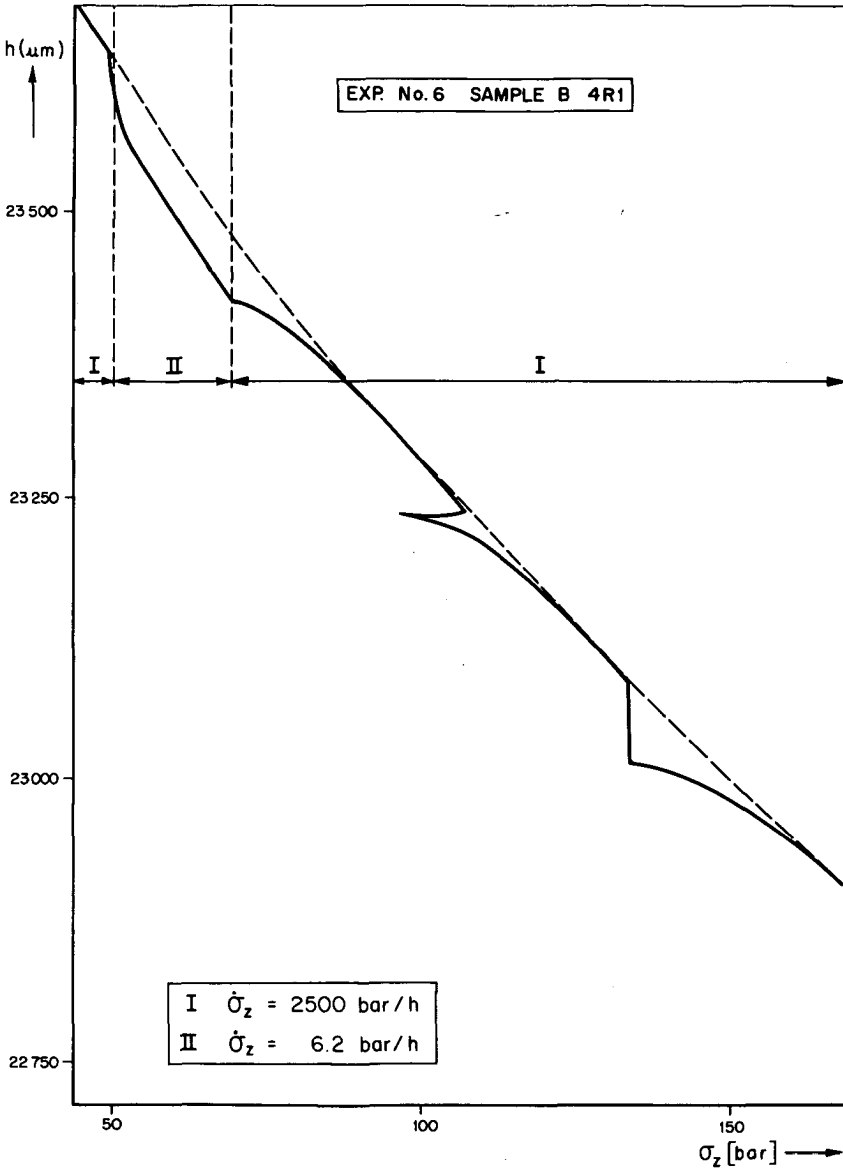OEDOMETER TEST) ORIGINAL AND
REMOULDED SAMPLE

FIG.A7 INFLUENCE OF CHANGES IN
LOADING RATE, PARTIAL UNLOADING
AND CREEP ON THE COMPACTION
BEHAVIOUR OF AN UNCONSOLIDATED
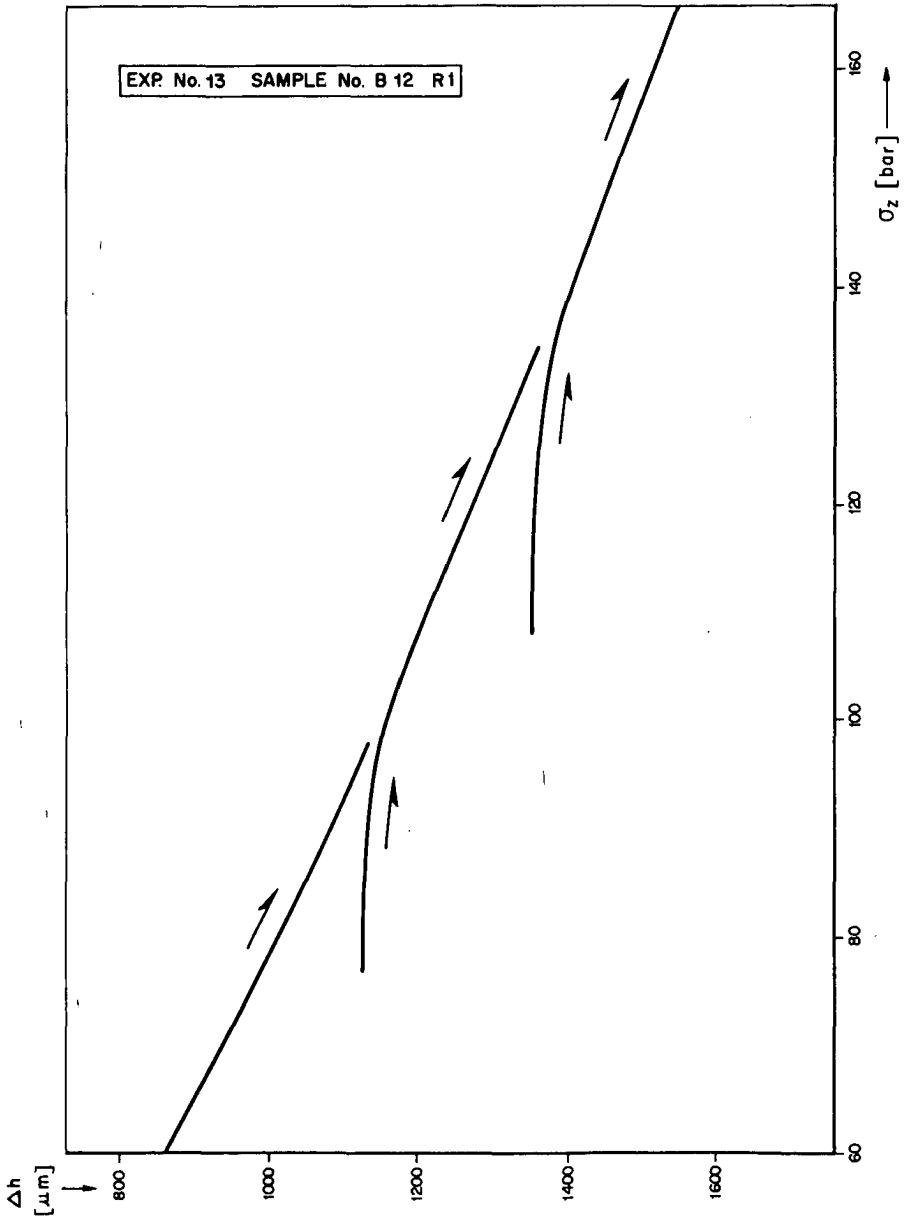RESERVOIR SAND. (RESERVOIR B,
OEDOMETER TEST)

FIG.A8 COMPACTION BEHAVIOUR OF
AN UNCONSOLIDATED RESERVOIR
SAND DURING RELOADINGS AFTER
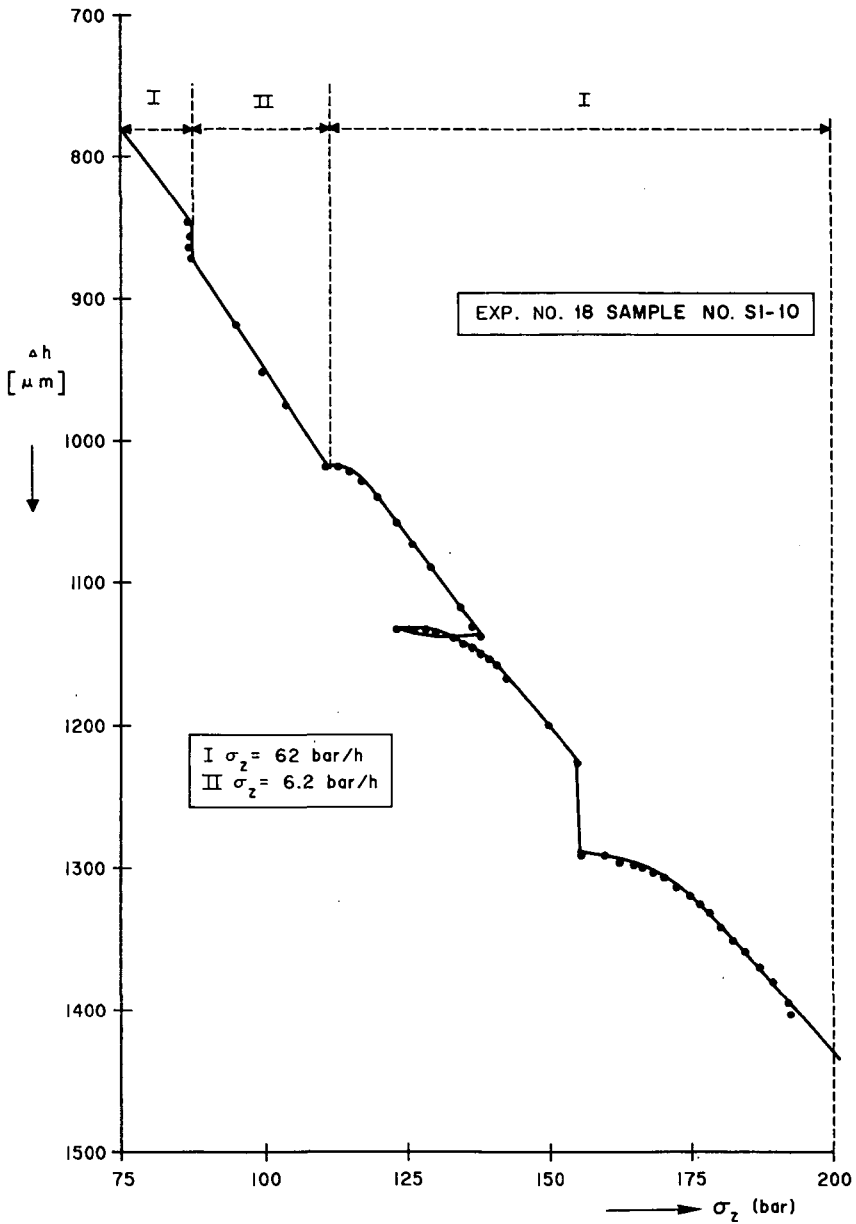PARTIAL UNLOADINGS. (RESERVOIR B,
OEDOMETER TEST)

FIG.A9 COMPACTION BEHAVIOUR OF
170 μ SAND AFTER A CHANGE IN
LOADING RATE, PARTIAL UNLOADING
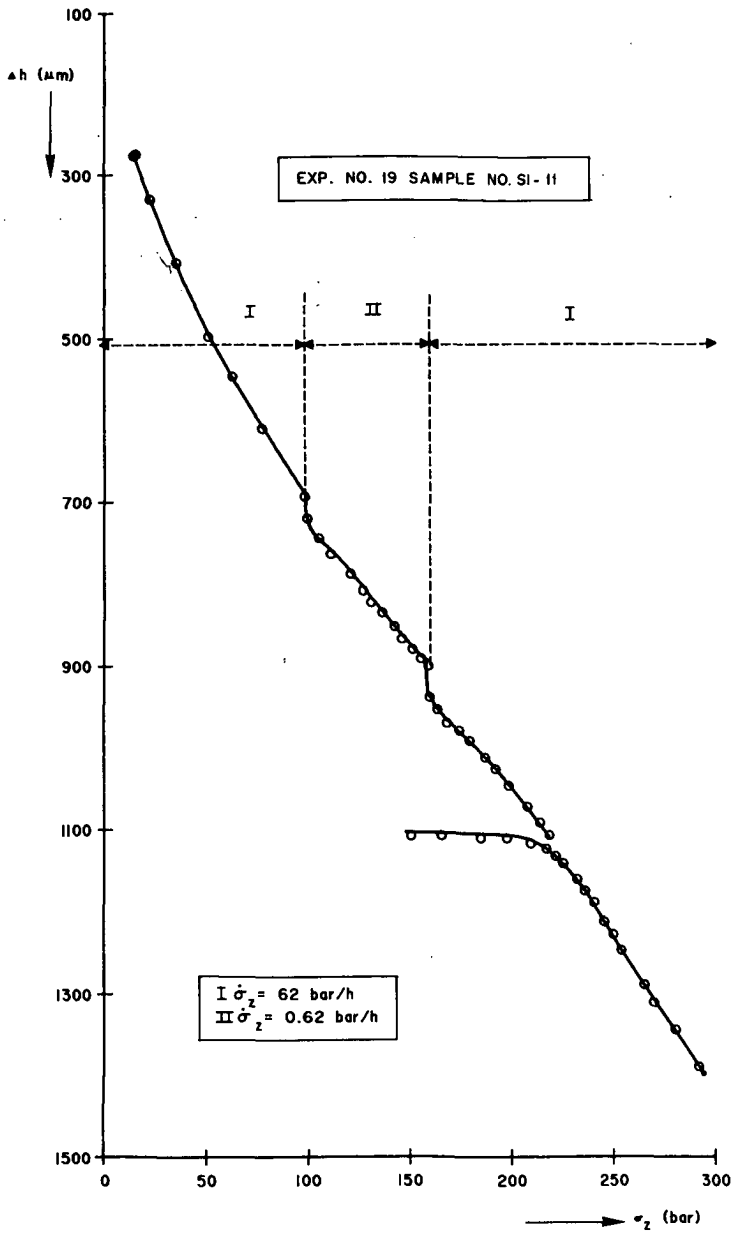AND CREEP (OEDOMETER TEST)

FIG.A10 COMPACTION BEHAVIOUR OF 170 μ SAND AFTER A CHANGE IN LOADING RATE, CREEP AND PARTIAL UNLOADING (OEDOMETER TEST)
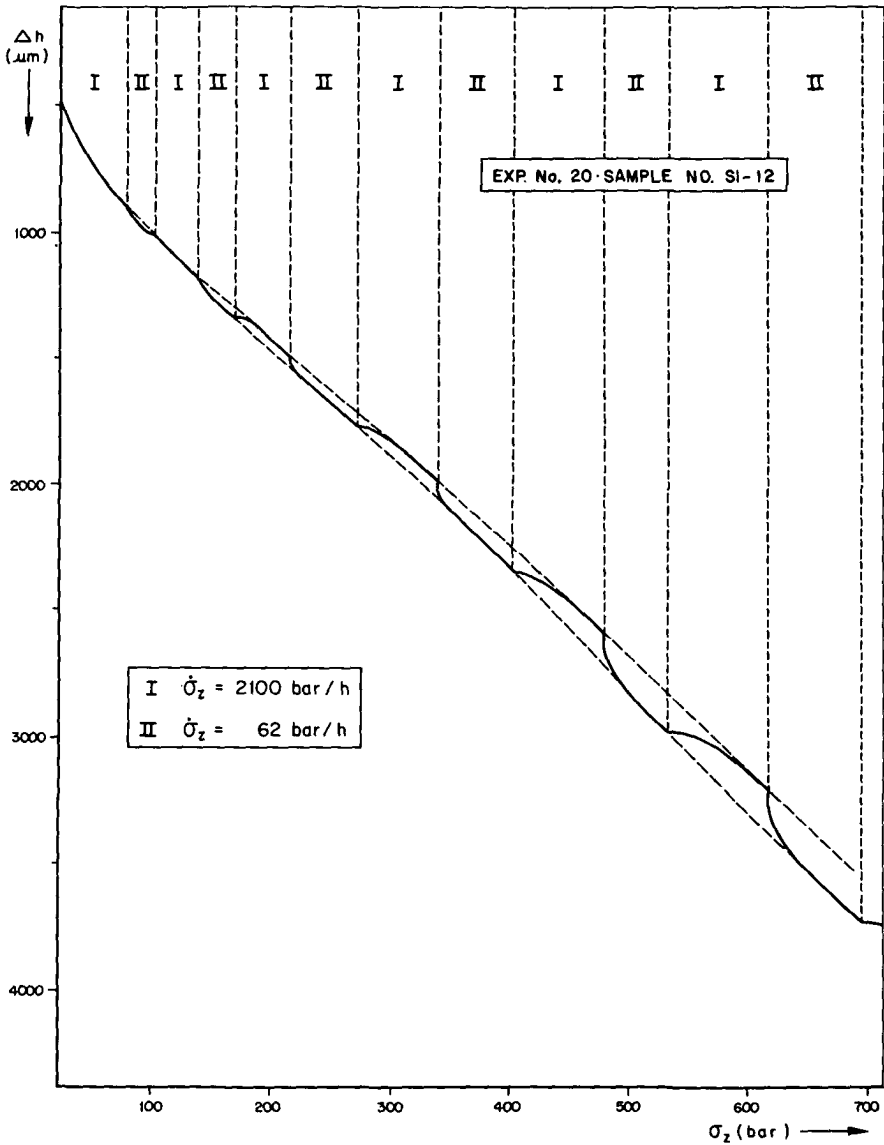
FIG.A11 COMPACTION BEHAVIOUR OF
170 μ SAND AS A RESULT OF CHANGES
IN LOADING RATE AT VARIOUS STRESS
LEVELS. (OEDOMETER TEST)

EXP. No. 22 SAMPLE NO. SI–13

σ_z [bar]

Δh [μm]

FIG.A12 COMPACTION BEHAVIOUR
AFTER PARTIAL UNLOADING OF 170 μ
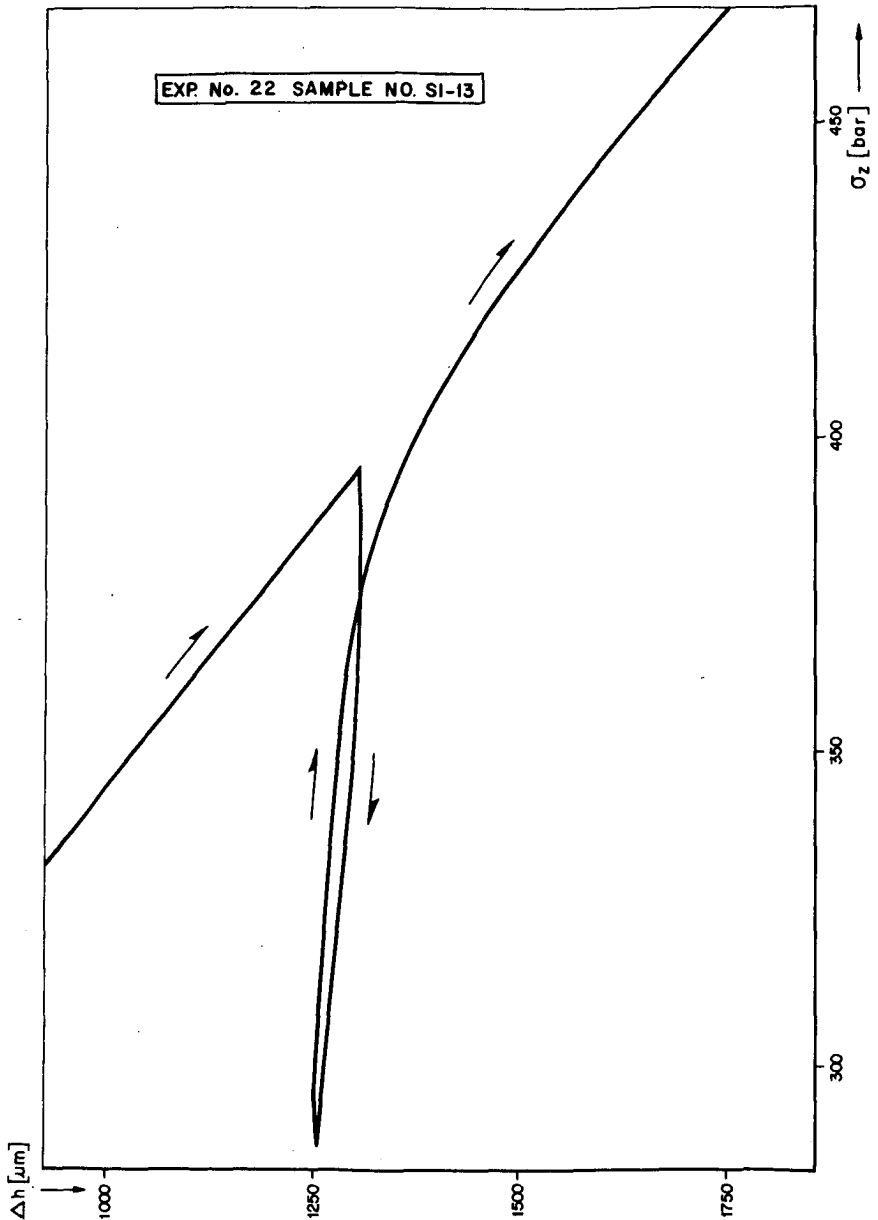SAND AT A HIGHER STRESS LEVEL.
(OEDOMETER TEST)

FIG.A13 COMPACTION BEHAVIOUR OF
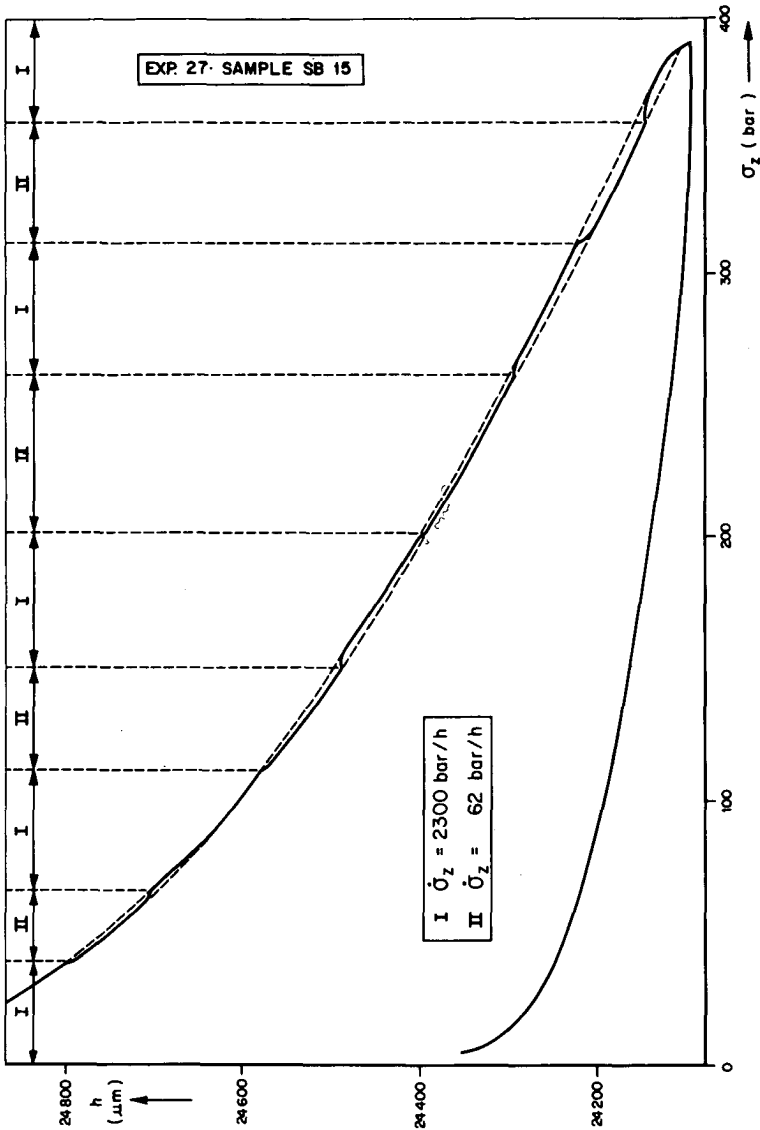170 μ STEAL BEADS AS A RESULT OF
CHANGES IN LOADING RATE AT
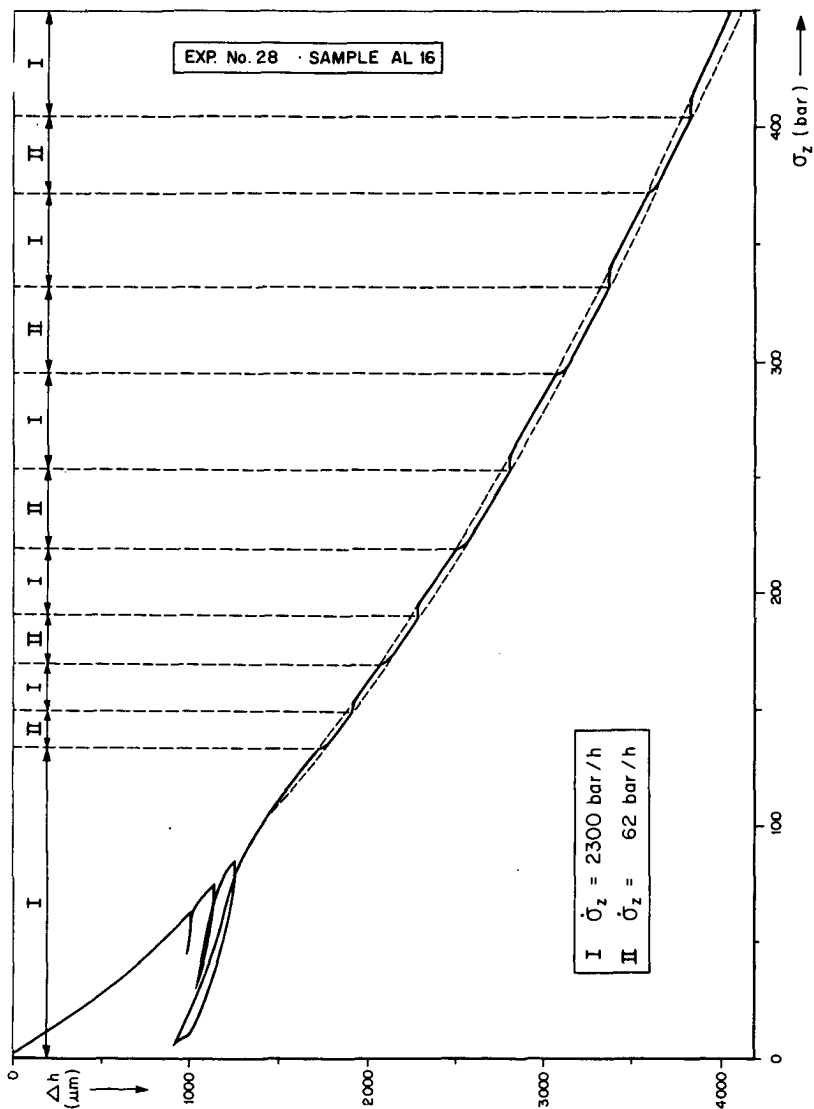VARIOUS STRESS LEVELS.
(OEDOMETER TEST)

FIG.A14 COMPACTION BEHAVIOUR OF
ALUMINIUM POWDER AS A RESULT OF
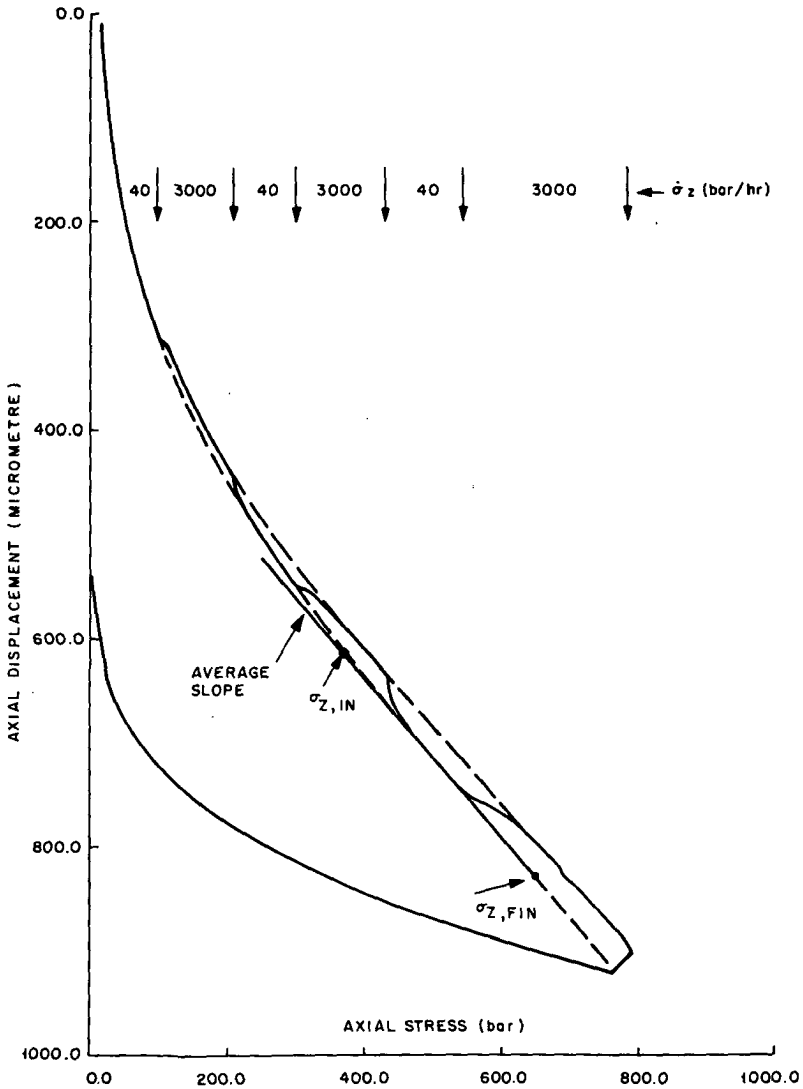CHANGES IN LOADING RATE AT
VARIOUS STRESS LEVELS.
(OEDOMETER TEST)

FIG.A15 EXAMPLE OF THE
COMPACTION BEHAVIOUR OF A
FRIABLE SANDSTONE AS A RESULT OF
CHANGES IN LOADING RATE AT
VARIOUS STRESS LEVELS
(SAMPLE E004, TRIAXIAL TEST)

SUMMARY

A proper understanding and accurate prediction of reservoir compaction and surface subsidence due to the withdrawal of fluids or gases from hydrocarbon or groundwater reservoirs is essential because of the possible environmental, technical and financial consequences. Over the last decade it has become apparent from a number of well documented field cases however, that the application of commonly accepted procedures to predict such reservoir compaction and the related surface subsidence, results in strong discrepancies between predicted and observed field behaviour. Therefore an extensive investigation has been carried out in an attempt to explain these discrepancies. The results of this investigation, culminating in the introduction of a new "rate type" compaction model (RTCM) strongly improving the capability to predict reservoir compaction and related surface subsidence, are presented in this thesis.

After outlining the historical development of the theoretical and experimental procedures to predict reservoir compaction and surface subsidence, the discrepancies between predicted and observed field behaviour are discussed in more detail. Next, the results of an experimental programme, resulting from an analysis of possible factors explaining these discrepancies, are presented. Based on these results, it is now understood that the observed discrepancies between laboratory predicted and field observed compaction behaviour are due to loading rate effects.

It is shown that after a sudden change in loading rate, as occurs in the field upon the start of depletion, the rock compressibility is strongly pressure dependent in a certain "transition zone". Similar transition zones occur after creep at constant stress and during reloading after partial unloading. In the transition zone, compressibility is initially very low. But it increases gradually, finally reaching values corresponding to conventional laboratory experiments. The behaviour in all these transition zones can be described by one unique (dimensionless) general compaction curve, independent of stress level, previous history or type of sandstone.

The above properties are similar to those of "rate type" materials and mathematical equations properly describing the observed compaction behaviour are derived from an existing constitutive equation developed for such materials. The governing differential equation is derived from a physical model in which the observed rate effects are related to time dependent friction at the intergranular contact points.

A procedure to apply the resulting rate type compaction model to field

conditions is given and it is shown that historical field compaction and subsidence data and those predicted by the new model are in good qualitative and quantitative agreement, thereby resolving the previously observed discrepancies.

SAMENVATTING

OVER DE INVLOED VAN BELASTINGS-SNELHEIDSVERANDERINGEN OP HET COMPACTIEGEDRAG VAN ZANDSTEEN RESERVOIRGESTEENTE

Een nauwkeurige voorspelling van reservoircompactie en bodemdaling ten gevolge van de onttrekking van gassen en vloeistoffen uit ondergrondse gesteentelagen is belangrijk in verband met mogelijke milieutechnische, operationele en financiele consequenties. Het is de laatste tien jaar echter duidelijk geworden dat de algemeen geaccepteerde methodiek om tot zulke voorspellingen te komen in een aantal goed gedocumenteerde praktijkgevallen heeft geleid tot grote verschillen tussen het voorspelde en het waargenomen veldgedrag. Daarom is een uitgebreid onderzoek uitgevoerd om te proberen deze verschillen te verklaren. De resultaten van dit onderzoek, die het onderwerp van het proefschrift zijn, hebben geleid tot een nieuw "rate type" compactie model (RTCM). Met behulp van dit model is een veel betere voorspelling van reservoircompactie en bodemdaling mogelijk geworden.

Na een historisch overzicht van de ontwikkeling van de theoretische en experimentele procedures om reservoircompactie en bodemdaling te voorspellen, worden de waargenomen verschillen tussen voorspeld en waargenomen veldgedrag meer in detail beschreven. Vervolgens worden de resultaten gegeven van een experimenteel onderzoek dat tot stand kwam op basis van een analyse van de mogelijke factoren die de verschillen konden verklaren. Uit de verkregen resultaten blijkt dat deze verschillen het gevolg zijn van belastingssnelheidseffecten.

Aangetoond wordt dat een plotselinge grote verandering in belastingssnelheid zoals die in het veld optreedt bij de aanvang van de depletie, resulteert in een gesteentecompressibiliteit die gedurende een bepaalde "overgangszone" sterk drukafhankelijk is. Soortgelijke overgangszones treden op gedurende toenemende belasting na een kruipperiode bij constante effectieve druk en gedurende toenemende belasting na een gedeeltelijke daling van de effectieve druk. In de overgangszone is de compressibiliteit aanvankelijk erg laag, maar hij neemt gestaag toe en bereikt uiteindelijk een waarde die ongeveer overeenstemt met die welke gedurende traditionele laboratoriumproeven gemeten wordt. Het gedrag in de verschillende overgangszones wordt beschreven door een enkele

(dimensieloze) algemene compactiekromme, die onafhankelijk is van het drukniveau, de belastingsgeschiedenis en het soort zandsteen.

De bovenstaande eigenschappen zijn karakteristiek voor "rate type" materialen. Wiskundige vergelijkingen die het waargenomen compactiegedrag goed beschrijven worden afgeleid uit een bestaande constitutieve vergelijking voor zulke materialen. De centrale differentiaalvergelijking wordt vervolgens afgeleid uit een eenvoudig fysisch model waarmee wordt aangetoond dat de waargenomen snelheidseffecten worden veroorzaakt door tijdsafhankelijke frictieverschijnselen op de korrelcontactpunten.

Een procedure om het "rate type" compactiemodel toe te passen op veldcondities wordt gegeven en aangetoond wordt dat historische gevallen van reservoir compactie en bodemdaling zowel qualitatief als quantitatief goed door het model worden beschreven, waarmee een bevredigende verklaring voor de vroeger waargenomen discrepanties is verkregen.

CURRICULUM VITAE

25-4-1953   Geboren te Amsterdam

1965 - 1971   6-jarige HBS-B te Amsterdam

1971 - 1977   Universiteit van Amsterdam, faculteit der Wiskunde
                     en Natuurwetenschappen, afstudeerrichting experi-
                     mentele natuurkunde.
                     Het afstudeeronderzoek werd uitgevoerd op het
                     Natuurkundig Laboratorium onder leiding van Prof.
                     I. Silvera en betrof het mechanisch en
                     thermodynamisch gedrag van vast waterstof en
                     deuterium bij cryogene temperaturen.

1977 - 1982   In dienst van het Koninklijke/Shell Exploratie en
                     Produktie Laboratorium te Rijswijk.

1982 - 1983   In dienst van het Bellaire Research Center te
                     Houston.

1983 - nu   In dienst van het Koninklijke/Shell Exploratie en
                     Produktie Laboratorium te Rijswijk. De nadruk van
                     het werk ligt op het onderzoek van de mechanische
                     en petrofysische eigenschappen van poreuze
                     gesteenten. Enkele voorbeelden zijn: het
                     electrische weerstandsgedrag in aanwezigheid van
                     koolwaterstoffen en geleidende kleimineralen; de
                     stroming van gassen en vloeistoffen; capillaire
                     krachten en de invloed ervan op de verdeling van
                     gassen en vloeistoffen in het gesteente.

STELLINGEN

1. De bewering van Helm dat een opwaartse beweging van de bodem van een compacterend reservoir fysisch onmogelijk is, is onjuist en kan met een eenvoudig symmetrie argument worden weerlegd.

   Helm, D.C., 1984, Field Based Computational Techniques for Predicting Subsidence Due to Fluid Withdrawal, Geol. Soc. of Am., Reviews in Engineering Geology, Volume VI, pp 1–22.

2. Het dient te worden onderzocht of de snelheidseffecten zoals die zijn gevonden in het compactiegedrag van zandstenen ook een rol spelen in het compactiegedrag van carbonaten en in het bijzonder welke invloed ze hebben op de positie van de zogeheten 'pore collapse trendlijnen'.

   Ditzhuizen, P.J.D. van and Waal, J.A. de, 1984, Reservoir Compaction and Surface Subsidence in the Central Luconia Gas Bearing Carbonates, Offshore Sarawak, East Malaysia, in: Proceedings 5th Offshore South East Asia, Singapore, February 21–24.

3. Het dient te worden onderzocht of de grote invloed van het type porievloeistof op het compactiegedrag van carbonaten zoals dat door Newman is gerapporteerd, kan worden verklaard uit het feit dat de 'pore collapse trendlijnen' voor olieverzadigde en waterverzadigde monsters verschillend zijn.

   Newman, G.H., 1981, The Effect of Water Chemistry on the Laboratory Compaction and Permeability Characteristics of some North Sea Chalks, SPE 10203.

4. De door Cook et al. gevonden negatieve uitzettingscoëfficiënt van vast waterstof is waarschijnlijk geen gevolg van een faseovergang maar een experimenteel artefact.

   Cook, G.A., Dwyer, O.E., Berwaldt, O.E. and Nevins, H.E., 1965, Pressure-Volume-Temperature Relations in Solid H_2, J. Chem. Phys. 43. 1313.

5. Het door Heaviside et al. gevonden grote effect van luchtdroging op de doorlaatbaarheid voor gas van illietfibers bevattende zandsteenmonsters is grotendeels reversibel.

   Heaviside, J., Langley, G.O. and Pallatt , N., 1983, Permeability Characteristics of Magnus Reservoir Rock, Paper A presented at the 8th European Formation Evaluation Symposium, pp 1–29, Londen, March.

6. De grote verschillen tussen het kationuitwisselend vermogen van zandstenen bepaald met membraanpotentiaalmetingen en met chemische titraties, zoals gevonden door Steward en Burck, zijn niet alleen een gevolg van het vermalen van de monsters ten behoeve van de titratiemeting, maar ten minste ten dele een gevolg van het niet geoorloofd gebruik van de membraanpotentiaalformule van Smits voor samples met hoge Qv's bij hoge molaliteit, zoals eerder waargenomen door Smits.

Steward, H.E. and Burck, L.J.S., 1985, Improved Cation Exchange/Qv Determination using the Multi-Temperature Membrane Potential Test, SPWLA 26th Annual Logging Symposium, June 17–20.

Smits, L.J.M., 1968, SP Log Interpretation in Shaly Sands, SPEJ, Vol. 9, pp 123–136, Trans. of AIME, Vol. 243.

7. Kennis van het interne vervormings- en bezwijkgedrag van gesteentemonsters tijdens laboratoriumproeven kan een belangrijke bijdrage leveren aan de verdere ontwikkeling van de gesteentemechanica. De röntgentomografietechniek biedt hiertoe in principe de mogelijkheid.

8. De conclusie van Chen en Stagg, dat de errorfunktie oplossing van Bourbie en Walls voor de interpretatie van pulspermeametermeting en alleen geldig is wanneer het porievolume kleiner is dan 0.6 maal het volume achter het monster, is op fysische gronden niet te begrijpen.

Chen, T. and Stagg, P.W., 1984, Semilog Analysis of the Pulse Decay Technique of Permeability Measurement, SPEJ, December, pp 639–642.

Bourbie, T. and Walls, J., 1982, Pulse Decay Permeability: Analytical Solution and Experimental Test, SPEJ, October, pp 719–721.

9. Naast aandacht voor vaardigheden en technieken is attitudeverandering ten aanzien van kinderen die anders zijn of zich anders ontwikkelen dan het verwachtingspatroon aangeeft, van wezenlijk belang voor het welslagen van de zorgverbreding binnen het basisonderwijs.

10 De discussie over het opnemen van reclame in academische proefschriften zou, wellicht ten onrechte, kunnen suggeren dat proefschriften frequent worden gelezen.

J.A. de Waal, mei 1986